Radiation Transfer characteristics and Transport Properties of Nitrogen-Polytetrafluoroethylene mixture plasma under Equilibrium and Non-equilibrium conditions

A thesis submitted to the University of Liverpool

By

Fei Yang

In partial fulfilment of the requirements for the degree of Doctor of Philosophy

Feb. 2016

Department of Electrical Engineering and Electronics

The University of Liverpool

Abstract

Nitrogen constitutes a natural part of air and is a non-global warming gas. There have been recent attempts to use it as a working medium in high voltage circuit breakers to replace SF_6, which is an excellent insulating and arc quenching gas but also a strong greenhouse gas with a Global Warming Potential (GWP) of 23,900 and a life time of 3,200 years. To employ the full potential of nitrogen for use in high voltage circuit breakers, the properties and radiation characteristics of its mixture with Polytetrafluoroethylene (PTFE) vapour, an electrical and thermal insulation material, need to be known, forming the objectives of the present work.

This research has investigated the capability of nitrogen and SF_6 on insulating and quenching an electric arc in a high voltage circuit breaker. Depending on the current of the electric arc range from 100 A to 330 A, the arc can be extinguished in 25-50 ms with nitrogen gas flow, while it takes 20-45 ms with SF_6. The peak voltage of the electric arc with SF_6 is 10% higher than it is with nitrogen. According to the preliminary data obtained in the experimental investigation, it seems possible that SF_6 can be replaced by nitrogen as the operation gas in high voltage circuit breakers. Research on the properties and radiation characteristics of a gas mixture of nitrogen and PTFE is required to allow modelling of a nitrogen filled circuit breaker.

Net Emission Coefficient (NEC) describes the radiation characteristics of the hottest area in an electric arc. The NEC of a nitrogen and PTFE mixture is computed by using the most advanced method considering both continuum and line radiation. The result shows that the influence of PTFE on the NEC cannot be neglected. The influence of uncertainty in atomic data on the calculated NEC is studied. A 50% adjustment in the uncertainty of the atomic data on high energy levels results in a 0.001% variation of the NEC because of the low population density of the particles with high energy levels involved. Due to the lack of experimental results of the mixture, the validity of the model is confirmed by a good agreement between the results calculated and those obtained by experiments or those predicted by the other research groups for pure nitrogen gas and pure PTFE vapour. Results show that influence of PTFE vapour on the NEC of the mixture is substantial. It has been determined that the NEC of the mixture cannot be estimated by NEC of the pure gases multiplied by their proportions in the mixture.

Re-absorption has to be considered when the temperature is lower than 25,000 K. To solve the Radiation Transfer Equation (RTE), the P1 and Discrete Ordinate Method (DOM) have been used to calculate the radiation with re-absorption. The P1 approximation is computationally cheaper but it has poor accuracy. The accuracy of DOM is determined by the number of calculation bands. It is obvious that the more bands used, the higher the accuracy. A comparison of the DOM 8-5 and 5-3 methods indicates a balanced compromise between accuracy and cost of calculation with DOM 8-5.

A two-temperature model was applied to solve the properties of the plasma in non-LTE condition when the temperature gradient is sufficiently high. A number of existing calculation methods are discussed. A modification of Godin's method has been proposed to satisfy the two-temperature model. Results of a gas mixture composition, obtained by different methods, are analysed. The modified method leads to results that agree very well with those from the existing methods but with better convergence that when the Newton-Raphson algorithm is used to obtain the solution. Results with different molar percentages of PTFE vapour have been presented and discussed. The results for pure nitrogen and pure PTFE vapour have been compared with existing data to verify the validity of the method.

Acknowledge

First of all, I would like to acknowledge and extend my heartfelt gratitude to my supervisor, Dr. J. D. Yan for his support and continuous encouragement throughout my study.

I would also like to thank Professor J. W. Spencer for useful discussions and advice.

I wish to thank other members of the Energy and Power Systems research group, especially Mr. J. Humphries who gave much help to me in the experiment. I also wish to thank the Department of Electrical Engineering and Electronics, University of Liverpool for providing me such a good environment for my research.

I thank my colleague, Mr. Q Zhang and Y. Pei for their support and help as well as all of my group members for their help and encouragement.

The last but not least, to my wife, my parents, I wish to express my greatest thanks for their love, endless support and encouragement which give me confidence, wisdom, strength, and endurance to pursue my dreams throughout all my study.

Table of Contents

List of Figures

List of Acronyms

CTE: Complete Thermal Equilibrium

DOM: Discrete Ordinate Method

HVCB: High Voltage Circuit Breaker

LTE: Local Thermal Equilibrium

MAC: Mean Absorption Coefficient

MMP: Mixed Mean Planck

NEC: Net Emission Coefficient

PTFE/C_2F_4: Polytetrafluoroethylene

RTE: Radiation Transfer Equation

SF_6: Sulfur-hexafluoride

Chapter 1 Introduction

1.1 Circuit breakers

Circuit breakers are designed to protect the electrical power transmission networks from damage when faults occur such as short circuits and overloads. In normal operation the contacts in circuit breaker are closed and it works as a good conductor. However, when a fault is detected, the contacts must be separated so it becomes an excellent insulator. Due to the high current (larger than 50 A) passing through the closed contacts, it generates an electrical arc by ionizing the gas between the contacts when they are separated. The electrical arc generates a sufficient high instant current that may damage the devices in the power network. The speed of interrupting the current flow determines the performance of the circuit breaker. Depending on the voltage of the circuit breaker used, it is divided into two classifications: low voltage (less than 1k V) circuit breaker and high voltage (greater than 1k V) circuit breaker.

1.1.1 Research on circuit breakers

The research on circuit breakers comprises two parts: modelling research and experimental investigation. The modelling research consists of simulating the progress of the circuit breaker operation, with the help of a computer, by mathematical and physical models. Experimental investigation is physically building a circuit breaker in a laboratory. Recording the sensor's data, oscilloscope and other monitoring equipment, can investigate the processing of operating and the behaviour of the electric arc when it interrupts the current flow. The purpose of the circuit breaker is to extinguish the electric arc in a very short time (less than 50 ms).

1.1.2 Nitrogen in circuit breakers

Currently, SF_6 is an excellent insulating and arc quenching gas but also a strong greenhouse gas with a Global Warming Potential (GWP) of 23900 and a life time of 3200 years. Nitrogen makes a natural part of air and is a non-global warming gas. There has been recent attempt to use it as a working medium in high voltage circuit breakers to replace the SF_6. To employ the full potential of nitrogen for use in high voltage circuit breakers, the properties and radiation characteristics need to be known.

1.2 Plasma

When a solid matter is heated adequately, its crystal lattices structure will be broken by the thermal motion of the atoms, which results in melting and a liquid is formed. When the liquid is heated sufficiently, the rate of atoms vaporising off the surface is higher than the rate of re-condensing, the matter transforms into gas. If the gas is heated enough, the atoms collide with each other and knock their outer shell electrons off, the matter is in a plasma state. Therefore, plasma can be regarded as the fourth state of matter.

Plasma, makes 99% of the matter in the universe. It was discovered by Davy[1] in 1808. Plasma physics has evolved into an advanced interdisciplinary science over past 30 years[2]. The plasma in the universe is generated naturally. A plasma can be created by heating a gas or subjecting it to a strong electromagnetic field applied with a laser or microwave generator. In plasma, electrons are generated by ionisation of molecules, atoms or ions. They are completely free to move. The freely moving electrons make the plasma electrically conducting.

After World War Two, there were rapid developments in the chemical and electrical industry. The technology of electrical arc and thermal plasma was

advanced owing to their unique characteristics of high temperature, energy density and flexibility in working gas. In the 1950s, plasma was widely used in material processing, such as for plasma cutting[3], plasma welding[4] and plasma painting[5]. In the 1960s great success was made in producing fine powders of refractory metal and cermet. It brought about immense success in material processing. Nowadays, there are more than 10 major research areas related to plasma, such as plasma diagnostics, plasma sheath phenomena and numerical plasmas and simulation.

1.2.1 Plasma in circuit breakers

Arc plasma in high voltage circuit breakers is generated by an electric discharge with a current above 50 A and a pressure greater than 0.1 bar. In a high voltage circuit breaker (HVCB), the electric arc is formed by separating the electric contacts. The current continues to pass through the arc even through the contacts have been separated. Due to Joule heating, the current results in a high temperature of greater than 20,000 K in the arc. The gas close to the arc is then ionized to become arc plasma. Theoretically, the arc plasma can exist in three states: Complete Thermal Equilibrium (CTE), Local Thermal Equilibrium(LTE) and non-LTE.

Complete Thermal Equilibrium (CTE)

For the arc plasma to be in the CTE state, it must satisfy the conditions below:

1. The temperature in the arc is unique.
2. The speed of particles in the plasma is according to the Maxwell-Boltzmann distribution and the population density of the excited states of particles follows the Boltzmann distribution.
3. All particle densities can be described by Saha equations.
4. The electromagnetic radiation field is that of blackbody radiation of intensity that can be described by the Planck function.

However, not only arc plasma but also an actual plasma and some natural plasmas cannot be in the CTE state. This is because most plasmas are optically thin and, the radiation temperature of the radiator is different from the kinetic temperature of the plasma.

Local Thermal Equilibrium (LTE)

In contrast to the CTE state, plasma in the LTE state does not require its radiation to correspond to the blackbody radiation intensity of the LTE temperature. The definition of LTE states that *collision processes (not radiative processes) govern transitions and reactions in the plasma.* The processes are micro reversible. LTE also requires local gradients of plasma properties such as temperature, number density and heat conductivity to be sufficiently small to allow the particles to arrive at equilibrium. The time required for the particles to reach equilibrium is much shorter than the diffusion time. As arc plasma has such a high temperature, especially in the arc core region, arc plasma can be considered to be in the LTE state. The plasma can be classified as thermal plasma if it meets all the requirements of LTE.

Non Local Thermal Equilibrium (non-LTE)

LTE is no longer valid when a large temperature gradient exists, such as in the region close to a cold wall or when the number density of electrons is not high enough to allow sufficient transfer of energy between the electrons and heavy-particles. In such a situation, plasma is in a non-LTE state.

Optical thin plasma

Optical thin plasma is a plasma that emits radiation with a wavelength longer than[2] $200\ \mathrm{nm}$ while radiation of wavelength shorter than $200\ \mathrm{nm}$ is partially or totally absorbed by the plasma. Many years ago, arc plasma was treated as optically thin, even at high temperature and high pressure. In the 1990s,

researchers have realised that the reabsorption of radiation from arc plasma is an important mechanism.

Blackbody radiator

A blackbody radiator in thermal plasma is an ideal emitter. The intensity of emitted blackbody radiation is independent of frequency, but is only determined by temperature. The radiation observed in plasma is usually much less than blackbody radiation, due to the influence of radiation absorption in optically thin and radiation reabsorption in optically thick.

Debye length and electric shielding

It is well known that due to Coulomb forces, on average, more than one electron surrounds a positive ion. The electrons act as shield for the positive ion, resulting in an electric field generated by a positively charged ion only existing within a sphere with diameter of Debye length; therefore, the Coulomb force on the electrons outside of the Debye sphere are significantly smaller on electrons within the sphere. The Debye length due to shielding effect then determines the ionization energy of atoms and ions.

1.2.2 Nitrogen-polytetrafluoroethylene plasma in circuit breakers

Polytetrafluoroethylene (PTFE) is one the most common materials used in high voltage circuit breakers. The arc plasma in the high voltage circuit breaker is ionized from the operation gas mixture with PTFE vapour. The presence of PTFE vapour in the arcing gas is a direct result of nozzle ablation induced by the strong radiative flux from the high current arc. The majority of a high current atmospheric pressure arc (instantaneous current >2 kA) at power frequency is in the LTE state. Only a small part near the arc edge where a strong temperature gradient exists deviates from LTE. However, this part of the arc contributes little to the conduction of a high current and the whole arc column can be modelled by an LTE arc model. In contrast, the low current arc during the current zero

period can deviate from LTE and a two-temperature model is often used to describe the different behaviours of electrons and heavy particles. Therefore, in present work, the nitrogen-PTFE plasma is considered to be under LTE and two-temperature non-LTE conditions.

1.3 Introduction to determination of equilibrium composition, thermal properties, transport coefficient and radiation for thermal plasma

Research work regarding radiation transfer in arc plasma is continuing because of the current interruption phenomenon in circuit breakers has not been elucidated clearly owing to the complex nature of this topic. Radiation dominates the mechanism of energy transport in arc plasma. It has been found that during the arc processing, the total radiation from an arc plasma is its energy loss, which determines the time required for the electric arc cooling down. Many papers have been published to introduce the different approximation methods that can be employed to approach the exact variation of radiation in an arc plasma. In this section, it is going to introduce the mechanism of radiation emission and absorption.

1.3.1 Equilibrium composition

The knowledge of the chemical equilibrium composition of a species is fundamental to the investigation of radiation transfer. The whole theoretical basis of equilibrium composition calculation is taken from Gibbs, who developed the formalism of statistical mechanics in 1902[6]. Stuart R. improved the theory to apply it to a system containing many constituents[7]. This method makes use of equilibrium constants to express some certain species. The weaknesses of this method are that it is limited to some specific species and

reactions, and it is quite cumbersome. In 1958, White improved the theory[8] and derived an equation that can be applied to all constituent species in a chemical reaction with no distinction between them. The Gibbs energy and number density of a specie can be related to the chemical potential, as represented below:

$$\mathrm{dG} = \sum_{a} \mu_a dN_a = 0 \qquad (1.1)$$

Where μ_a is the chemical potential and N_a is the number density for species a. Researchers continued to improve the calculation method. The composition and transport properties of SF_6 were calculated by Frost et al.[9] by applying minimization of Gibbs free energy. The temperatures of results are from 1,000 K to 45,000 K and pressures from 1 bar to 16 bar. In 2003, Godin and Trepanier[10] developed a new robust method to simplify the computation of equilibrium composition. They introduced a chemical basis in the calculation, which leads to be regardless reactions individually. Cressault[11] investigated thermal plasma properties for several kinds of mixtures of metal vapour. He calculated the plasma composition for metals with different molar proportions by applying Godin's method. The results were in good agreement with existing theoretical and experimental work.

The Saha equation, known as the Saha-Langmuir equation, was developed by Saha[12] in 1920. It is another popular method related to the species number density, temperature and pressure. The following equations describe the ionization reaction and dissociation reaction, respectively.

$$\frac{n_a n_b}{n_{ab}} = \frac{Q_a Q_b}{Q_{ab}} \left[\frac{2\pi kT}{h^2}\right]^{3/2} \left[\frac{m_a m_b}{m_{ab}}\right]^{3/2} \exp\left[-\frac{E_d}{kT}\right] \qquad (1.2)$$

$$n_e\left[\frac{n_{r+1}}{n_r}\right] = 2\left[\frac{Q_{r+1}}{Q_r}\right]\left[\frac{2m_e\pi kT}{h^2}\right]^{3/2}\exp\left[-\frac{E_{I,r+1}-\Delta E_{I,r+1}}{kT}\right] \quad (1.3)$$

In Eq.(1.2), n_a, n_b and n_{ab} are the population of species ab and its products of dissociation reaction *a* and *b*, k is the Boltzmann constant, and h is the Planck constant. E_d indicates the dissociation energy of the reaction $ab \Leftrightarrow \mathrm{a} + b$. In Eq.(1.3) n_{r+1} represent the population of species r that loses an electron and n_e indicates the population of electrons. $E_{I,r+1}$ is the ionization energy for the reaction $r \Leftrightarrow [\mathrm{r}+1] + e^-$ and $\Delta E_{I,r+1}$ is the lowering of the ionization energy. The Q in both equations represents the internal partition functions.

Saha equations are applied for LTE conditions. However, Van de Sanden[13] proposed another form of equations that are suitable for non-LTE conditions. Potapov et al.[14] derived other equations based on the Saha equations for non-LTE but chemical equilibrium.

1.3.2 Transport

The transport coefficient calculation usually employed overcomes the various integral equations of Boltzmann, explaining the development of application in the Chapman–Enskog (CE) approach[15]. A study by Hirschfelder *et al*.[16] completed in-depth examinations in this regard. Despite the fact that it was presented in mind of weakly ionised gases, such a technique has been regarded as valid in relation to thermal plasmas[17]. The transport coefficients are estimated by using Sonine polynomials. Knowledge of the equilibrium composition of the particles is necessary before calculating the transport coefficient, as well as the integrals of collision $\Omega_{m,n}^{(l,s)}$, which are known to be dependent on the ability to characterise the interaction between two particles m and n. Following[16] Hirschfelder's research, these integrals can be expressed as:

$$\Omega_{m,n}^{(l,s)} = \left(\frac{k_B T}{2\pi\mu_{m,n}}\right)^{1/2} \int_0^{\infty} \exp(-\gamma_{m,n}^2)\gamma_{m,n}^{2s+3} Q_{m,n}^{(l)}(\varepsilon_r) d\gamma_{m,n} \qquad (1.4)$$

Where k_B is the Boltzmann constant, $\gamma_{m,n} = \left(\frac{\varepsilon_r}{k_B T}\right)^{1/2}$, ε_r is the kinetic energy, $\mu_{m,n}$ is the reduced mass, and $\frac{1}{\mu_{m,n}} = \frac{1}{m_m} + \frac{1}{m_n}$ and $Q_{m,n}^{(l)}(\varepsilon_r)$ are the total transport cross section, which can be carried out by the interaction potential of different species and will be described in Chapter 4. Chapman[15] summarised a method to calculate diffusion coefficients, viscosity and electrical conductivity.

There are four important terms in calculating thermal conductivity. They are the translational thermal conductivity of heavy-particles, electrons, internal and reaction respectively[18]. The fundamental term is due to the different chemical reactions, and is representative of the energy transportation by dissociation and the species' and molecules' ionisation and recombination.

The complete diffusion coefficient, taking into consideration temperature and pressure gradients, and ambipolar diffusion, has been suggested by Devoto[19]. Murphy published a paper[20] that states the importance of diffusion coefficients to mixture gas modelling. Weizong[21] computed the thermal properties and transport coefficient of pure nitrogen gas. However, there is lack of calculation relating to nitrogen mixtures such as with PTFE.

1.3.3 Radiation

Radiative transfer, is an important energy transport process within thermal plasmas. It plays a significant role in determining the temperature in high current electrical arcs. Moreover, it also affects the electrical and other transport properties of the plasma. Due to the importance of radiation transfer

in energy balance, it is necessary to clearly understand the mechanisms of radiation emission.

Generally, the direction of radiation transfer within an arc plasma starts from the arc core (hot regions). The energy is emitted from the arc core to the cold regions, such as the edge of the plasma. Energy can be absorbed completely in hot regions. However, it has to be absorbed partially in relatively cool regions. When the radiation reaches the cold region, the remaining energy will be absorbed.

The absorption coefficient indicates the probability of a photon being absorbed along the path. This absorption effect leads to a reduction of radiation intensity. It can be expressed according to the equation below:

$$\frac{dI_v}{dr} = K_v B_v - K_v I_v \qquad (1.5)$$

Where I_v is the radiation intensity at the point of interest *r* with frequency *v*, which can be defined as radiation power per unit solid angle and per unit apparent surface. r is the distance from the point of interest to the arc core. B_v is the blackbody intensity, which expresses the radiation intensity emitted from the arc core. K_v is the absorption coefficient. The term $K_v B_v$ is defined as power emitted from the arc core through a unit volume of the plasma per unit solid angle at frequency *v*.

$$\frac{\varepsilon_v}{K_v} = B_v = \frac{2hv^3}{c^2[\exp\left(\frac{hv}{kT}\right) - 1]} \qquad (1.6)$$

The absorption coefficient is the key parameter to investigate radiation transfer within an arc plasma. It can be contributed by atoms, molecules and ions. According to the radiation mechanism, it can be classified such four

contributions: atomic continuum, atomic line, molecular continuum and molecular line radiation.

In 1971, Lowke and Liebermann[22] computed the atomic continuum and line radiation for SF_6 arc plasma. A detailed method was derived for the calculation of the absorption coefficient contributed by the atomic continuum and line radiation. Gongassian and Schluter[23] developed a more elaborate theory for the calculation of atomic continuum radiation. A deduction effect of the contribution of radiative recombination to the total continuum radiation was found by applying a new calculation method of photoionization cross sections. The photoionization cross section of an atom and a molecule dominate the magnitude of continuum radiation that can be observed from experimental investigation. Lee[24] reported cross sections for 10 kinds of species including nitrogen from experiment. However, estimation of the cross section from theoretical investigation is an efficient way to obtain the cross section for thousands of species in nature. Hudson[25] reviewed the photoabsorption cross section for molecules of some popular species with wavelengths of less than 300 nm. Fennelly [26] tabulated the cross section for nitrogen atoms and molecules taking into account the dense structure and autoionization structure in the cross section. Robinson[27] developed a method of estimating the cross section for negative ions. Itikawa[28] complied the table of the cross sections for molecular nitrogen in 1984.

Radiation due to transition between electronic excitation energy levels results in spectral lines. The broadening of spectral lines can be caused by different mechanisms. Lowke described the methods to calculate line spectral broadening due to different mechanisms. The line profile is a function describing the spectral line shape with a given broadening from all mechanisms. Gleizes [29] and Drawin [30] introduced a two-line profile in their radiation calculations. In Gleizes's case, he neglected the influence of line overlapping

and applied the Gaussian line profile for calculating line radiation. The radiation results matched existing theoretical and experimental work but were slightly higher. Darwin applied the Lorentzian line profile in his calculation. The Lorentzian line profile has been more popular in recent years: Franke [31] calculated radiation in a free-burning arc employing the Lorentzian line profile for the line radiation. Liani[32] computed the net emission coefficient (NEC) for a CH_4 mixture with H_2 by applying the Lorentzian line profile.

In 1974, Lowke[22] introduced the concept of the NEC, a novel theory to estimate radiation for isothermal plasma. He demonstrated the use of NEC to express the divergence of the radiative flux at the centre of the arc plasma. It is believed that the arc core is the hottest region of the arc plasma and can be treated as an isothermal plasma[33]. The calculation equation is expressed below:

$$\varepsilon_N(T, p, R_p) = \int_0^\infty \kappa_\nu(T, p) B_\nu(T) \exp\left(-\kappa_\nu(T, p) R_p\right) d\nu \qquad (1.7)$$

Where NEC ε_N is a function related to temperature, pressure and thermal radius. The thermal radius indicates the radius of the isothermal plasma.

Many researchers have investigated arc plasma radiation based on NEC theory: Gleizes calculated the NEC for pure nitrogen, SF_6 and their mixture arc plasma that has good agreement with experimental results[29]. Cressault[34] investigated the radiation properties of several metal vapours by employing the NEC as the indicator. The calculation results matched with published work. Billoux [35] calculated the NEC for CO_2 mixture with copper vapour. He found that the NEC cannot indicate radiation transfer at low temperature because species reabsorption is neglected. Some work has been done on the NECs for other pure gases or mixtures: air[36], CH_4-H_2[32], H_2O-air-$MgCl_2$/$CaCl_2$/NaCl[37] and SF_6[38].

Arc plasma with real radiation transfer, however, is not an isothermal plasma. Plasma reabsorption dominates the radiation transfer in the cool region where NEC is no longer valid. The physical quantity that describes radiation transfer is

radiation flux. However, it is expensive in computation costs to resolve the actual radiation flux model. Therefore, some approximation methods have been developed to simplify the calculation model of radiation flux in an arc plasma. A partial characteristics method has been developed by Sevast' Yanenko[39], who identified two parameters, Som and $\Delta \mathrm{Sim}$, which describe the absorption and emission of radiation in a given direction. Those two values can be tabulated for a specific gas before starting the simulation work. It is complex as well, but the simulation is rapid. P1 approximation is the other effective method of calculating radiation flux for plasma modelling. P1 approximation was first developed by Jeans[40] in 1917, but Kourganoff further described this method in 1952[41]. The value of this method is the governing equation, which is a simple partial differential equation (PDE), which means that approximation can be solved in low order equations. The computation cost is much less than that required for solving radiation transfer equation (RTE), and it has good accuracy for media that is near-isotropic radiative intensity [42] . Gelbard improved the P1 method to high-order approximation to increase its accuracy; it is known as SP_N. The discrete ordinate method (DOM) is another approximation method to simplify RTE. Details of DOM have been given by Charest[43].

1.3.4 Nitrogen-PTFE plasma under thermal and non-thermal equilibrium

There has been much interest directed towards plasma devices that function with nitrogen due to the fact they function with common tungsten-based refractory electrodes, provide an environment that is radical non-oxidising with high temperature for a number of different plasma processing and plasma chemistry functions, and deliver higher plasma power when contrasted alongside argon via the higher voltage drop across the plasma[44-47]. Within these devices, there may be temperature variations spanning several thousand

degrees Kelvin, although ultimately this depends on the electrodes' geometry and the operating conditions, where pressure could vary from a number of atmospheres to sub-atmospheres, and where there could be a significant variation of electron temperature from corresponding heavy species, although this is dependent on location[48]. The presence of gradients of temperature, species densities and pressure, as commonly experienced in these devices, makes it necessary to ensure good insight into the notably non-linear behaviours of associated transport and thermal properties. In recent times, numerical simulation of devices has been gaining much momentum as a cost- and time-saving method geared towards understanding the behaviours of devices within various operating parameters and device designs. Transport properties and thermodynamic data represent the most pressing prerequisites for such simulations.

In the past, various theoretical and experimental efforts have been directed towards understanding the transport and thermodynamic properties of nitrogen plasma in direct consideration of thermal equilibrium[49 - 60]. With the exception of very minor deviations from various collision integral sets applied in other works, the majority of these calculated properties display a generally sound consensus. Regarding LTE, the work carried out by Murphy and Arundell[58] warrants specific consideration. An in-depth examination into the transport properties and thermodynamic data associated with atmospheric-pressure nitrogen was carried out in the temperature range 300–30,000 K. The pressure dependence of the properties is further addressed in the work of Murphy[59]. Nonetheless, works surrounding the estimation of transport property and thermodynamic data of nitrogen plasma within conditions of non-equilibrium is selective[61]. Colombo *et al*.[61] completed the first work in this field and, together with argon and oxygen, various transport and thermodynamic properties associated with atmospheric pressure nitrogen were established in

relation to the thermal non-equilibrium parameter (h, ratio of electron temperature to heavy species temperature) up to 3. The data available in the literature, thus far, have not undergone in-depth comparison. Subsequent to the aforementioned work, Wang *et al*.[21] completed a study that showed that within thermal non-equilibrium the calculated properties significantly depend on the definition of screening length, particularly at higher temperatures. The issue centred on whether only electrons or both ions and electrons should be recognised in the definition surrounding shielding length under screened Coulomb potential. Despite the fact that there was no reason to question whether the effect of ions should not be taken into account in the shielding when they can quite clearly impact the shielding mechanism, work besides that by Wang *et al*. demonstrated shielding by electrons only for the calculation of thermodynamic and transport properties.

In a study conducted by Ghorui *et al*.[62], selection of the most suitable shielding distance form in the prediction of collision integrals within screened Coulomb potential for two-temperature non-equilibrium plasma has been questioned. The shielding distance definition has been revised with an alternative suggested in close alignment with the experimentally observed[62] results. This is centred on the view that greater electron mobility can achieve redistribution in any change in the potential at the rate of electron temperature (T_e), whilst the single temperature T_e could be used whilst both ions and electrons are being incorporated and taken into account in the prediction of potential screening. The current work implements such a method and further establishes the complete set of transport properties and thermodynamic values for the nitrogen plasma within conditions of both thermal non-equilibrium and equilibrium[62]. In this particular calculation, the range of temperature amongst the electrons is 300–50,000 K, where the ratio (θ) of T_e to the heavy particle temperature (T_h) ranges from 1–20, whilst the pressure range is 0.1–

7 atmospheres. In the field of atmospheric pressure, the findings garnered for thermal equilibrium ($T_e = T_h$) can be contrasted with a significant number of published results in comparable settings. Due to the fact that much discussion has been centred on the behaviours of various diffusion coefficients under thermal non-equilibrium[63], thus far, this paper has not presented any data on diffusion coefficients.

In the area of chemical non-equilibrium, various densities within the plasma can be affected through diffusive particle fluxes stemming from temperature gradients and species.

1.4 Objectives of research and outline of thesis

As discussed in the last section, the thermal plasma radiation, thermodynamic properties, transport coefficient are often fundamental for computer simulations for the investigation of arc behaviour. An experimental investigation to justify if nitrogen can be used in circuit breakers will be presented before the calculation work. After that, this thesis will focus on the calculation of fundamental data for thermal and non-thermal equilibrium conditions of plasma.

The contents of this thesis are arranged into six chapters. The first chapter gives a brief introduction to the thesis, including background, importance and the calculation process.

In chapter two, an experiment investigating arc behaviour with nitrogen gas flow will be introduced. The arc is sustained by a slowly decreasing, low magnitude direct current, which is supplied by a capacitor bank. The details of the experimental apparatus and calibration of the equipment will be described. Three sets of results with current levels of 100 A, 160 A and 333 A will be given. The experimental results will be compared with the results with SF_6 as the operation gas obtained Weizong using the same experimental apparatus.

Chapter three is focused on the determination of NEC of nitrogen-PTFE plasma under LTE conditions. A modified Gibbs's free energy minimisation method is employed to calculate the equilibrium composition of the gas mixture with different molar percentages of PTFE. A comparison of the NECs with different mole proportions of nitrogen and PTFE at different pressures will be made. The influence of uncertainty in atomic data on the calculated NECs will be studied. The objective of this chapter is to investigate how PTFE vapour affects the NEC of nitrogen arc plasma. Because there is no existing radiation data for nitrogen and PTFE gas mixtures, this work will give an introduction to determining the NEC for this arc plasma mixture.

Chapter four will focus on describing the radiation balance within an arc plasma under LTE conditions. Two approximation methods, the discrete ordinate method (DOM) and P1 approximation, will be introduced in this chapter. The computation of directly solving RTE costs too much in terms of computer resources, so these two methods can reduce the computation cost significantly. However, the drawback of both methods is that it is not as accurate as RTE. The calculation of radiation transfer in the nitrogen arc plasma mixture with PTFE vapour will be done. The objective of this chapter is to find an effective way to obtain the divergence of radiative flux for the nitrogen arc plasma mixture with PTFE. As the radiation results for the nitrogen and PTFE gas mixture are not available in the literature, the results will give researchers an image of the radiation balance in nitrogen and PTFE gas mixture arc plasmas.

Chapter five gives a two-temperature model for calculating species composition, thermodynamic properties and transport coefficients of the nitrogen-PTFE arc plasma under non-LTE conditions. This chapter will focus on an improved version of Godin's method that can be applied under non-LTE conditions. Transport coefficient calculation will be based on the Chapman-Enskog approach. Since the electron and heavy-particles temperature are

different in two-temperature model, the transport coefficients of both kinds of particles are calculated separately with different non-equilibrium degrees $\theta = \frac{T_e}{T_h}$. The influence of the different mole proportions of the PTFE mixture with nitrogen on the thermodynamic properties and transport coefficient at a given pressure will be discussed. The objective of this chapter is to give an image of the different properties of nitrogen and PTFE gas mixtures under LTE and non-LTE conditions. Non-LTE exists in some regions in circuit breakers, and the work on nitrogen arc plasmas in chapter three, four and five will help further the theoretical investigation of high voltage circuit breakers with nitrogen as the cooling gas.

Finally, chapter six, appropriate conclusions are drawn and possible future work discussed.

1.5 References

[1]. H. Davy, *Elements of chemical philosophy*, Vol.1, Smith and Elder, London, 152, (1812).

[2]. M. I. Boulos, P. Fauchais and E. Pfender. *Thermal plasmas fundamentals and applications,* Volume 1, Springer, (1994).

[3]. P. R. Houldcraft, *The importance of laser for cutting and welding*, Welding and Metal Fabrication, 42, N. 9, 1, (1974).

[4]. T. Boniszewski, *Basic fluxes and deoxidation in submerged arc welding of steel,* Metal Construction and British Welding Journal N, 6, 216, (1972).

[5]. Y. Takahashi, K. Fukuta and T. Kaneko, *Plasma treatment for painting of polypropylene bumper*, SAE Technical Paper 850320, (1985).

[6] F. Reif, *Fundamentals of statistical and thermal physics*, McGraw-Hill, (1965).

[7] S. R. Brinkley, *Calculation of the equilibrium composition of systems of many constituents*, J. Chem. Phys. 15, 107, (1947).

[8] W. B. White, S. M. Johnson and G. B. Dantzig, *Chemical equilibrium in complex mixtures*, J. Chem. Phys. 28, 751, (1958).

[9] L. S. Frost and R. W. Liebermann, *Composition and transport properties of SF and their use in a simplified enthalpy flow arc model*, Proc. IEEE, 59, 4, (1971).

[10]. D. Godin and J. Y. Trepanier, *A Robust and efficient method for the computation of equilibrium composition in gaseous mixtures*, Plas. Chem. Plas. Proc., 24, 3, (2004).

[11]. Y. Cressault, A. Gleizes, *Thermal plasma properties for Ar–Al, Ar–Fe and Ar–Cu mixtures used in welding plasmas processes: I. net emission coefficients at atmospheric pressure*, J. Phys. D: Appl. Phys., 46, 415206, (2013).

[12]. M. N. Saha, *LIII. Ionization in the solar chromosphere.* Philosophical Magazine Series 6, 40, 472, (1920).

[13]. M. C. M. van de Sanden, P. P. J. M Schram, A. G. Peeters, J. A. M.van der Mullen, and G. M. W. Kroesen, *Thermodynamic generalization of the Saha equation for a two-temperature plasma*, Phys. Rev. A. 40, 5273, (1989).

[14]. A. V. Potapov, *Chemical equilibrium of multi temperature systems*, High Temp. 4, 48, (1966).

[15]. S. Chapman and T. G. Cowling, *The mathematical theory of non-uniform gases*, Cambridge University Press, (1958).

[16]. J. Hirschfelder, C. F. Curtis and R. B. Bird, *Molecular theory of gases and liquids,* Wiley, (1964).

[17]. L. Spitzer, Jr. and R. Harm, *Transport phenomena in a completely ionized gas*, Phys. Rev. 89, 977, (1953).

[18]. J. N. Butler and R. S. Brokaw, *Thermal conductivity of gas mixtures in chemical equilibrium*, J. Chem. Phys. 26, 1636, (1957).

[19]. R. S. Devoto, *Simplified expressions for the transport properties of ionized monatomic gases*, Phys. Fluids 10, 354, (1967).

[20]. A. B. Murphy, *Thermal plasmas in gas mixtures*, J. Phys. D: Appl. Phys. 34, 151, (2001).

[21]. W. Z. Wang, M. Z. Rong, J. Yan, A. B. Murphy, J. W. Spencer, *Thermophysical properties of nitrogen plasmas under thermal equilibrium and non-equilibrium conditions*, Phys. Plas. 18, 113502, (2011).

[22]. R. W. Liebermann and J. J. Lowke, *Radiation emission coefficients for sulphur hexafluoride arc plasmas*, I. Quont. Spectrosc. Radial. *Transfer,* 16, 253, (1976).

[23]. M. Gongassian, *Etude théorique du rayonnement émis par un plasma d'hexafluorure de soufre*, Ph.D. thesis, University Paul Sabatier, Toulouse, France, (1986).

[24]. L. C. Lee, R. W. Carlson, D. L. Judge and M. Ogawa, *The absorption cross sections of N_2, O_2, CO, NO, CO_2, N_2O, CH_4, C_2H_4, C_2H_6 and C_4H_{10} from 180 to 700 A*, Qwmr. Specrmc. Radiat. Tra., 13, 10234031, (1973).

[25]. R. D. Hudson, *Critical review of ultraviolet photoabsorption cross sections for molecules of astrophysical and aeronomic interest*, Reviews of Geophysics and Space Physics, 9, (1971).

[26]. J. A. Fennelly and D. G. Torr, *Photoionization and photoabsorption cross sections of O, N_2, O_2, and N for aeronomic calculations*, Atomic Data and Nuclear Data Table, 51, 321, (1992).

[27]. E. J. Robinson and S. Geltman, *Single- and double-quantum photodetachment of negative ions*, Physical Review, 153, (1966).

[28]. Y. Itikawa, A. Ichimura, K. Onda, K. Sakimoto AND K. Takayanagi, *Cross sections for collisions of electrons and photos with nitrogen molecules*, J. Chem. Phys. Ref. Data. 15, 985, (1986).

[29]. A. Gleizes, B. Rahmani, J. J. Gonzalez and B. Liani, *Calculation of net emission coefficient in N_2, SF_6 and SF_6-N_2 arc plasmas*, J. Phys. D: Appl. Phys. 24 1300, (1991).

[30]. H. W. Drawin and F. Emard, *Comparative study of existing theories for volume ion-electron recombination in plasmas*, Beitr. Plasmaphysik, 13, 143, (1973).

[31]. S. Franke, R. Methling, D. Uhrlandt, R. Bianchetti, R. Gati and M. Schwinne, *Temperature determination in copper-dominated free-burning arcs*, J. Phys. D: Appl. Phys. 47, 015202, (2014).

[32]. B. Liani, M. Rahmouni, A. H. Belbachir, H. Riad and A. Gleizes, *Temperature determination in copper-dominated free-burning arcs*, J. Phys. D: Appl. Phys. 30, 2964, (1997).

[33]. J. J. Gonzalez, J. B. Belhaouari and A. Gleizes, *Influence of demixing effect on the temperature in wall-stabilized SF_6 arcs*, J. Phys. D: Appl. Phys. 29, 1520, (1996).

[34]. Y. Cressault and A. Gleizes, *Thermal plasma properties for Ar–Al, Ar–Fe and Ar–Cu mixtures used in welding plasmas processes: I. Net emission coefficients at atmospheric pressure*, J. Phys. D: Appl. Phys. 46, 415206, (2013).

[35]. T. Billoux, Y. Cressault, V. F. Boretskij, *Net emission coefficient of CO_2-Cu thermal plasmas: role of copper and molecules*, J. Phys.: Conf. Series, 406, 012027, (2012).

[36]. Y. Naghizadeh-Kashani, Y. Cressault and A. Gleizes, *Net emission coefficient of air thermal plasmas*, J. Phys. D: Appl. Phys. 35, 2925, (2002).

[37]. R. Hannachi, Y. Cressault, Ph. Teulet, Z. B. Lakhdar and A. Gleizes, *Net emission of H_2O–air–$MgCl_2$/$CaCl_2$/NaCl thermal plasmas*, J. Phys. D: Appl. Phys. 41, 205212, (2008).

[38]. H. Z. Randrianandraina, Y. Cressault and A. Gleizes, *Improvements of radiative transfer calculation for SF_6 thermal plasmas*, J. Phys. D: Appl. Phys. 44, 194012, (2011).

[39]. V. G. Sevast'yanenko, *Radiant heat transfer in a real spectrum*, *Hear Tramfir Sov. Res. 9* 36, (1977).

[40]. J. H. Jeans, *The Equations of Radiative Transfer of Energy*, Monthly Notices Roy. Astronom. Soc., 78, 28, (1917).

[41]. V. Kourganoff, *Basic methods in transfer problems*, Dover Publications, New York, (1963).

[42]. M. F. Modest, *Radiative heat transfer*, Academic Press, (2013).

[43]. M. R. J. Charest, C. P. T. Groth, and O. L. G¨ ulder, *Solution of the equation of radiative transfer using a Newton–Krylov approach and adaptive mesh refinement*, J. Comp. Phys. 231, 8, 3023, (2012).

[44]. E. Pfender, *Thermal plasma technology: where do we stand and where are we going?*, Plas. Chem. Plas. Proc. 19, 1, (1999).

[45]. P. Fauchais, *Topical review: understanding plasma spraying*, J. Phys. D: Appl. Phys. 37, 86, (2004).

[46]. P. Fauchais, G. Montavon, M. Vardelle, *Development in direct current plasma spraying*, Cedelle J., Surf Coat Technol, 201, 1908, (2006).

[47]. F. Monerie-Moulin, F. Gitzhofer, P. Fauchais, M. Boulos, *Metals and material society*, Warrendale, 125, (1992).

[48]. S. Ghorui, J. Heberlein, E. Pfender, *Thermodynamic and transport properties of two-temperature oxygen plasmas*, J. Phys. D: Appl. Phys. 40, 1966, (2007).

[49]. K. Yun, S. Weissman, *High-temperature transport properties of dissociating nitrogen and dissociating oxygen*, Mason E., Phys. Fluids, 5, 672, (1962).

[50]. F. A. Guevara, B. B. Mclnteer, W. Wageman, *High temperature viscosity ratios for hydrogen, helium, argon, and nitrogen*, Phys. Fluids, 12, 2493, (1969).

[51]. N. Tsitelauri, *Candidate's dissertation*. ENIN Academy of the Sciences of the USSR, (1969).

[52]. W. Hermann, E. Schade, *Transportfunktionen von sticksoff bis 26000 K,* Zeitschrift für Physik A Hadrons and nuclei, 233, 333, (1970).

[53]. U. Plantikow, *Bestimmung von transportkoeffizienten des stickstoffs bis 13 000 K*, Zeitschrift für Physik A Hadrons and nuclei, 237, 388, (1970).

[54]. E. Asinovsky, A. Kirillin, E. Pakhomov, V. Shabashov, *Experimental investigation of transport properties of low-temperature plasma by means of electric arc*, Proc. IEEE, 59, 592, (1971).

[55]. M. Capitelli, R. Devoto, *Transport coefficients of high-temperature nitrogen*, Phys. Fluids, 16, 1835, (1973).

[56]. A. Neuberger, *Composition, electrical conductivity, and total radiation of nitrogen plasma*, AIAA J. 13, 3, (1975).

[57]. M. Capitelli, C. Gorse, P. Fauchais, *Transport coefficients of high temperature N_2-H_2 mixtures*, J. Phys. 38, 653, (1977).

[58]. A. B. Murphy, C. Arundell, *Transport coefficients of argon, nitrogen, oxygen, argon-nitrogen, and argon-oxygen plasmas*, Chem. Plas. Proc. 14, 451, (1994).

[59]. A. B. Murphy, *Chemical physics of low-temperature plasmas*, Chem. Phys. 398, 64, (2012).

[60]. M. Boulos, P. Fauchais, E. Pfender, *Thermal plasmas fundamentals and applications*, vol 1. Plenum Press, New York, (1994).

[61]. V. Colombo, E. Ghedini, P. Sanibondi, *Thermodynamic and transport properties in non-equilibrium argon, oxygen and nitrogen thermal plasmas*, Prog Nucl Energy 50, 921, (2008).

[62]. S. Ghorui, A. K. Das, *Collision integrals for charged-charged interaction in two-temperature non-equilibrium plasma*, Phys. Plas. 20, 093504, (2013).

[63]. K. C. Meher, N. Tiwari, S. Ghorui, A. K. Das, *Multi-component diffusion coefficients in nitrogen plasma under thermal equilibrium and non-equilibrium conditions*, Plas. Chem. Plas. Proc. 34, 949, (2014).

Chapter 2 Introduction of experimental investigation of nozzle arc behaviour with super-fast nitrogen gas flow

2.1 Introduction

Current interruption is the main function of a high voltage circuit breaker. It is related to the physical phenomena of an electric arc. The separation of two electrodes leads to an electric arc discharging between them. The gas around the arc is ionized to plasma due to energy released by the arc discharging and then returning to the insulating gas. The energy transferring from the arc core to the surrounding area determines the performance of the electrical arc. The ability of the interrupting current in a short period is a sign of the capability of the circuit breaker. One of the most important theoretical aspects of investigating arc behaviour is to determine the radiation properties, thermodynamic properties and transport coefficients which will be introduced in subsequent chapters. However, experimental work for investigating arc behaviour cannot be neglected.

Many experimental investigations have been published indicating methods of data measurement, such as arc voltage across the electrode, current through the arc and arc resistance. An experiment for investigating the dynamic characteristics of nitrogen arcs in a super-fast nozzle is presented in this chapter.

2.2 Experimental apparatus

The arcing chamber

Fig. 2-1 shows the assembly of the experimental equipment, including the solenoid driving mechanism, movable contact, arcing chamber, observation

windows and connecting pipe. The arcing chamber is designed to measure physical properties, such as gas pressure, and electrical properties such as arcing voltage and current. Because the arcing chamber is airproofed, there are four watching windows installed. The connecting pipe connects the gas tank and the arcing chamber; it is a tube that transfers the gas flow from the gas tank to the nozzle. The diameter of the connecting pipe is 38 mm and its length is 150 mm. The solenoid driver is placed above the arcing chamber. The solenoid driving mechanism provides the power for the movable contact to separate from the static contact. Fig. 2-2 shows the structure of the system.

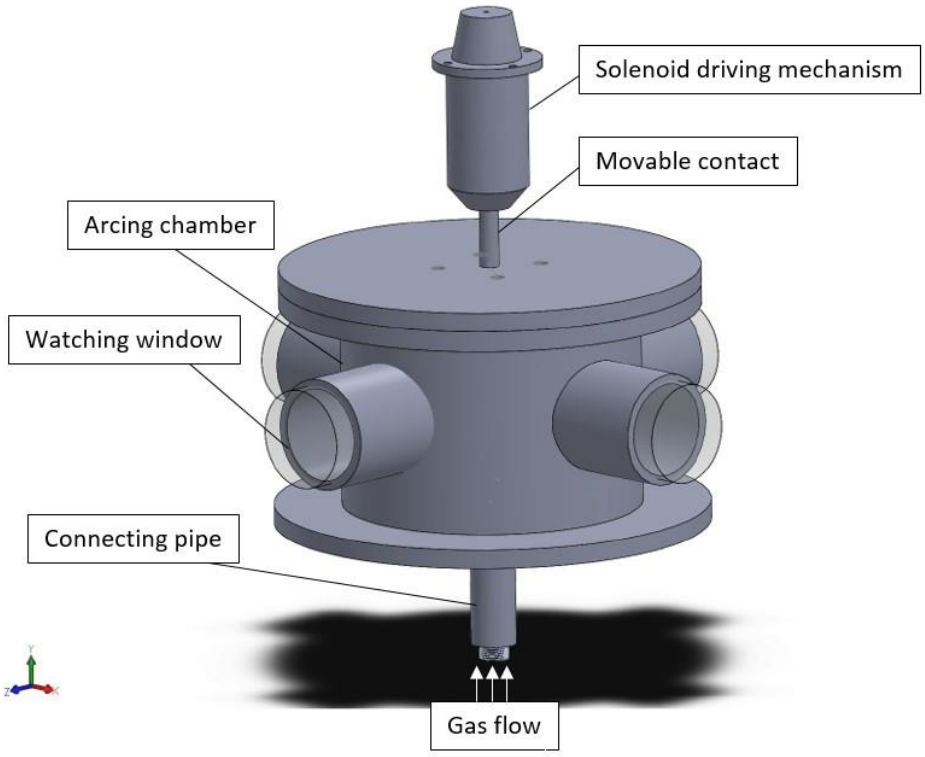

Fig. 2-1: Top view of main experiment equipment

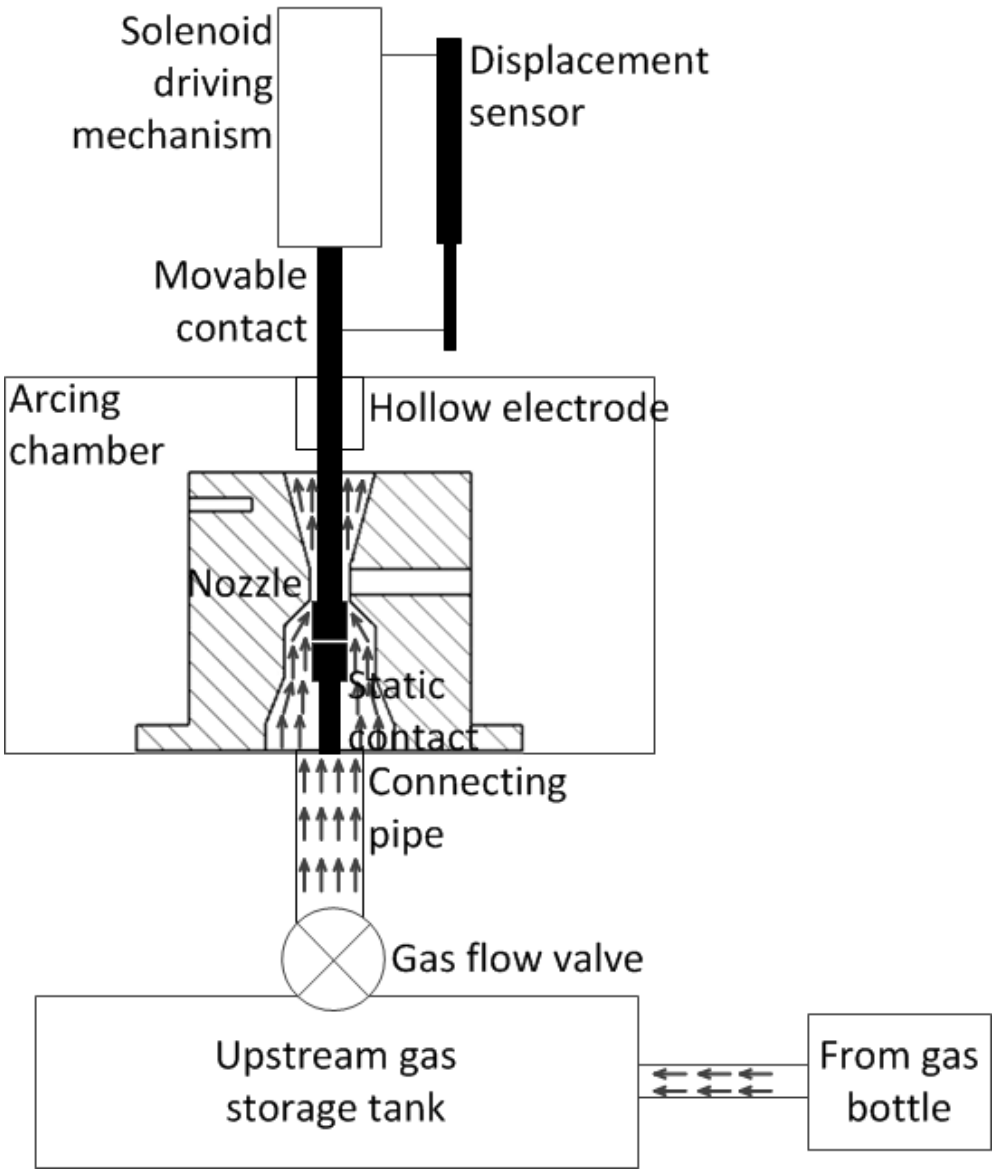

Fig. 2-2: Diagram showing the structure of a two-pressure gas flow system

The electrodes are placed at the terminal of movable contact and static contact. The contact rod is made of zinc. The electrodes are composed of 80% copper and 20% tungsten in a cylinder shape with diameter of 10 mm and length of 15 mm. During the arc processing, the movable contact is powered by the solenoid driving mechanism and the two electrodes are separated by 60 mm in 60 ms after the movable contact starts to move. The anode is connected to the

static contact and is fed via a high voltage cable from the power bank. It should be noted that the connecting pipe feeds the chamber from a PTFE nozzle. The experimental earth is the reference. It is connected with the arcing chamber which has same electrical potential with moving contact. The fixed hollow contact is introduced in order to ensure that the arc has a fixed length in each experiment. The displacement sensor is used to monitor the movement of the movable contact versus time.

The nozzle is made of PTFE (polytetrafluoroethylene, C_2F_4) whose vapour has good insulation compared to other materials. During the electric arc processing, the temperature of the nozzle surface is so high, that it generates PTFE vapour.

Fig. 2-3 shows that the diameter of the nozzle throat is 12.5 mm with length of 10 mm. As mentioned above, the diameter of the electrode is 10 mm and, there is a 1.25 mm thick space between the electrode and the nozzle.

Power bank

Fig. 2-4 shows the supplier of the electric arc, which consists of a series of capacitors, ignitrons, resistors and inductors. The control unit is used to synchronize activation of ignitrons to generate the current wave for the electric arc. The capacitance of the capacitor is 33 mF. There is an inductor with 184 μH inductance. The 0.9 $m\Omega$ resistor is a shunt resistor.

At the beginning of experiment, the capacitors will be charged. The energy stored in the capacitors can be adjusted by the control unit. Before the power bank discharges, all five ignitrons are disabled which keeps the circuit open. When ignitron one is fired and an electrode gap is generated by separating the two electrodes, it will produce a pseudo-DC arc across the electrode gap.

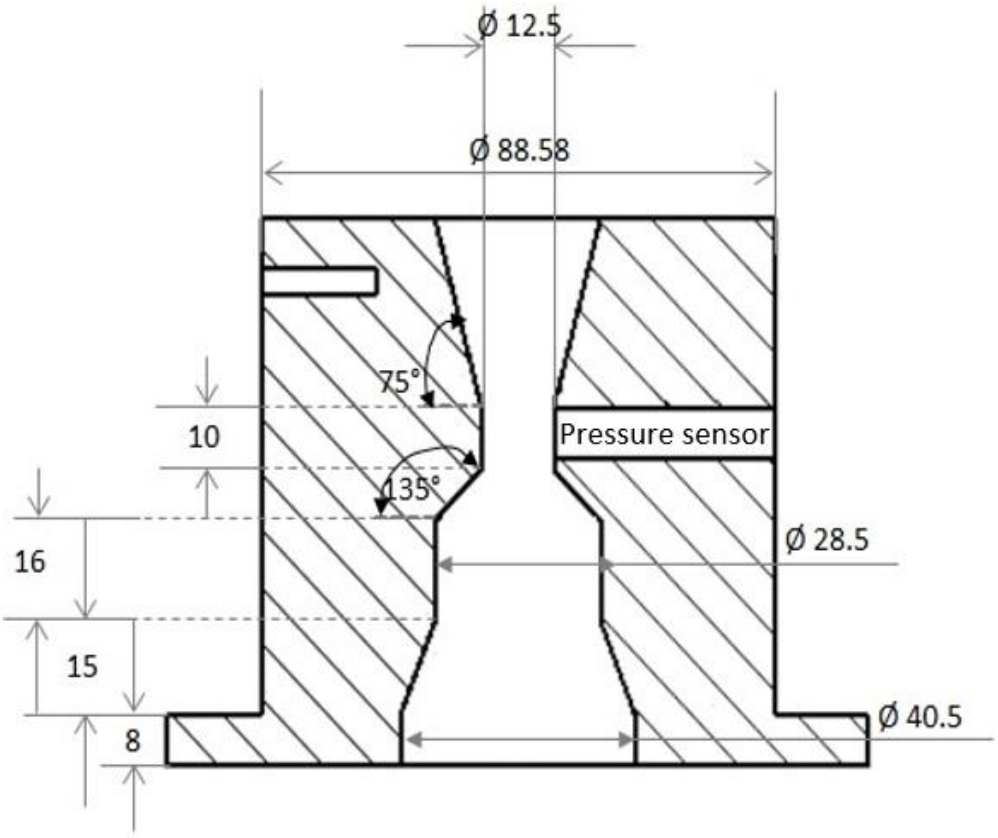

Fig. 2-3: Geometry of arc nozzle with dimension (unit: mm)

Depending on the duration of the DC arc, it costs about 30-50% of the total energy stored in the capacitor. Following the configuration of control unit, the second step is to activate ignitrons two and three. Once those two are fired, the rest of the energy stored in the capacitors will be released immediately. It will generate a sinewave but with a 60% reduction from each previous half cycle. However, in this experiment, the arc is always extinguished in the first half cycle at the first current-zero position. Once the arc is extinguished, the third step is fire ignitrons four and five, which sends the energy remaining in the capacitor to ground so that the energy is safely disposed of.

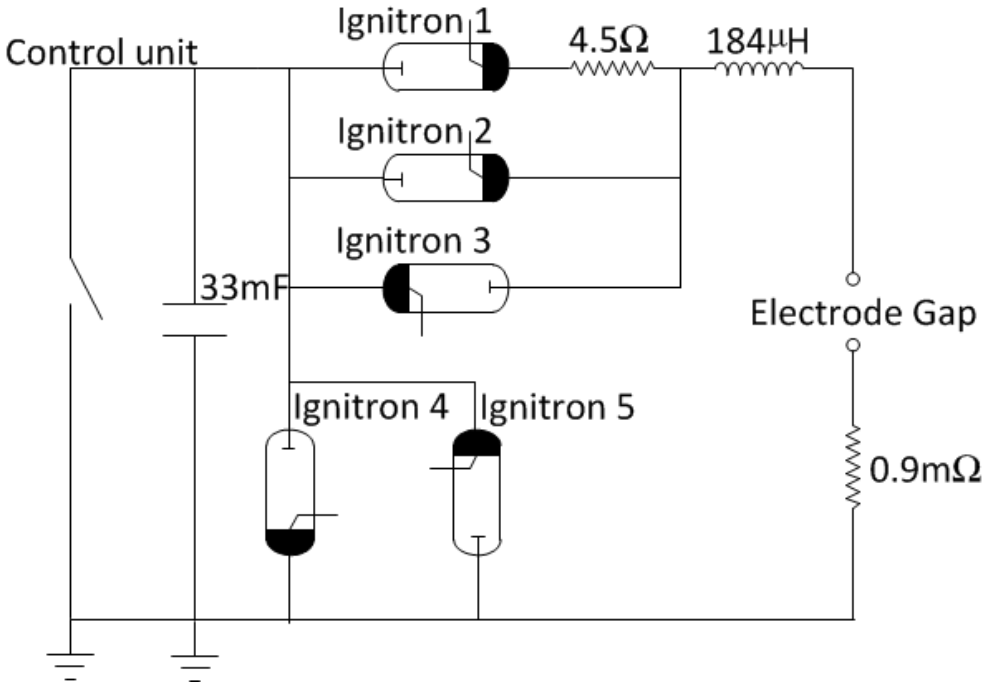

Fig. 2-4: Schematic diagram of the power supply

Gas supply equipment

The 20 L gas tank of is placed below the connecting pipe with an SMC VXZ2360-10F-5D1 valve to control the gas flows into the nozzle. The control circuit has been designed to control the valve opening time, which can be triggered by a signal from the control unit.

Synchronisation of control unit

The control unit generates the trigger signals for all the equipment. This trigger signal is a pulse signal emanated by the control unit with a magnitude of 200 volts and duration of 1μs. As mentioned above, the sequence of each trigger signal is set up by the control unit in order to initiate an electric arc and activate the measurement equipment to record the experimental data at the appropriate proper time. There is a delay in the trigger signal emanated from the control unit, which is about 25 ms.

2.2.1 Calibration of equipment

Current and voltage measurement probe

It has been shown that the electrical characteristics of an arc determine the efficiency of arc extinguishing. The voltage measurement in this experiment is achieved using a Tektronix P6015A passive high voltage probe with a compensation box of 7-49 pF range. In order to safely measure using an oscilloscope, 1000 times attenuation of the probe results in the data input to the oscilloscope being 1/1000 of the real volts. The measurement data can be converted to its real value by setting up the oscilloscope.

Pressure sensor

The gas flow is always used in circuit breakers to help cool down the arc. The pressure change is usually an important characteristic that affects the behaviour of the arc and the properties of the arc plasma. The pressure sensor used in this experiment is a Kistler 601A. The sensor utilises the piezoelectric effect of a quartz crystal. The sensor generates a small current signal; when the pressure on the sensor changes, the current will change as well. Thus, a charge amplifier is used to convert this small current signal to a proportional voltage signal that can be monitored by oscilloscope. The type of charge amplifier used is a Kistler 5001 and the oscilloscope type is a Tektronix 2230.

Displacement sensor

The displacement sensor is used to record the position of the movable electrode during the experiment. Because the distance between the movable electrode and the static electrode determines the arc length, this is one of the most important factors that decides the arc behaviour.

The sensor is a Honeywell linear displacement sensor, which can transform a mechanical linear displacement signal to an electrical signal. The principle of the sensor is a wiper attached to an operating shaft. The wiper is connected to

a conductive track and when the shaft is moved, the resistance will change as well. Moreover, the resistance is proportional to the displacement of the shaft.

2.3 Experimental investigation results

The upstream gas tank has an initial pressure of 10 bar at room temperature. It provides the nitrogen gas flow. The pressure of downstream exhaust space is fixed at 1 bar. The voltage changes across the electrodes and the position of rod electrode tip as a function of time is recoded for three capacitor bank charging voltages of 450 V (Case 1,Fig. 2-6), 720 V (Case 2,Fig. 2-7) and 1500 V (Case 3,Fig. 2-8). The measure of each case is taken for two scenarios, one with the valve shut and the other opened at a specified instant. Odd numbered curves (1 and 3) indicate arc with gas flow while even numbered curves indicate arc without gas flow.

In Fig. 2-6, the current starts from 80 A for both scenarios. The rate of decreasing is at 0.64 A/ms. It is a result of power consumption in the circuit, especially in the resistor. At 93 ms and 100 ms, the electrode separation starts respectively. It can be found that in both scenarios, the sudden increase of voltage across the electrodes is from 2.69 V to 22.91 V for the arc with the valve opened later while the current has a drop of 4.39 A. The resistance can be calculated when the arc voltage is 2.69 V and arc current 71.65 A, which is 37.54 mΩ. It is dominated by the electrode contact resistance between the two electrode surfaces. The pressure in scenario one has a drop when the arc starts, the reason is the arc consume the gas in nozzle but gas flow hasn't yet reach nozzle. Once the gas flow reach nozzle, the pressure is recovered. With the steady gas flow, the nozzle pressure can reach 2.6 bar. While the pressure data of scenario two indicates the free-burning arc consume the gas in nozzle, after the arc extinguished, the pressure is recovered.

When an arc is struck between the two electrodes, this electrode contact resistance is replaced by the electrode sheath layers. Therefore, the value of 22.91 V is the sum of the anode and cathode sheath drops at a current of 71.65 A without externally forced gas flow because the valve only starts to open at 100 ms. The voltage of the arc column should therefore be derived by taking the initial voltage rise at electrode separation from the recorded voltage.

In contrast with the measurement with the valve opened at 100 ms, the arc without forced gas flow continues to burn beyond 150 ms. Because the rod electrode in this scenario starts to move at 98 ms, its arc length is smaller (middle diagram of Fig. 2-6) and convection cooling is weaker in comparison to the scenario where the valve is opened. This gives a lower arc resistance, which explains the higher arc current and lower arc voltage for this scenario, as clearly shown in Fig. 2-6.

The arc current starts to decrease rapidly at 134 ms with an instantaneous value of 37.87 A in the forced gas flow scenario and extinguishes at 135 ms, as a result of the capacitor bank being no longer able to sustain the arc at a current of 37.87 A (curve 1 in Fig. 2-6). The arc takes 1 ms to extinct. The voltage across the electrodes increases rapidly and reaches the voltage of the capacitor bank (275 V) when the current ceases to flow.

Case 2 follows a similar pattern to Case 1. The current starts at a value of 160 A. Electrode separation takes place at 95ms and 105 ms for the two scenarios. Because of the increased initial current, the sudden current drop corresponding to electrode separation is no longer apparent and the power consumption in the arc column is negligible. The voltages cross the electrodes at their separation are respectively 2.23 V and 2.18 V. The arc starts to extinguish at 136 ms with a current of 69.53 A.

The starting current in Case 3 is much higher than the other two cases with a value of 330 A at 50 ms (Fig. 2-8). The increases in voltage across the electrodes corresponding to electrode separation are respectively from 2.5 V to 22.44 V and from 1.4 V to 17.2 V for the two scenarios with and without the valve opened. The arc current and voltage behave differently at the stage when gas flow is established. There are two distinct voltage increases starting at 117 ms and 134 ms, respectively. The valve in this case is scheduled to open at 100 ms with a full opening time of 25 ms. The first voltage increase is expected to be the effect of arc confinement by gas flow from the tank following the opening of the valve. The effect is modest because the rod electrode still blocks the nozzle and gas can only exhaust into the downstream space through the gap between the rod electrode and the nozzle throat with a thickness of 1.25 mm. The second increase of nearly 100 V is a consequence of the rod electrode clearing the nozzle throat and the establishment of high speed gas flow. The flow leads to enhanced arc cooling and increases the arc resistance.

Corresponding to the voltage climbing, there is an apparent drop in arc current. Despite the increased travel speed of the rod electrode, the arc voltage and current after 138 ms experiences a temporary change in the opposite direction. This is believed to be caused by the rapid change of flow field downstream the nozzle throat when the rod electrode continues to move away from the nozzle throat and causes the arc resistance to increase. It is highly likely that a shock is formed in the diverging section of the nozzle causing broadening of the arc column[1].

The arc current starts to decrease again from 141 ms with a rate of 1.54 A/ms until 149 ms when the current with an instantaneous value of 149.8 A begins a rapid drop at a rate of 37.63 A/ms leading to arc extinction at 152 ms. The corresponding rate of increase of voltage between 149 ms and 153 ms is approximately 217.9 V/ms. There are voltage fluctuations immediately before

arc extinction due to possible instability of the arc column. The electrode gap length varies from 26.17 mm to 37.62 mm over the period of 141 ms to 149 ms. The arc with no forced flow continues to burn beyond 160 ms. The arc voltage varies between 130.2 V at 141 ms and 134.7 V at 149ms. A more complete picture of the arcing process is given in Fig. 2-8 where the electrode movement is also given.

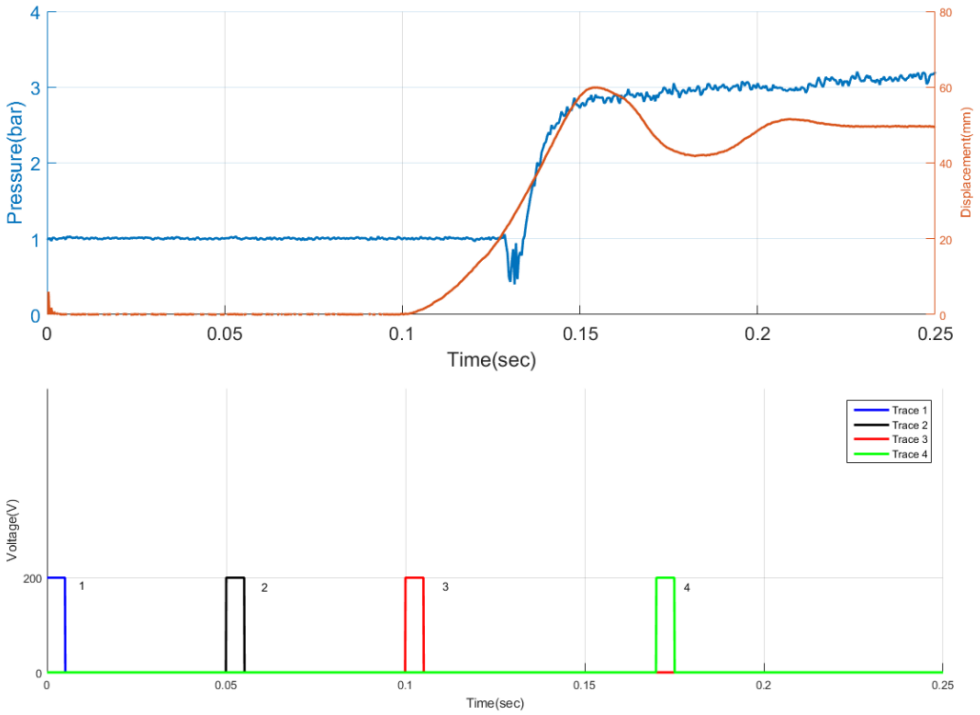

Fig. 2-5: Electrode travel curve (top) and sequence of triggering pulses (bottom) for different parts of the system. Curve (top): 1-Pressure in throat. 2-displacement sensor. Curve (bottom): 1-Oscilloscope. 2-DC current. 3-Gas flow valve. 4-Main current

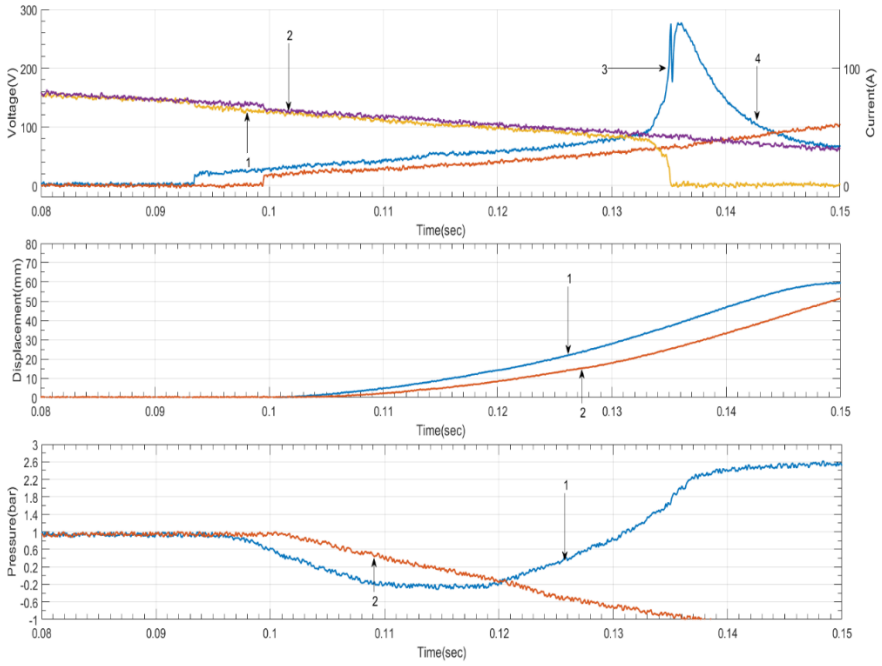

Fig. 2-6: Arc voltage and current with/without gas flow for a charging voltage of 450 V. Curves 1 and 3 are arc current and voltage respectively with nitrogen gas flow. Curves 2 and 4 are arc current and voltage respectively without nitrogen gas flow (keys also apply to other figures).

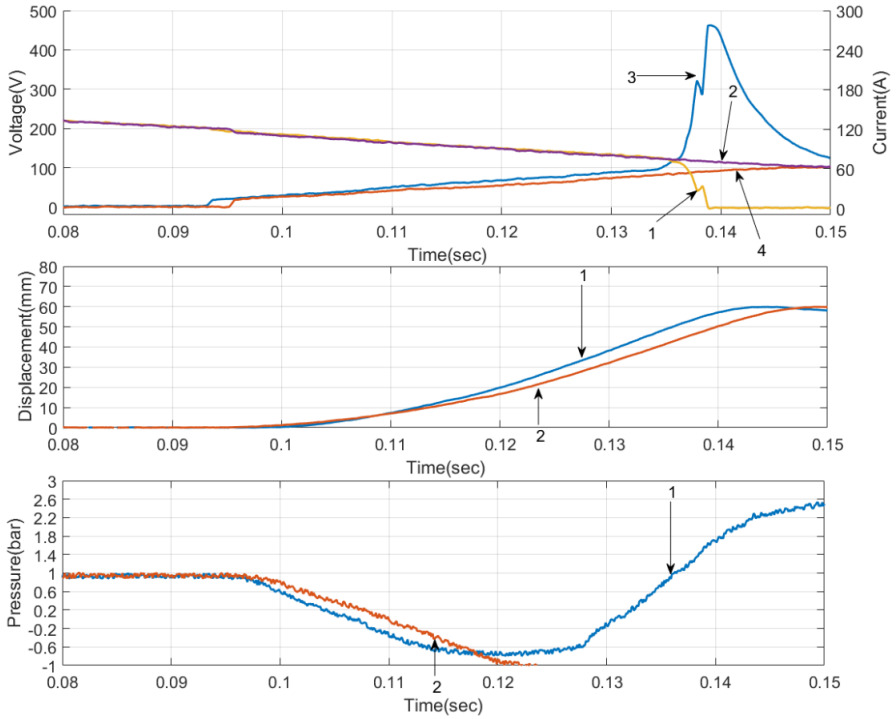

Fig. 2-7: Voltage and current records for a capacitor bank discharging voltage of 750 V

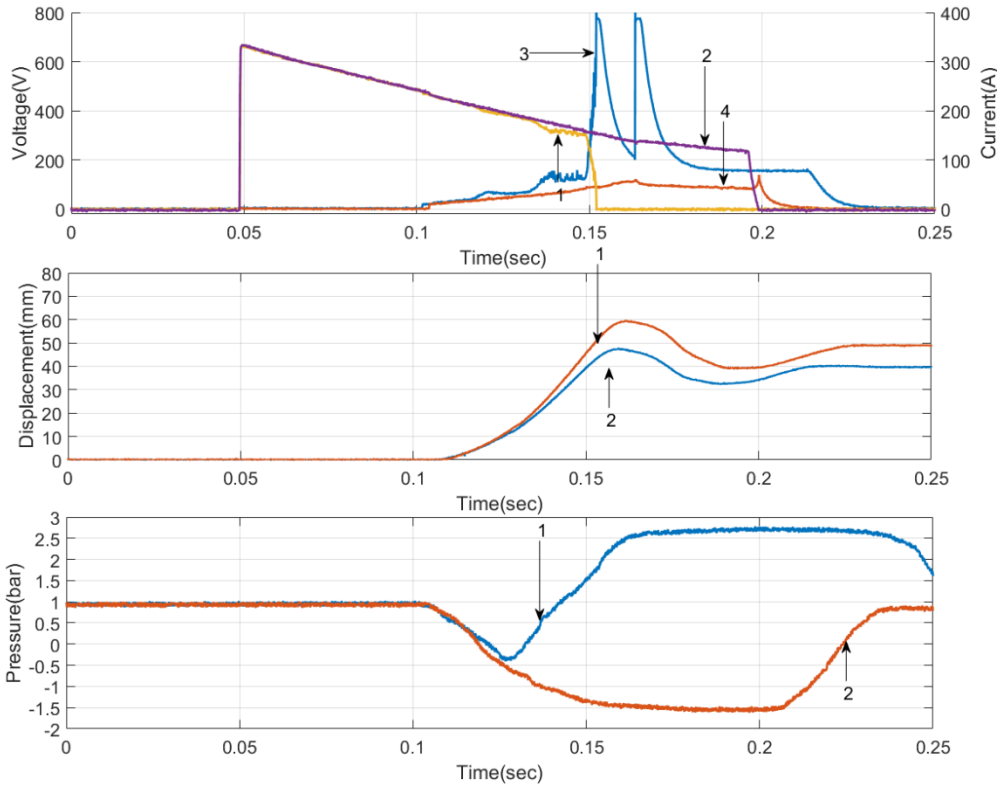

Fig. 2-8: Voltage and current records for a capacitor bank charging voltage of 1500 V.

2.3.1 Influence of a different operational gas

Experiment with SF_6 as operational gas have been taken place to justify the capability of extinguishing electric arc by nitrogen. The experiment has been done at same experimental apparatus. Fig. 2-9 and Fig. 2-10 show the current interrupting capability by using three different gas: SF_6, N_2 and CO_2. SF_6 has the best performance on current interrupting in circuit breaker. By comparing with three different operation gas, the capability of interrupting current flow by N_2 and SF_6 is closed to each other while CO_2 is much poorer than those two gases. The voltage extinction peak of SF_6 and N_2 are higher than CO_2 due to the fast rising arc resistance.

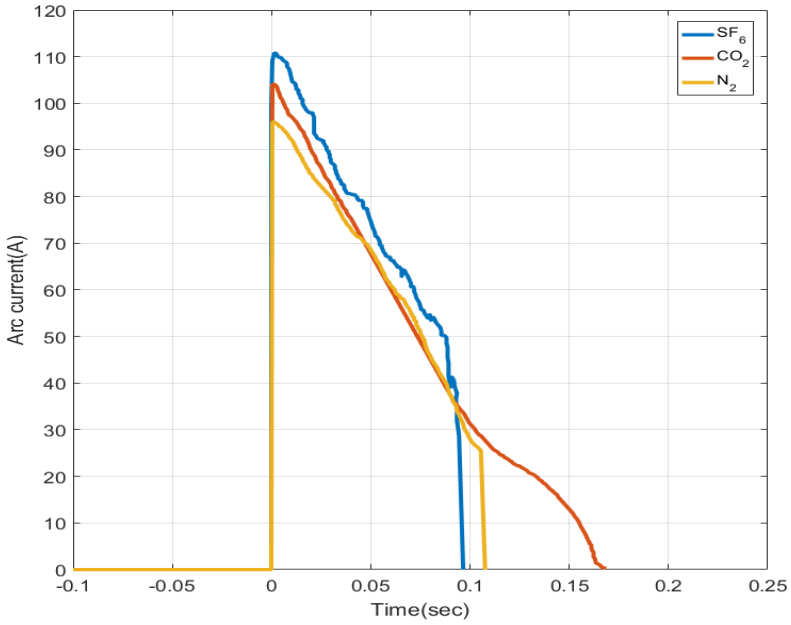

Fig. 2-9: Electric arc current with gas flow: SF_6, CO_2, N_2

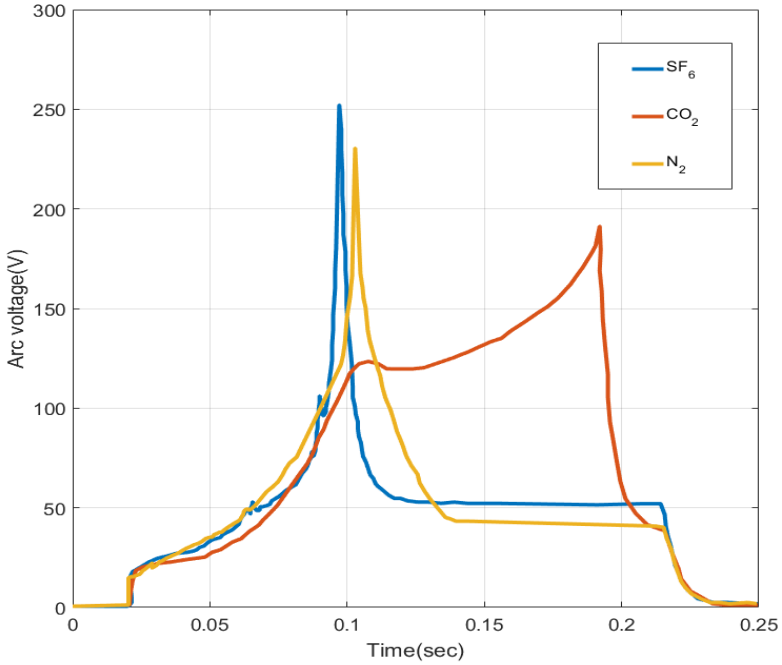

Fig. 2-10: Electric arc voltage with gas flow: SF_6, CO_2, N_2

2.4 Summary

An experimental investigation of arc behaviour with nitrogen gas flow was carried out. The arc is sustained by a slowly decreasing low direct current from a capacitor bank. Two temperature system is designed to provide gas flow. The current and voltage cross electrodes were measured for the arc with three initial currents: 80 A, 130 A and 333 A. It was observed that with gas flow the arc is easier to extinguish while without gas it lasts for a longer time. Some improvements to the experiment can be made in the future, such as by adding more pressure monitors and using a higher initial current across the electrodes when starting the arc. By comparing the arcing behaviour with different gases, nitrogen shows good capability to interrupt the current flow.

2.5 References

[1]. J. D. Yan, M. T. C. Fang, *Electrical and aerodynamic behaviour of arcs under shock conditions*, IEEE Trans. On Plas. Sci. 25, 840, (1997).

Chapter 3 Radiation transfer calculation based on net emission coefficient for N_2-PTFE plasma

3.1 Introduction

Radiative transfer inside and around a high temperature thermal plasma is an important energy transfer mechanism. It heavily influences the arc behaviour in a high voltage circuit breaker[1]. However, the radiative flux does not obey blackbody laws based on complete thermal equilibrium (CTE). One of the reasons is that plasma temperature changes along with space, and the second reason is that this space is limited. Local thermal equilibrium (LTE) is usually assumed for atmospheric arc plasma. In LTE, particles are allowed to achieve thermal equilibrium due to the local gradients of plasma properties being small enough. In recent years, research on thermal plasmas has primarily been driven by potential industrial applications and by the ever-increasing demand for existing plasma technology.[2,3,4,5,6,7,8]

To understand the processes involved in thermal plasmas that stem from arc discharge, numerical modelling of arc behaviour is commonly used. It requires the inclusion of radiation transfer in energy equations based on the radiation transfer equation (RTE). Due to the complexity of the absorption spectra of ionised gas, directly solving the RTE is computationally expensive[9]. The concept of net emission coefficient (NEC) was firstly introduced by Lowke.[10,11] It greatly simplified radiation transfer calculation, thus making numerical modelling much more applicable to industrial applications[12]. An electric arc can be divided into three regions based on the typical temperature profile. Fig. 3-1 shows a typical temperature profile in an electric arc. Region one is the core region. In

this region, because the temperature is normally higher than 25,000 K and there is a low gradient within this region, plasma reabsorption can be neglected. Thus, radiation within this region can be treated as pure emission radiation.

The net emission coefficient, which corresponds to the local radiative power, takes into account both the emission and the self-absorption in the plasma. This limits the application of NEC so that it can be only applied in the arc core region.

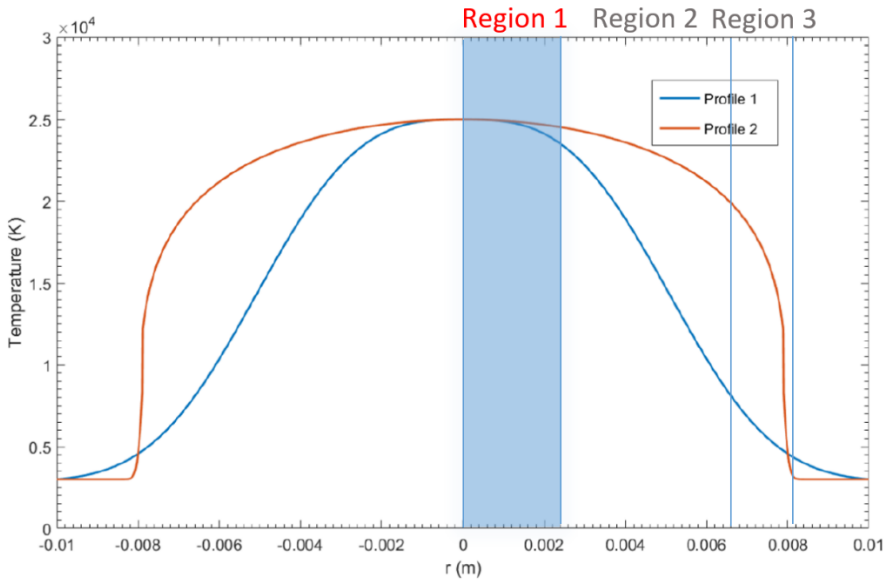

Fig. 3-1: Typical temperature profile of electric arc

In this chapter, a method of NEC calculation for N_2-PTFE under LTE conditions will be introduced in detail. The calculation includes the following:

1. Equilibrium composition of species in N_2-PTFE plasma
2. Line and continuum radiation due to different mechanisms of particle transition
3. The absorption coefficient as a function of frequency at a specific temperature
4. The NEC of N_2-PTFE plasma

The calculation focuses on N_2-PTFE gas mixtures with different initial molar proportions and pressures. The calculation is performed by an in-house program written in C++.

There is no NEC data for N_2-PTFE gas mixtures so a comparison of the NEC of pure nitrogen plasma obtained in the present work with published results will be carried out. A study on the influence analyse of basic atomic data on the NEC will be also conducted to analyse the reliability of the data.

3.2 Methodology of NEC calculation for N_2-PTFE plasma

3.2.1 Method for the determination of plasma composition

The radiation emission characteristics and transport properties of a thermal plasma depend on the species and their concentrations. Thus, the first step of calculation is to obtain the number density of each species. In this chapter, a robust and efficient method from Godin and Trepanier[13] is used to calculate the equilibrium composition of the plasma. Certain previously developed equations can effectively describe the equilibrium composition that derived by Gibbs[14]. Under thermal equilibrium temperature and pressure are to be given to solve a system of nonlinear equations. Chemical equilibrium condition is achieved by the minimisation of a thermodynamic potential. Gibbs free energy $\Delta \mathrm{G}$ is one of the thermodynamic potentials that describes enthalpy difference between a system or a reaction and product at a constant temperature and pressure. The minimised of Gibbs free energy is an indicator of system reaching chemical equilibrium. The minimisation of Gibbs free energy can be expressed according to the Gibbs-Duhem relationship:

$$\Delta \mathrm{G} = \sum_{a} \mu_a dN_a = 0 \qquad (3.1)$$

where μ_a is chemical potential and N_a is population of particle a.

For example, the dissociation of C_2F_4into C_2F_2 and the fluorine atom ($C_2F_4 \Leftrightarrow C_2F_2 + 2F$) in symbolisation. It can be presented as:

$$\sum_{a}^{species} c_a A_a = 0 \qquad (3.2)$$

where the parameter can be specified as:

$$A_a = \{C_2F_4, C_2F_2, F\}$$

$$c_a = \{1, -1, -2\}$$

where c_a is the coefficient of reactants and products in the dissociation reaction.

Chemical potential μ_a can be derived from the partition function:

$$\mu_a = -kTln(\frac{Q_a}{n_a}) \qquad (3.3)$$

where *Q* and *n* are, respectively, the partition function per unit volume and the number density of specie a. T is the temperature in [K].

In terms of the equations associated with the mass action law, the primary equations are as follows:

$$\prod_{a}^{species} n_a^{c_a} = \prod_{a}^{species} Q_a^{c_a} \qquad (3.4)$$

The calculations are represented in a wide pressure range (1 atmosphere to 100 atmospheres) and temperature range (from 300 K to 30 000 K). A total of 34 species are taken into account in the calculation of the plasma composition.

e^-, N^+, CN, C_2F_2, N_2, C_2, F_2, N ,N^{2+},N^{3+},F , F^+ , F^{2+} , F^{3+} , F^{4+} , C , C^+ , C^{2+}, C^{3+}, C_2F_4, C_2F_6, CF_2, CF_3, C_2F_3N, CF_4 , CN^-, $CN_2(CNN)$, $CN_2(NCN)$, CF, C_3, C_2N_2, FN, C_2N, C_4N_2.

According to Godin's method, a concept of chemical basis has been defined. It is denoted by z containing the M chemical basis and by z^*, the subset of the other N-M species not belonging to it. In this calculation, there are 4 chemical bases and the remaining 30 species are listed below:

z = {e^-, N^+, CN, C_2F_2}

z*={N_2, C_2, F_2, N ,N^{2+},N^{3+},F , F^+ , F^{2+} , F^{3+} , F^{4+} , C , C^+ , C^{2+} , C^{3+} , C_2F_4 , C_2F_6, CF_2 , CF_3 , C_2F_3N , CF_4 , CN^- , $CN_2(CNN)$, $CN_2(NCN)$, CF, C_3 C_2N_2 , FN, C_2N, C_4N_2}

$$\left\{ n_{z_j^*} = Q_{z_j^*} \prod_{i=1}^{M} \left(\frac{n_{z_i}}{Q_{z_i}}\right)^{c_{j,i}} \right\}_{j=1}^{N-M} \quad (3.5)$$

Eq.(3.5) shows an expression that use number density of chemical basis and partition function to express number density of particle in z*. In the equation, Q is the partition function of species z or z^*, c is the coefficient related to the chemical basis which is listed below:

Species are set as the chemical basis in consideration of the number of chemical elements present in the plasma and the charge (N, C, F, and charge). Therefore, the remaining 22 species are set as chemical species and mass action law is applied. The principles of conservation of atomic nucleus, electrical neutrality and ideal gas law are used to obtain a system of plasma. A total of 26 equations are obtained, which include two equations for conservation of nuclei (ratio of C:F in PTFE + N:F between PTFE and N_2), one equation for charge neutrality, one from the ideal gas law and another 22 equations describing the mass action law for the 22 chemical species.

Table 3-1: Coefficient c of each chemical species

Coefficient c					
		z_i			
		e^-	N^+	CN	C_2F_2
z_j^*	N_2	2	2	0	0
	C_2	-2	-2	2	0
	F_2	2	2	-2	1
	N	1	1	0	0
	N^{2+}	-1	1	0	0
	N^{3+}	-2	1	0	0
	F	1	1	-1	0.5
	F^+	0	1	-1	0.5
	F^{2+}	-1	1	-1	0.5
	F^{3+}	-2	1	-1	0.5
	F^{4+}	-3	1	-1	0.5
	C	-1	-1	1	0
	C^+	-2	-1	1	0
	C^{2+}	-3	-1	1	0
	C^{3+}	-4	-1	1	0
	C_2F_4	2	2	-2	2
	CF_2	1	1	-1	1
	CF_3	2	2	-2	1.5
	C_2F_3N	2	2	-1	1.5
	CF_4	3	3	-3	2
	C_2N_2	0	0	2	0
	FN	2	2	-1	0.5

These equations are solved using the Newton-Raphson method to obtain the number density of all 26 species. Logarithm was taken on both sides of the

chemical species equations, which results in 22 linear equations and greatly simplifies the calculation. The linear equations are then substituted in the base equations to reduce the number of unknowns to only 4. This gives a smaller size of the Jacob matrix in the solution procedure using the Newton-Raphson Method, which substantially promotes the convergence of the calculation.

3.2.2 Partition function

Partition function in this thesis is related to a function of describing the distribution of electrons on different energy level. A total partition function of a species i is written as

$$\mathrm{Q}_i^{total} = Q_i^{trans} \times Q_i^{int} \times Q_i^{reac} \tag{3.6}$$

Q_i^{trans}, Q_i^{int}, Q_i^{reac} are translational, internal and reaction partition function respectively.

The translational partition function of species i can be expressed below:

$$\mathrm{Q}_i^{trans} = \left(\frac{2\pi m_i k T_i}{h^2}\right)^{3/2} V \tag{3.7}$$

where V is the volume and T_i is the temperature of particle i, k and h are Boltzmann constant and Planck constant respectively. m_i is the mass of particle i. According to the element number, particles can be divided as: monatomic, diatomic and polyatomic species.

Monatomic species

Monatomic species usually dominate the plasma composition when the temperature is higher than 10,000 K. The partition function of a monatomic species consists of electronic energy that can be expressed as:

$$\mathrm{Q}_i^{total} = \frac{V}{h^3}(2\pi mkT)^{3/2} \cdot Q_{int} \cdot Q_{reac} \quad (3.8)$$

The internal partition function of specie i can be expressed below:

$$Q_{int} = Q_{ele} = \sum_j^{\varepsilon_I} g_{e,j}\exp(-\frac{\varepsilon_j}{kT}) \quad (3.9)$$

Where ε_I is the ionization energy, $g_{e,j}$ is the statistical weight. The internal partition function of monatomic specie is its electron partition function Q_{ele}.

$$Q_{reac} = \exp(\frac{-E_{reac}}{kT}) \quad (3.10)$$

Q_{reac} represents reaction partition function, E_{reac} is the energy which depends on the reaction for generating the specie.

Two tables are shown in Table 3-2 describes all chemical reactions at equilibrium. There are 26 ionization and dissociation reactions are taken in account.

Table 3-3 lists the reference energy of all species which is obtained by energy balance of reaction. The partition function of monatomic species is calculated by summation over all energy level is below the ionization limit. However, the number of energy levels is infinite as gap between the high energy levels becomes smaller and smaller, so the calculation involving high energy levels can be replaced by an integral.

Table 3-2: Chemical reactions in the calculation

Chemical reactions in the calculation			
No.	Chemical reaction	No.	Chemical reaction
1	$N_2 \leftrightarrow N + N$	12	$F \leftrightarrow F^+ + e^-$
2	$N \leftrightarrow N^+ + e^-$	13	$F^+ \leftrightarrow F^{2+} + e^-$
3	$N^+ \leftrightarrow N^{2+} + e^-$	14	$F^{2+} \leftrightarrow F^{3+} + e^-$
4	$N^{2+} \leftrightarrow N^{3+} + e^-$	15	$F^{3+} \leftrightarrow F^{4+} + e^-$
5	$C_2F_4 \leftrightarrow C_2F_2 + F_2$	16	$C \leftrightarrow C^+ + e^-$
6	$C_2F_2 \leftrightarrow C_2 + F_2$	17	$C^+ \leftrightarrow C^{2+} + e^-$
7	$F_2 \leftrightarrow F + F$	18	$C^{2+} \leftrightarrow C^{3+} + e^-$
8	$C_2 \leftrightarrow C + C$	19	$C^{3+} \leftrightarrow C^{4+} + e^-$
9	$C_2F_3N \leftrightarrow CF_3 + CN$	20	$CF_2 \leftrightarrow C + F + F$
10	$CN \leftrightarrow C + N$	21	$CF_4 \leftrightarrow CF_3 + N$
11	$CF_3 \leftrightarrow CF_2 + F$	22	$FN \leftrightarrow F + N$

Table 3-3: Reference energy of species

Reference energy of species					
Specie	Reaction E	Specie	Reaction E	Specie	Reference E
$\mathbf{e^-}$	0	$\mathbf{N_2}$	0	$\mathbf{C_2}$	0
$\mathbf{F_2}$	0	$\mathbf{N}$	4.88eV	$\mathbf{C}$	3.2eV
$\mathbf{F}$	0.82 eV	$\mathbf{N^+}$	19.42 eV	$\mathbf{C^+}$	14.460 eV
$\mathbf{F^+}$	18.242 eV	$\mathbf{N^{2+}}$	49.025 eV	$\mathbf{C^{2+}}$	38.845 eV
$\mathbf{F^{2+}}$	53.214 eV	$\mathbf{N^{3+}}$	96.451 eV	$\mathbf{C^{3+}}$	86.733 eV
$\mathbf{F^{3+}}$	115.922 eV	$\mathbf{C^{4+}}$	151.226 eV	$\mathbf{F^{4+}}$	203.097 eV
$\boldsymbol{C_2F_2}$	-9.118 eV	$\mathbf{C_2F_4}$	-18.8 eV	$\boldsymbol{CF_2}$	-5.81 eV
$\mathbf{CF_3}$	-10.657 eV	$\boldsymbol{CN}$	0.307 eV	$\mathbf{C_2F_3N}$	-15.211 eV
$\mathbf{CF_4}$	-15.504 eV	$\mathbf{C_2N_2}$	-5.314 eV	$\boldsymbol{FN}$	2.083 eV

Diatomic and polyatomic species

For a diatomic specie, the internal partition functions can be expressed by

$$\mathrm{Q}_{int} = \mathrm{Q}_{ele} Q_{vib} Q_{rot} = \sum_j g_{e,j} \exp\left(-\frac{\varepsilon_j}{kT}\right) \sum_v \exp\left(-\frac{\varepsilon_{vib}(v)}{kT}\right) * \sum_J (2J+1)\exp(-\varepsilon_{rot}(v)/kT) \tag{3.11}$$

where Q_{ele}, Q_{vib} and Q_{rot} are electron, vibrational and rotational partition function separately. The expression for those partition functions are shown below:

$$\begin{aligned} Q_{ele} &= \frac{1}{\sigma} \sum_{T_e} g_e \exp\left(-\frac{S_e}{k\,T}\right) \\ Q_{vib} &= \sum_{v=0} g_v \exp\left(-\frac{G_v(S_e)}{k\,T}\right) \\ Q_{rot} &= \sum_{J=0} g_J \exp\left(-\frac{F_v(J)}{k\,T}\right) \end{aligned} \tag{3.12}$$

σ is a constant, it is equal to 2 for homonuclear molecules and 1 for heteronuclear molecules. The electronic levels S_e are limited to the number of states. G_v corresponds to the vibrational energies and depend on the spectroscopic constants expressed in Eq.(3.13)

$$G_v = \left(v+\frac{1}{2}\right)\omega_e - \left(v+\frac{1}{2}\right)^2 \omega_e x_e + \left(v+\frac{1}{2}\right)^3 \omega_e y_e \tag{3.13}$$

$F_v(J)$ corresponds to the rotational energies which is present below:

$$\begin{aligned} F_v(J) &= B_v J(J+1) - D_v J^2 (J+1)^2 + .. \\ B_v &= B_e - \alpha_e \left(v+\frac{1}{2}\right) + .. \\ D_v &= D_e - \beta_e \left(v+\frac{1}{2}\right) + .. \end{aligned} \tag{3.14}$$

Those parameters: ω_e , $\omega_e x_e$, $\omega_e y_e$, α_e , β_e , B_e , D_e are the spectroscopic constants which are available in Janaf table.

If the vibration-rotation interactions can be neglected, the internal partition function for polyatomic species is same as diatomic species in Eq.(3.11).

However, as the polyatomic species exist at low temperatures, the population of the fundamental level is important. The contribution of Q_{ele} to the total internal partition function can be treated as the ground state quantum weight P_s. The vibrational partition function can be expressed as:

$$Q_{vib} = \prod_{i=1}^{N} \left[1 - \exp(\frac{-v_i hc}{k\,T})\right]^{-d_i} \qquad (3.15)$$

Where d is the degeneracy of the vibrational frequency v. It can be obtained from Janaf table. For contribution of the rotation part to total partition function, it is shown in Eq.(3.16) and Eq.(3.17).

For linear molecules:

$$Q_{rot} = \frac{1}{\sigma}\frac{k\,T}{hcB_0} \qquad (3.16)$$

For non-linear molecules:

$$Q_{rot} = \frac{1}{\sigma}\sqrt{\frac{\pi}{ABC}(\frac{k\,T}{hc})^3} = \frac{1}{\sigma}6.93510^{57}\sqrt{T^3 I_A I_B I_C} \qquad (3.17)$$

The constant of rotation A, B, C or the momenta of inertia I_A, I_B, I_C can be found from Janaf Table.

3.2.3 Molar weight and mass density

There are several thermodynamic properties in thermal plasma, such as molar weight, mass density, they can be calculated once the composition of a thermal plasma is determined at a temperature and pressure. Molar weight and mass density are expressed below:

Molar weight

$$\rho = \sum_i m_i n_i \tag{3.18}$$

Where m_i is the mass of species i, n is the number density.

Mass density

$$M = \sum_i x_i M_i \tag{3.19}$$

$$x_i = n_i / \sum_i n_i \tag{3.20}$$

Where x_i and M_i are the molar fraction and molar mass of species i.

3.2.4 Radiation emission and absorption

In the applications of thermal plasmas, the media involved are usually gases and metallic vapours. Radiation is an efficient energy transfer mechanism in high pressure arcs commonly encountered in high voltage circuit breakers. Radiation emission and absorption are the two main mechanisms. The emission of spectral lines is caused by electronic transitions of excited neutral particles (atoms and molecules) or ions from higher energy levels to lower[15]. Thus, radiation by this mechanism is referred to as bound-bound. Theoretically, radiation in the form of line radiation is only a small fraction of the total radiation.

When an electron is captured by an atom or ion into its orbit, the recombination process leads to the emission of free-bound radiation. In general, this

mechanism can apply to all possible energy levels of a molecule, atom or ion. Therefore, all species can emit continuum spectra resulting from free-bound radiation.

Bremsstrahlung (free-free transition) is another process that leads to continuum radiation. A free electron may lose part of its kinetic energy due to interaction with other charged particles through Coulomb field of the charged particles. Radiation in this case is converted from the lost kinetic energy of the charged particles.

Recombination and Bremsstrahlung contribute most towards the continuum radiation. Sometimes a plasma contains molecular species (molecular species are usually present when plasma temperature is lower than 8,000 K at 1 atm) and the spectrum also contains bands of molecules. The molecular bands consist of extinction of rotational and vibrational energy of molecules.

The total radiation due to various emission mechanisms cannot completely leave the plasma without attenuation, unless it is considered optically thin. Some thermal plasmas can be treated as optically thin. However, strong absorption of line and band radiation may still occur and it will increase with the pressure.

Eq.(3.21) describes the relationship between monochromatic intensity I_{ν} and $\mathrm{I}_{\nu 0}$, radiation intensity from the core over a thickness L in the medium.

$$\mathrm{I}_{\nu} = \mathrm{I}_{\nu 0} \exp\left(-\int_0^L \kappa_{\nu} dx'\right) = \mathrm{I}_{\nu 0} \exp(-\tau_{\nu}) \qquad (3.21)$$

where κ_{υ} is the absorption coefficient at frequency ν, it is generally expressed in cm^{-1}.

The absorption coefficient is applicable to line and continuum radiation. Due to the influence of line overlapping on radiative transfer, all overlapped spectral lines must be taken into account in the calculation of the absorption coefficient. It will be discussed in results section.

The absorption coefficient for a spectral line *'i'* in species *'a'* can be denoted as[10]:

$$\kappa_{a,\nu}^{i}(T,P) = \pi \mathrm{r}_0 c f_{mn}^{a,i} N_n^a(T,P) L^i(\nu,T,P) \qquad (3.22)$$

where r_0 is the classical electron radius, $f_{mn}^{a,i}$ indicates the absorption oscillator strength of spectral line i corresponding to an electronic transition from higher energy level m to lower energy level n of specie a. N_n^a represents the population density of lower energy level n of specie a. L^i is the normalized line profile:

$$2\int_0^\infty L^i(\nu,T,p)\, d\Delta\nu = 1 \qquad (3.23)$$

Where $\Delta\nu$ is the frequency difference between ν and the line centre. L^i is the line shape which is assumed to be dispersion or Lorentz profile[10]. It can be expressed as:

$$L^i(\nu,T,p) = \frac{1}{\pi\omega^i(T,P)(X^2+1)} \qquad (3.24)$$

where

$$\mathrm{X} = (\nu - \nu_c^i)/\omega^i(T,P) \qquad (3.25)$$

$$\nu_c^i = \nu_0^i + d^i(T,P) \quad (3.26)$$

$$\nu_0^i = \frac{E_m - E_n}{h} \quad (3.27)$$

In the above expressions, ν_c^i is the centre frequency of spectral line *i*, ω^i is its half width corresponding to at the half peak value in the profile. However, due to perturbation on energy states of atoms or ions, the frequency of peak absorption is slightly shifted from the true line centre which is at ν_0^i. Eq.(3.26) represents the relationship of shifted and true centre frequency of the spectral line. Both the line shift $d^i(T,P)$ and the half width $\omega^i(T,P)$ will be described in the next section. The undisturbed line centre has a frequency as given in Eq.(3.27)

The absorption oscillator strength f is obtained from database which mentioned in last section and Wiese et al[16].

The absorption coefficient for continuum radiation associated with recombination and bremsstrahlung has to be treated as different cases. For the absorption associated with recombination, as it is collision dominated, the photon absorption cross section significantly affects the absorption coefficient.

$$\kappa_\nu^{rec} = \sum_i \sigma_{i,\nu}^a N_i^a \quad (3.28)$$

Eq.(3.28) describes the absorption coefficient due to free-band radiation of specie 'a' at energy state of E_i^a. $\sigma_{i,\nu}^a$ is the photon absorption cross section at frequency ν by a particle at tis energy level i. N_i^a is the population density of specie 'a' at E_i^a.

3.2.5 Broadening of spectral lines

Radiation due to transition between electronic excitation energy levels results in broadening of line spectrum. The broadening of spectral lines can be caused by different mechanisms. Broadening mechanisms due to different interactions contribute to different spectral line broadening will be discussed in this section.

Stark broadening

When the population of charged particles dominates the total population of particles in a thermal plasma will be generated and perturb the normal energy levels. It results in Stark broadening. Griem has developed a theory for both atomic spectral lines[17] and ionic lines[18]. Eq.(3.29) and Eq.(3.30) describe the half width and spectral shift for ionic lines[18]. Considering a band-band transition from energy level m to n, the total angular momentum quantum numbers of m and n are respectively J' and J .

$$\omega_{stark}^{i} = \mathrm{C}(\mathrm{T},\mathrm{P}) \cdot \left[\sum_{J''} \frac{S(J'',J)}{2J+1} g_{Se}\left(X_{J''J}\right) + \sum_{J''} \frac{S(J'',J')}{2J'+1} g_{Se}\left(X_{J''J'}\right)\right] \tag{3.29}$$

and

$$\mathrm{d}_{stark}^{i} = \mathrm{C}(\mathrm{T},\mathrm{P}) \cdot \left[\sum_{J''} \frac{\Delta E_{J'',J}}{\left|\Delta E_{J'',J}\right|} \frac{S(J'',J)}{2J+1} g_{Sh}\left(X_{J''J}\right) - \sum_{J''} \frac{\Delta E_{J'',J'}}{\left|\Delta E_{J'',J'}\right|} \frac{S(J'',J')}{2J'+1} g_{Sh}\left(X_{J''J'}\right)\right] \tag{3.30}$$

where $S(J'',J)\ and\ S(J'',J')$ indicate all transition to and from J and J'. Function C is related to the population of free electrons.

$$\mathrm{C(T,P)} = 16\left(\frac{\pi}{3}\right)^{\frac{2}{3}} cR_\infty a_0^3 N_e \left(\frac{hcR_\infty}{kT}\right)^{1/2} \quad (3.31)$$

R_∞ is the Rydberg constant, a_0 is Bohr radius. S is the line strength which can be obtained by Eq.(3.32):

$$S(J', J) = 3(2J + 1)\lambda R_\infty f_{J'J} \quad (3.32)$$

Eq.(3.29) and Eq. (3.30) take into account all possible transitions to and from level m and n. X are empirical functions given by Griem[18].

Although the Stark broadening should be obtained by considering all transitions to and from the lower and upper energy levels, transitions between energy levels whose effective quantum numbers exceed 5 are normally ignored.

Resonance broadening

Resonance broadening can enhance the half width of a spectral line, if transition between the ground state and either of the lower or upper energy level of the line is allowed. The resonance broadening of the half width of a spectral line is given by Lowke[10].

$$\omega_{Res}^{i} = \frac{3r_0 c^2}{4\pi}\left[\frac{G_1}{G_K}\right]^{1/2} \frac{f_{K1}}{\nu_{Res}} N_1^a \quad (3.33)$$

where K refers to the lower or upper energy level that is allowed to transit to ground level. When K = 1, it refers ground state. $G_K = (2S_K + 1)(2L_K + 1)$, L is related to L-S coupling, and L is the total orbital angular momentum. $\nu_{Res} = (E_K - E_1)/h$.

Van der Waals broadening

Van der Waals force exists among particles in thermal plasma. It is a much weaker force than chemical bond. However, it still perturbs the emitting particles[19]. Eq.(3.34) describes the half width of a spectral line attributing to Van der Waals force.

$$\omega_v^i = \frac{a_0^2}{2}\left[\frac{9\pi\alpha c}{4}\right]^{\frac{2}{5}}\left[(\bar{R}_n^2)^{\frac{2}{5}} + (\bar{R}_m^2)^{\frac{2}{5}}\right]\sum_{P\neq a}\left(\frac{R_\infty}{E_p}\right)^{4/5} V_p^{3/5} N_1^P \qquad (3.34)$$

where α is the fine structure constant, V_p is perturber relative velocity, E_p the characteristic energy of the perturbing specie, $\bar{R}_n$ and $\bar{R}_m$ the mean radial matrix elements. The relative velocity of perturbers can be calculated in Eq.(3.35).

$$\mathrm{V}_p = \left[\frac{8kTN_0}{\pi}\left(\frac{W_a + W_p}{W_p \cdot W_a}\right)\right]^{\frac{1}{2}} \qquad (3.35)$$

where W is the atomic weight with the subscript a and p species 'a' or 'p'. The mean radial matrix element $\bar{R}_X$ is expressed as[17]:

$$\bar{R}_X{}^2 = \left(\frac{\mathrm{N}_X^{*2}}{2\mathrm{Z}_a^2}\right)\left[5\mathrm{N}_X^{*2} + 1 - 3\mathrm{l}_X(\mathrm{l}_X + 1)\right] \qquad (3.36)$$

where Z_a present in both Eq.(3.36) and Eq.(3.37) is the net charge of the specie a. X here can be m or n in Eq.(3.34), l_X is the orbital angular momentum quantum number and N_X^* indicates the effective principal quantum number which is given below:

$$\mathrm{N}_X^{*2} = \frac{\mathrm{Z}_a^2 E_H}{E_\infty^a - E_X^a} \qquad (3.37)$$

E_{∞}^{a} and E_{X}^{a} are, respectively, the ionisation energy and energy on level X of species a. Similarly, E_H is the ionization energy of a hydrogen atom.

3.2.6 Continuum absorption

Atomic continuum

Continuum radiation from a plasma is due to two mechanisms, free-bound electron recombination and free-free bremsstrahlung radiation. Lowke and Liebermann[11], Gleizes and Gongassia[20], Naghizadeh-Kashani and Cressault[21], calculated the continuum radiation for SF_6, SF_6-N_2 and Air. Under LTE condition, as the plasmas are collision dominated in terms of energy exchange and transition of electronic states, Kirchhoff's law can then be applied to relate spectral absorptivity to emission coefficients. Thus, the spectral absorptivity can be related to photon absorption cross section σ^a.

The main problem in the calculation of continuum absorption is to obtain the cross section data. There is a lack of experimental results about photon absorption cross section. Thus, in present work, the cross sections are estimated using theoretical methods.

Quantum Defect Method[21] and its variants[22] is chosen to generate the photon absorption cross sections for atomic species. This method has been used by Lowke.[10] An LS coupling scheme is required first:

$$\mathrm{E}_{i}^{a}(nlSL) = \sum g(J)E^{a}(nlSLJ)/g(nlSL) \qquad (3.38)$$

where $g(J) = 2J + 1$ and $g(nlSL) = (2\mathrm{S} + 1)(2\mathrm{L} + 1)$. S and L are, correspondingly the spin angular momentum and orbital angular momentum in LS coupling. Eq.(3.38) defines the threshold energy for photon absorption. The frequency ν_{nl} of the energy level is then worked out. The cross section of photon absorption is then expressed as Eq.(3.39).

$$\sigma^{a}_{nlSL} = 8.559 \times 10^{-23}\left(\frac{\mathrm{E}^{a}_{i}(nlSL) + k^{2}}{\mathrm{E}^{a}_{i}(nlSL)^{2}}\right) \sum_{l'=l\pm1} C_{l'}|nl;Sl|^{2} \qquad (3.39)$$

where $k^2 = z_f^2 S$ is the energy of the ejected electron in Rydberg unit. z_f here is the charge on the final ion. The unit of cross section from Eq.(3.39) is in m^{-2}. According to the theory of free-bound transition, the frequency that the cross section in Eq.(3.39) corresponds to a threshold frequency. The cross section higher than the threshold frequency varies as $1/\nu^3$

$$\sigma^{a}_{\nu,i} = \sigma^{a}_{\nu_{th},i}(\nu_i/\nu)^3 \qquad (3.40)$$

where $\sigma^{a}_{\nu_{th},i}$ is the cross section obtained from Eq.(3.39). ν_i corresponds to the frequency of the level with energy $\mathrm{E}^{a}_{i}(nlSL)$.

The photon absorption cross section for ions can be estimated using hydrogenic approximations. Combining with the estimation of frequency beyond threshold, Eq.(3.41) expresses the photon absorption cross section for ions:

$$\sigma^{a}_{\nu,i} = \alpha a_0^2 4\pi^2 \frac{N_i^*}{Z_a^2}\left(\frac{\nu_i}{\nu}\right)^3 \qquad (3.41)$$

where N_i^* is the effective principal quantum number of i^{th} energy state. Z_a is the net charge of the atom or ion as seen by the valence electron. As the high energy levels tend to have small gaps, the absorption coefficient $\sum_i \sigma^{a}_{i,\nu} N^{a}_{i}$ can be treated as an integral. The Eq.(3.42) describes all high energy levels bound-free and all free-free radiation

$$\kappa_{\nu}^{bf+ff}(T,P) = \frac{kT\alpha^3 c^2}{4h\nu^3}\sum_{a}\frac{N_a}{U_a}Z_a^2\eta_a\sum_{K}G_K exp\left\{-(E_{\infty}{}^{a,K} - \Delta E_{\infty}{}^{a} - h\nu')/kT\right\} \qquad (3.42)$$

where η_a is a correction factor for species 'a', it usually is set as two[10] , G_K is the statistical weight of the K^{th} parent term, $E_{\infty}{}^{a}$ is the ionisation energy of

species 'a', $\Delta {E_\infty}^a$ is the lower ionisation energy. ν' is defined as $\nu' = v_n = ({E_\infty}^{a,K} - {E_n}^{a,K})/h$ if $\nu \geq v_n$ and if $\nu < v_n$ then $\nu' = \nu$. ${E_n}^{a,K}$ is the lowest smeared energy state of species 'a', it is usually picked up from a high energy level.

Molecular continuum

For molecular continuum radiation, the calculation method is similar to atomic species. The cross section of some of the species can be found from literature, such as for C_2F_4 [23], CF_4 [24,25,26], C_2 [27], F_2 [28] and N_2 [29]. The cross sections of the remaining species such as C_2N_2, CF_3, CF_3N, C_2F_2 and FN, are estimated by two empirical laws[30]. Fig. 3-2 is taken as an example to explain the estimation method. Three regions of molecular cross section with respect to wavelength can be assumed. The cross section in region 1 can be considered as constant of 10^{-17} cm^2 and 10^{-18} cm^2 in region 3. In region 2, there is a parabolic relationship between the logarithm cross section axis and the wavelength, which is expressed in Eq.(3.43). It is required to determine the boundaries for each species that do not have experimental photon absorption cross section.

According to the number of atoms contained in a molecule, the species can be divided into two groups. The first one is small molecules which include no more than three atoms, such as FN. The second group is formed by the molecules with more than three atoms such as: C_2N_2, CF_3, CF_3N, C_2F_2.

Following method[30], the boundaries used in molecular cross section estimation are listed in Table 3-4.

3.2.7 Net emission coefficient (NEC)

The Net Emission Coefficient (NEC) was proposed by Lowke[10]. The NEC corresponds to the effective radiation emitted from the axis of an infinitely long isothermal cylinder. Usually, the calculation of radiative transfer in the central region of a thermal plasma is based on the NEC.

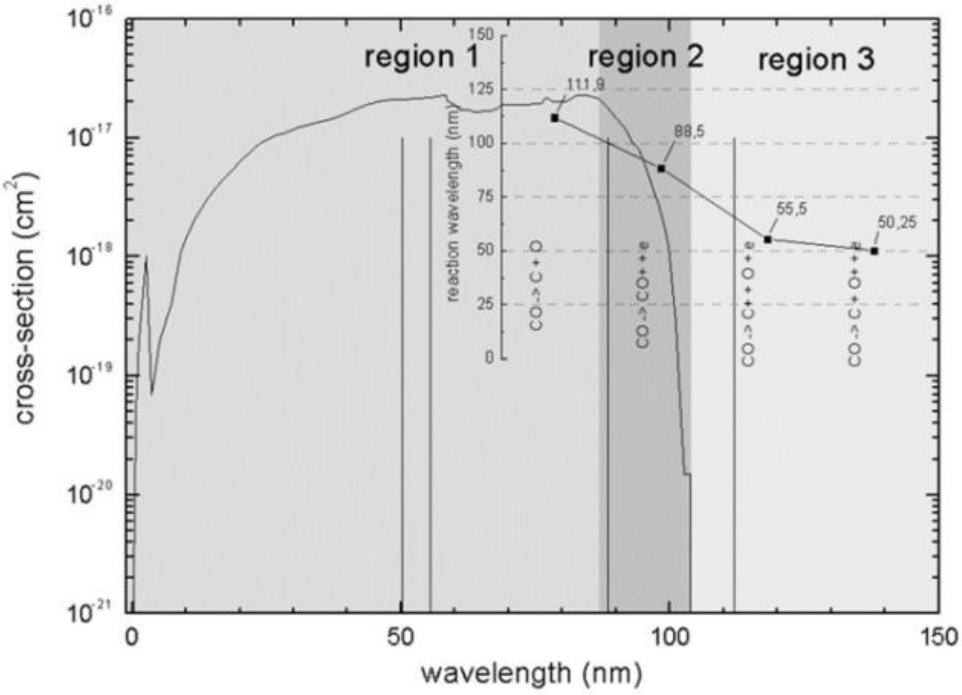

Fig. 3-2: CO molecular photon absorption cross-section with respect to wavelength.[30]

$$\sigma_{region\,2} = 10^{a\lambda^2+b\lambda+c} \tag{3.43}$$

It is defined as:

$$\varepsilon_N(T,p,R_p) = \int_0^{\infty} \kappa_\nu(T,p) B_\nu(T) \exp\left(-\kappa(T,p)R_p\right) d\nu \tag{3.44}$$

where $\kappa_\nu(T,p)$ is the spectral absorption coefficient corresponding to Eq.(3.22). $B_\nu(T)$ represents the Planck function for blackbody radiation. As it is stated before, Kirchhoff's law is applicable, the emission coefficient ε_ν is $\varepsilon_\nu = \kappa_\nu(T,p)B_\nu(T)$. Eq.(3.44) considers the absorption of radiation in the isothermal cylinder. To reduce the calculation time, the integration operation is discrete as:

$$\varepsilon_N(T,p,R_p) = \sum_{\nu^K=\nu^{K-1}+d\nu} \kappa_\nu(T,p)B_\nu(T)\exp\left(-\kappa(T,p)R_p\right)d\nu \qquad (3.45)$$

where ν^{K-1} is the frequency at position K-1 on the frequency axis and the next frequency point is equal to $\nu^{K-1}+d\nu$. Because of the narrow profile of line spectra, $d\nu$ has to be very small. A value of $10^{11}Hz$ is used in the calculation.

Table 3-4: List of the values for region 1-2 and region 2-3 used in molecular cross-section estimation.

Molecule	Boundary of Region 1-2	Boundary of Region 2-3
FN	115.3	135.3
C_2N_2	122	163.4
CF_3	135.2	165
CF_3N	138.9	173.7
C_2F_2	83.7	108.6

3.2.8 Data source

The energy level data of atoms that are employed in the calculation were gathered from the database of the National Institute of Standards and Technology (NIST)[31]. The Atomic Spectra Database (ASD) includes observed transitions and energy levels of most known chemical elements. The wavelengths of spectral lines included in ASD are from 0.002 nm to 60 nm. The data of spectral lines in ASD includes radiative transition probabilities and the energies of ground states and ionization. For the data observed for the experiment, the accuracy is also included in the database. As the calculation results in this thesis are based on the ground data from the NIST, it is certainly affected by the accuracy of the ground data. A discussion of how the results are apportioned to inputs of different uncertainty will be mentioned in the later content.

Another database is compiled from Kurucz (University of Hannover)[32]. Similarly, University of Harvard includes the spectral lines and atomic data for most common chemical elements.

3.2.9 Calculation program

The calculation program was developed using C++ and the Armadillo library. The Armadillo library is a high-quality linear algebra library. The only feature of the Armadillo library employed in the program is to carrying out the matrix inverse in the Newton-Raphson method. The program runs on a personal computer with a Windows 10 operation system with Intel i5-2320 and 8 Gb RAM.

3.3 Results

3.3.1 Equilibrium composition

Two sets of equilibrium composition of nitrogen and PTFE mixture have been figured below in Fig. 3-3(case 1) and Fig. 3-4(case 2). The percentage in the figure captions, indicates the molar percentage of nitrogen or PTFE at the temperature of 300 K. The temperature range is from 300 K to 35,000 K and at 1 bar pressure. In both cases, due to the free particles recombination, CF_4, C_2N_2, C_2F_3N are formed at around 800 K. However, the weak chemical bond of these three species result in a saturation of their number density. Starting from 1,200K, the density of CF_3 rapidly increased. Rapid dissociation of C_2F_4 starts at 3,000 K, which results in a large amount of carbon and fluorine atoms in the plasma. That is the reason that number density of CF_2, C_2F_2, CN are increased at the temperature from 2,800 K to 3,200 K. When the temperature is higher than 4,000 K, remaining molecule species starts dissociation. The number density of free electron is getting large. Almost complete ionization of all atoms

takes place at around 16,000 K. The molecule species number density is not only determined by the temperature of plasma, but also the initial composition. This is also happened to the number density of atomic species at the temperature higher than 20,000 K. For example, at temperature of 20,000 K, the number density of ions F^+ and C^+ are more than N^+ in case 1, but they are less in case 2. Thus, the radiation transfer will be different due to the difference in number density.

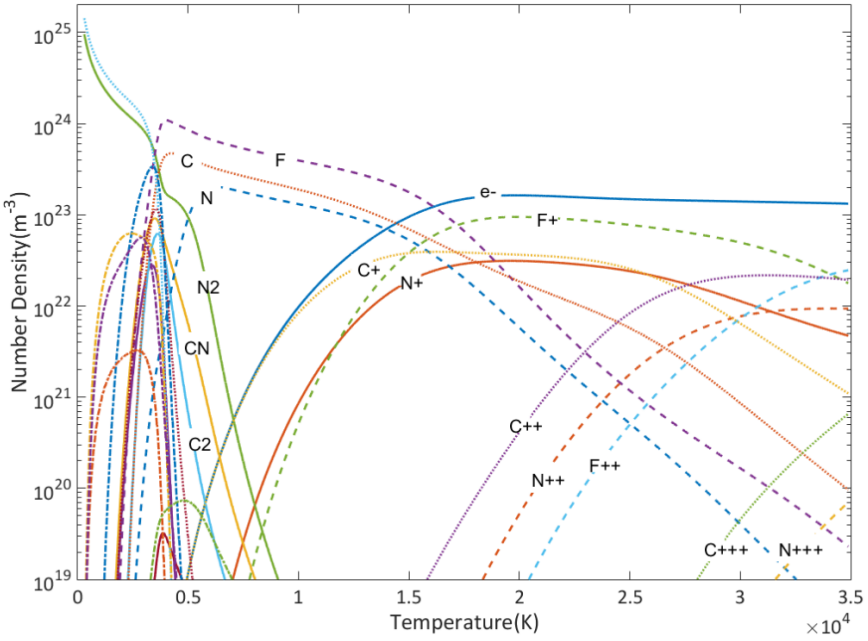

Fig. 3-3a

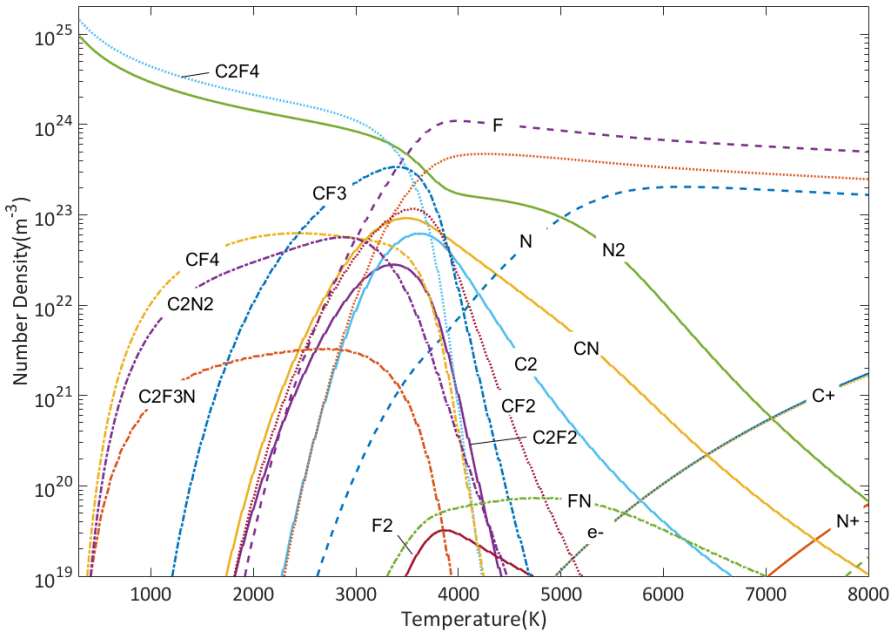

Fig. 3-3b

Fig. 3-3: calculated composition of 50%N_2-50%PTFE mixture gas plasma with temperature range from 300 K-35,000 K(a), 300 K-8,000 K(b)

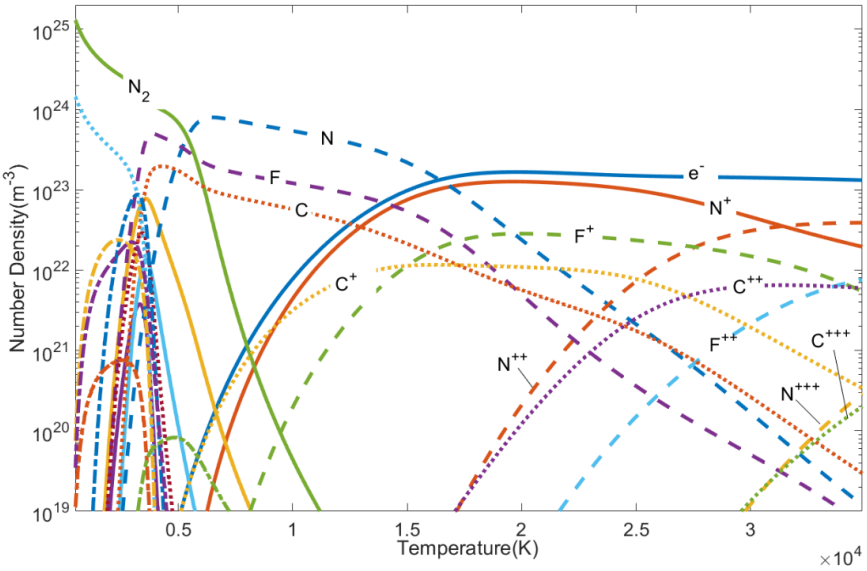

Fig. 3-4a

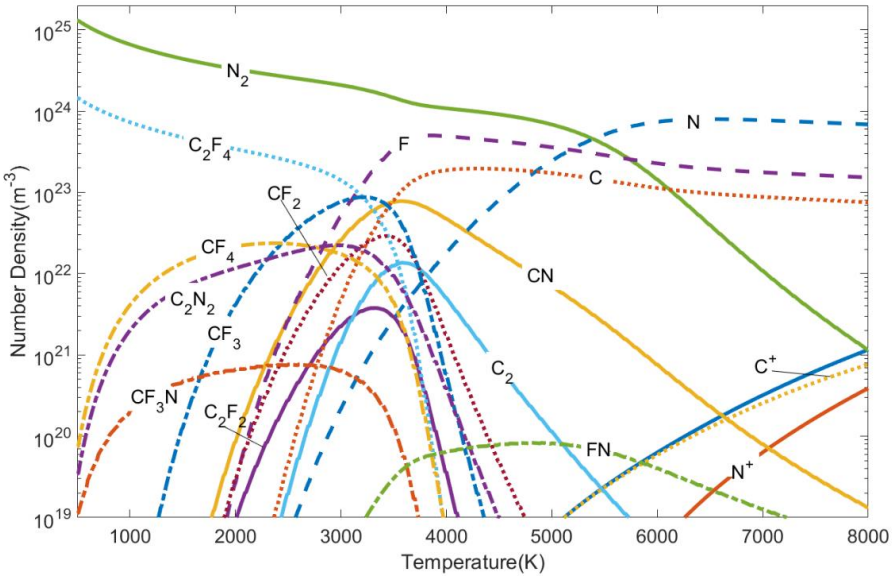

Fig. 3-4b

Fig. 3-4: calculated composition of 90%N_2-10%PTFE mixture gas plasma with temperature range from 300 K-35,000 K(a), 300 K-8,000 K(b)

3.3.2 Thermodynamic properties and dominant factors

Mass density and molar weight

The composition is a function of pressure as well. Fig. 3-5 shows the temperature dependence of molar fraction of nitrogen atom and electrons in 90% N_2 – 10% PTFE gas mixture. As the continuous dissociation of nitrogen molecule, the molar fraction of nitrogen atom increases rapidly at low temperature and starts to decrease at high temperature due to high ionization potential. From Fig. 3-5a, it is obviously, that pressure increase suppresses the dissociation and ionization reactions. This is corresponding to Le Chatelier's pressure principle. Due to ionization, the molar fraction of free electrons increases rapidly. Similarly, this increasing is also suppressed as pressure increase.

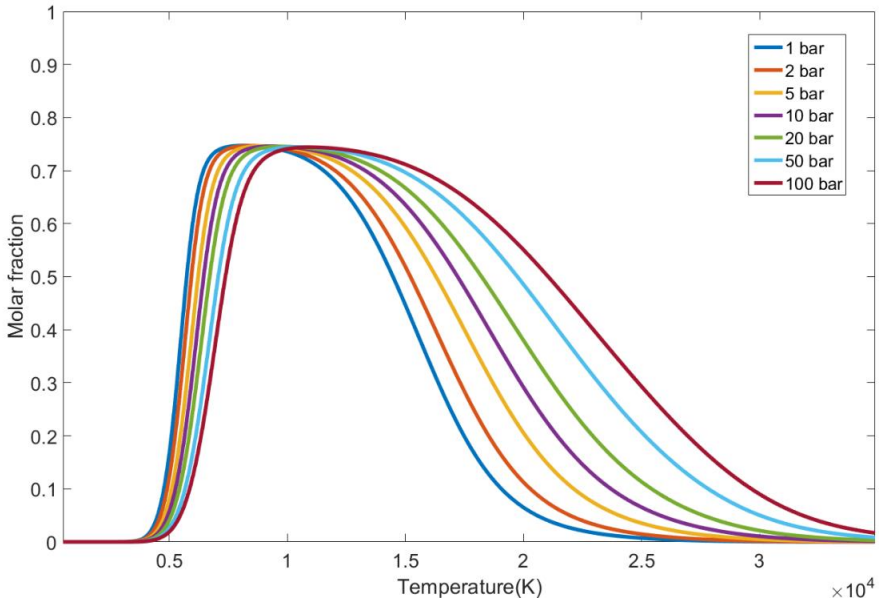

Fig. 3-5a

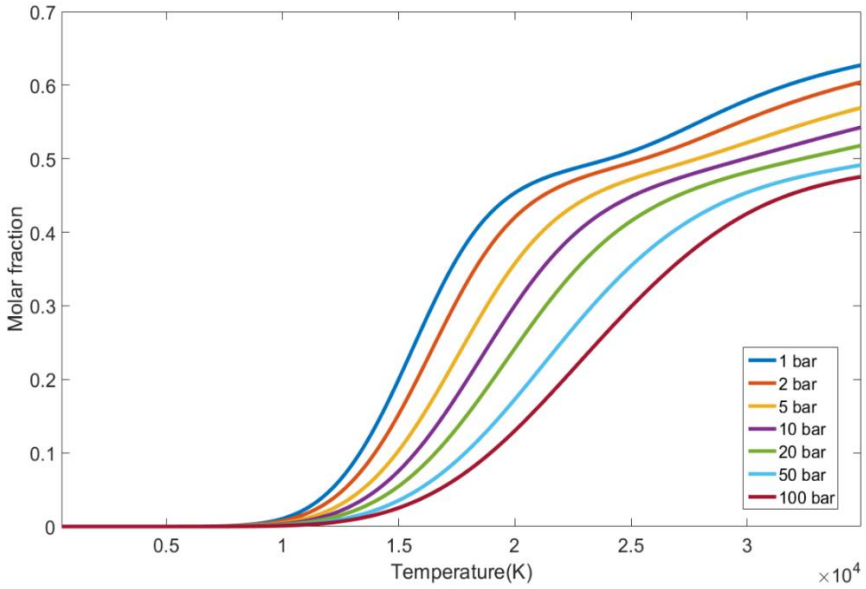

Fig. 3-5b

Fig. 3-5: molar fraction of nitrogen atoms (a) and electrons (b) in 90%N_2-10%PTFE plasma with the pressure ranging from 1 bar(atmosphere) to 100 bar.

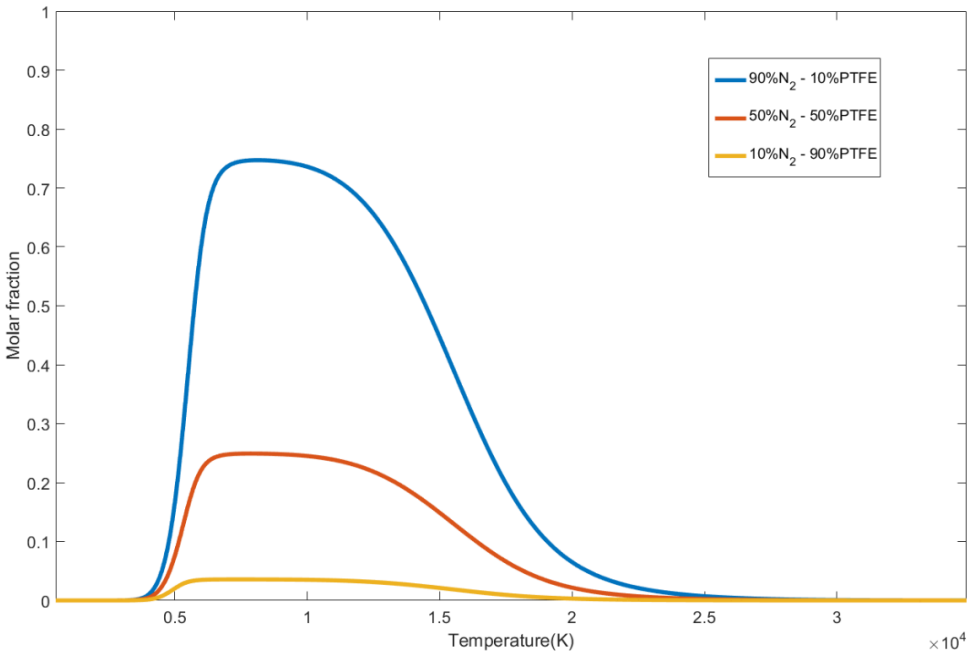

Fig. 3-6a

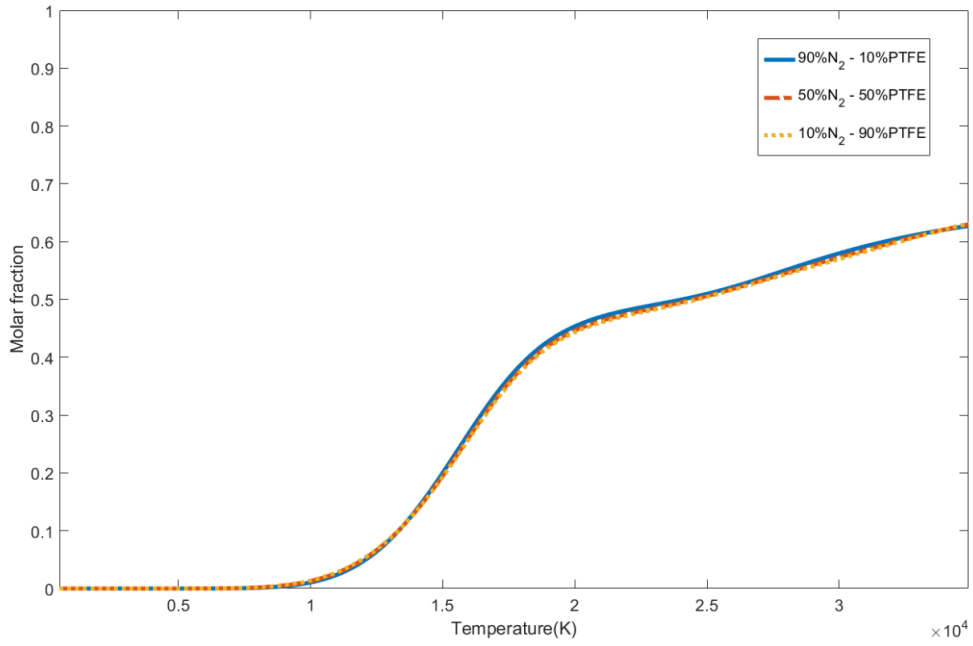

Fig. 3-6b

Fig. 3-6: molar fraction of nitrogen atoms (a) and electrons (b) in different ratio of N_2 to PTFE mixture gas plasma with the pressure range of 1 bar (atmosphere).

The variation of mass density and molar weight as a function of temperature are presented in Fig. 3-7 and Fig. 3-8, respectively. The pressure range shown in the figure is from 1 bar to 100 bar. In the absence of chemical reactions, such as dissociation or ionization, the mass density varies inversely with the temperature and the molar weight should keep constant for an ideal gas. However, dissociation and ionization reactions result in non-ideal variations as a function of temperature. The pressure increase brings the mass density and molar weight to higher value at same temperature. Also, the location of gradient of mass density curve moves to higher temperature as the pressure increase.

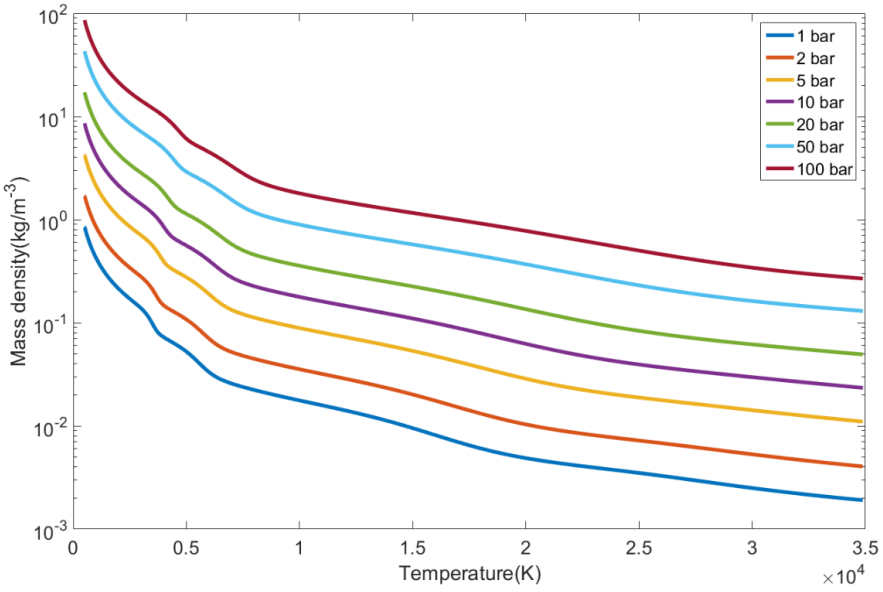

Fig. 3-7: Mass density of 90%N_2-10%PTFE mixture gas plasma in the pressure range from 1 bar (atmosphere) to 100 bar.

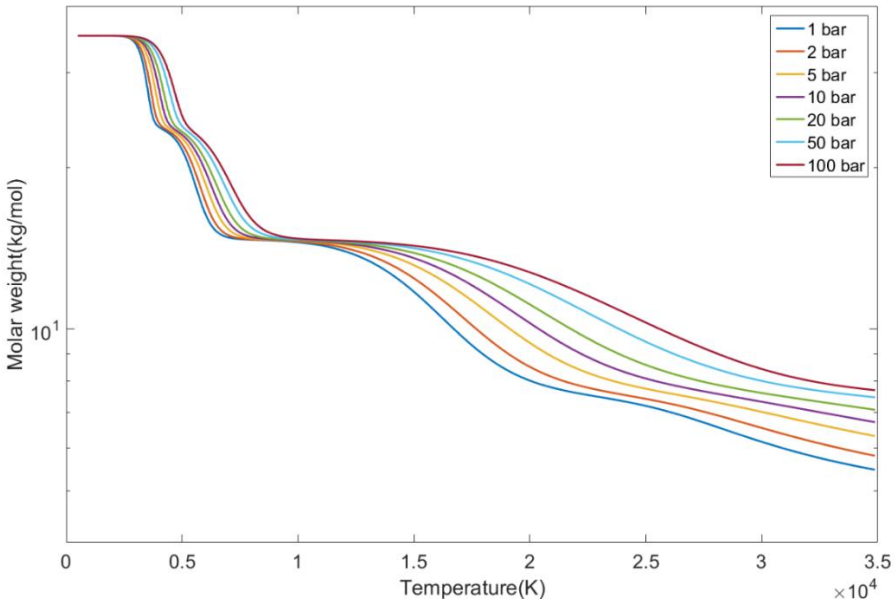

Fig. 3-8: Molar weight of 90%N_2-10%PTFE mixture gas plasma in the pressure range from 1 bar (atmosphere) to 100 bar.

3.3.3 Absorption coefficients

Line spectral

The total number of atomic lines considered in the calculation is 32644. The absorption oscillator strength is obtained from NIST database[31]. Stark broadening operates in most of the atomic lines. In addition, both Doppler broadening and Van der Waals broadening are taken into account. The calculation of radiation due to electronic transition between different energy levels is described in paper[10].

Continuum radiation

Results from Kokoouline[22] appears to show smaller photoionization cross section for CN^-, C_3N^- and C_5N^- in comparison with other ions. It appears that radiative electron attachment is negligible compared to neutral particle induced attachment. Radiative recombination makes the most contribution to the continuum radiation. The calculation makes use of the Scaled Thomas-

Fermi potential. The latest energy levels from NIST[31] and the work of Kurucz[32] are used. The Bremsstrahlung coefficient, known as the Gaunt factor[33], is used to correct the hydrogen-like approximation. The coefficient is calculated based on the method by Stewart[33].

Radiation emission and absorption

Different frequency steps in different regions are used in the NEC calculation, due to the performance limitation of computer. The spectral frequency of radiation is swept from frequency range of 0.1 Hz to 10 PHz. When temperature increase to 5,000 K, the most of molecular species are dissociated. The number density of electrons dominates composition of plasma when temperature above 15,000 K. And the electric arc usually has a temperature of 30,000 K in its core area. Thus, the calculated radiation absorption coefficients for temperatures of 5,000 K, 15,000 K, 30,000 K with a pressure of 1 bar will be shown in Fig. 3-9 (a), (b), (c), respectively. Also the spectral absorption coefficient of room temperature (300 K) is shown on each figure as reference.

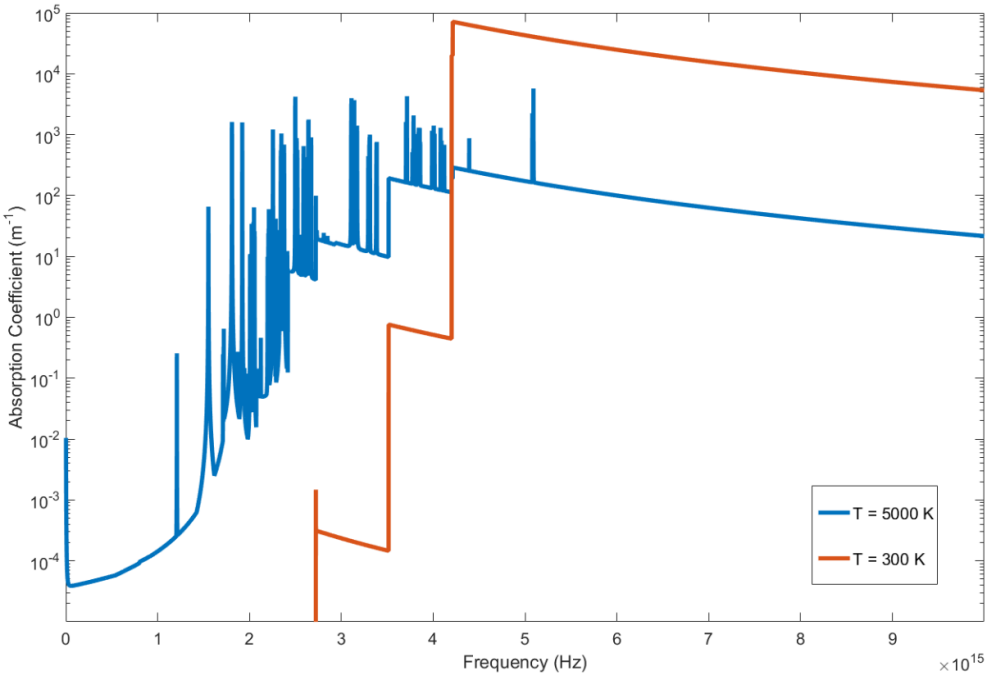

Fig. 3-9a

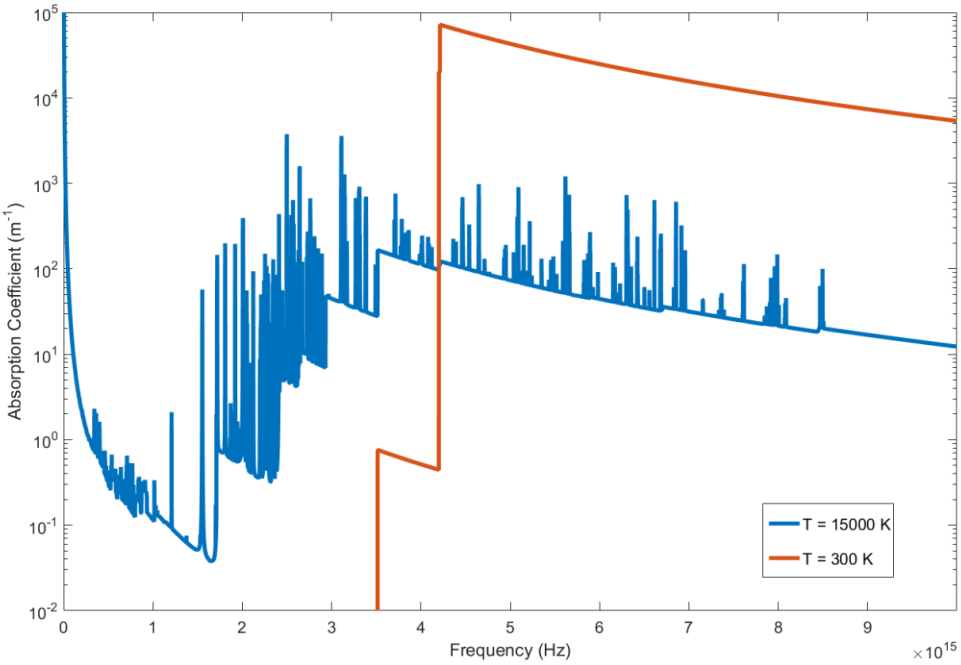

Fig. 3-9b

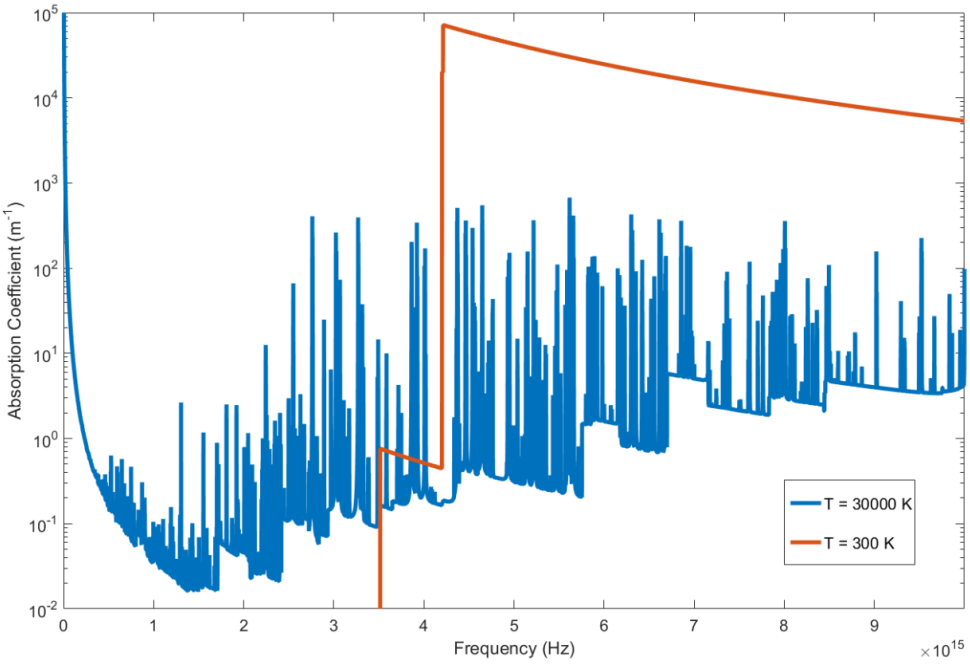

Fig. 3-9c

Fig. 3-9: Spectral line and continuum absorption coefficient for 90% N_2- 10% PTFE at temperature of 5,000K (a), 15,000K (b), 30,000K (c) referenced with the result at 300K.

A comparison of the absorption coefficient at different pressures but the same temperature is illustrated in Fig. 3-10. The main influence of increasing pressure is increasing of the amplitude of absorption coefficient. The higher pressure leads to larger absorption coefficient contributed by continuum radiation. The most important reason of this change is due to the number density of species increasing due to pressure rising. However, the rate of increase in absorption coefficient gets weaker as the temperature increases.

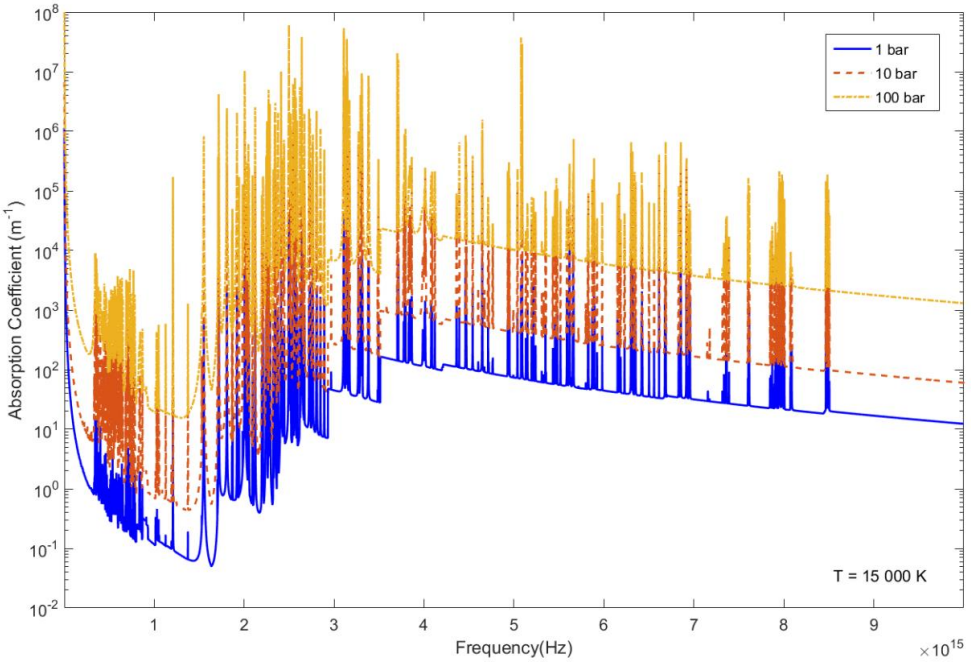

Fig. 3-10a

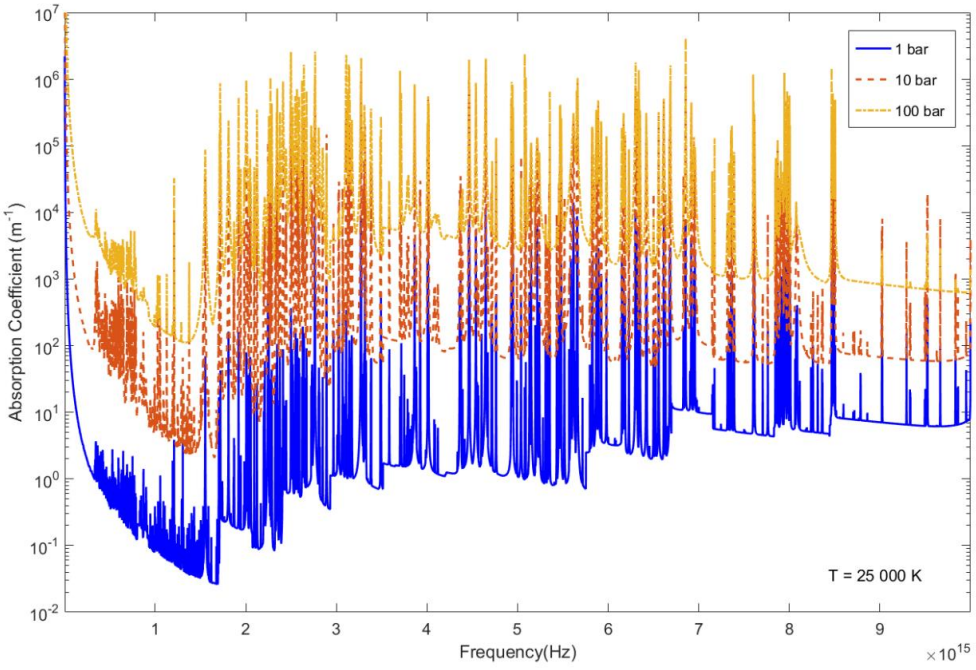

Fig. 3-10b

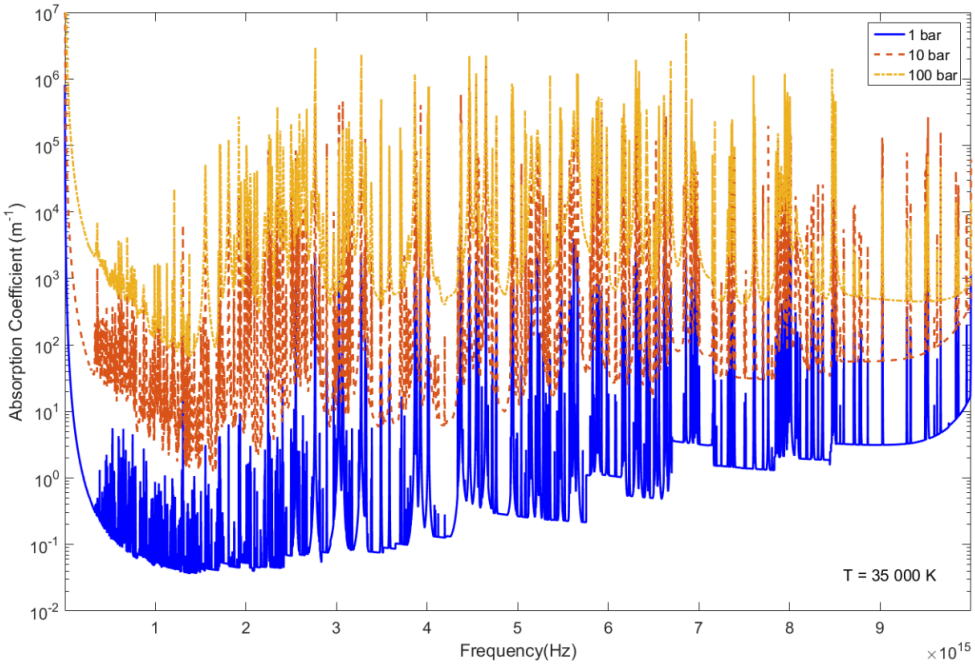

Fig. 3-10c

Fig. 3-10: Spectral line and continuum absorption coefficient for 90% N_2- 10% PTFE with pressure of 1bar, 10bar and 100 bar, at temperature of 15,000K (a), 25,000K (b), 35,000K (c).

3.3.4 NEC

Fig. 3-11 shows the NEC for 90% nitrogen – 10% PTFE mixture with different plasma column radii. As the NEC is quite low at low temperature, results presented here are for temperature higher than 8,000 K. Initially the NEC increases rapidly with temperature. The rate of increase slows down when the temperature reaches 14,000 K. It is interesting to note that this pattern of rate of change of the NEC seems to be closely linked to the total number density of the ions. The rate of change of the NEC becomes higher again when the temperature exceeds 18,000 K, due to the increase in the population of the ions. In the gas mixture calculation, two cases with 10% nitrogen - 90% PTFE (Case 1), and 90% nitrogen – 10% PTFE (Case 2) were selected as the initial composition. Fig. 3-12 shows the NEC of r=0 with different compositions. The

maximum difference in the NEC between the two cases below 15,000 K is about 35%. The difference increases again when the temperature is higher than 22,000 K. The NEC of Case 2 is 65% higher than that of the Case 1 at 34,000 K. This indicates that the influence of PTFE on the NEC can be significant, especially at high temperature (T > 22,000 K).

Fig. 3-13 presents the comparison of NEC between high pressure (100 bar) and low pressure (1 bar). Results indicate that the value of NEC can be significantly affected by the gas pressure, but not in a linear relationship.

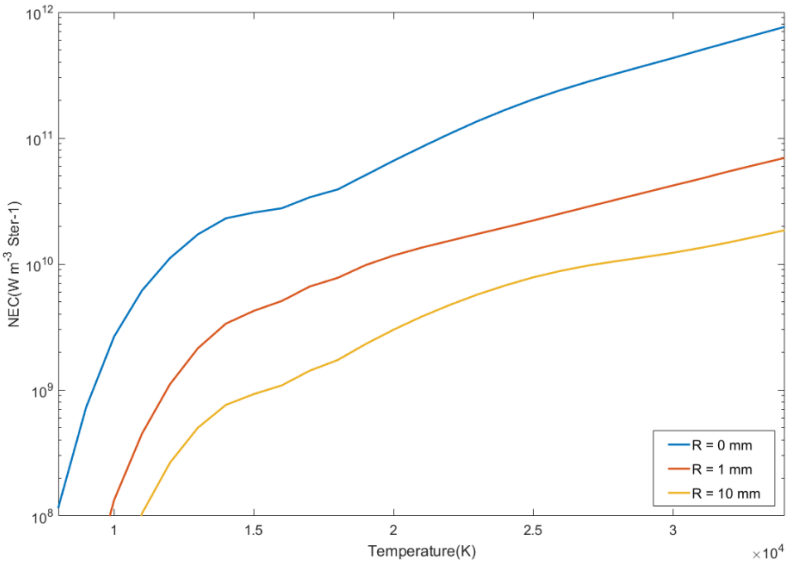

Fig. 3-11: NEC of 90% N_2 – 10% PTFE gas plasma with different R at 1bar.

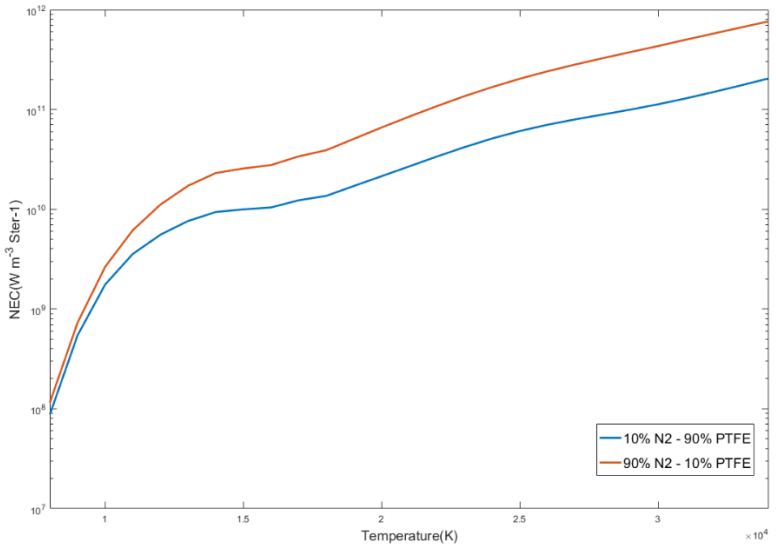

Fig. 3-12: Comparison of NEC of 10% N_2 – 90% PTFE and 90% N_2 – 10% PTFE initial molar proportions at pressure of 1 bar.

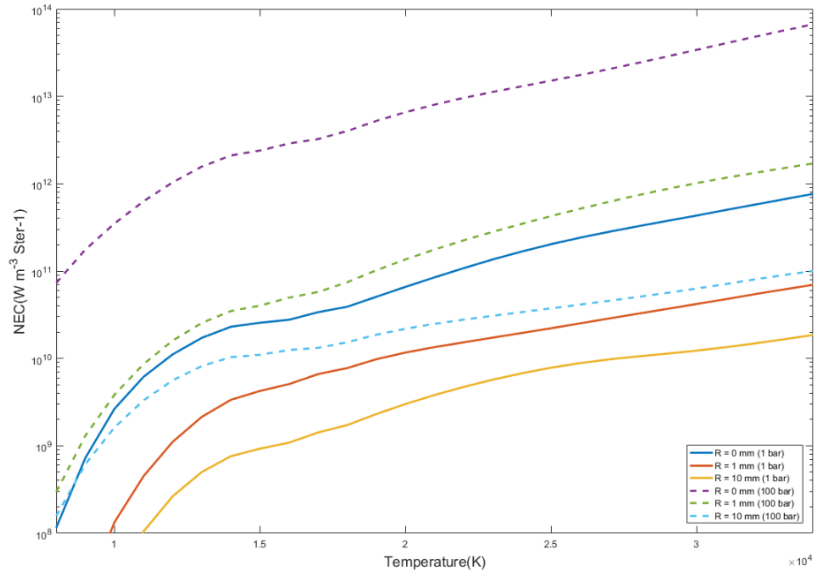

Fig. 3-13: Comparison of high pressure NEC 90% N_2 – 10% PTFE

3.3.5 A sensitivity study on the results

Sensitivity analysis is a common way to study how the uncertainty in the input data affects the results. This study is an important way to investigate the influences of different sources on the output, especially in the radiation transfer calculation for thermal plasma, as the accuracy of the basic data could be low. Although the data are obtained from NIST and Kurucz's database, the energy of the excited or ground levels of atoms, spectral line data due to the transition of particles, molecular energy bands and other relative basic data are obtained by observation from experiment. The Table 3-5 lists atomic spectra level data of nitrogen atom.

Table 3-5: Data accuracy of atomic spectral energy band.

	Accuracy	Number with certain accuracy	Ratio to total level number
Total level number: 311	A $\leq 3\%$	31	10%
	B $\leq 10\%$	165	53.1%
	C $\leq 25\%$	47	17.1%
	D $\leq 50\%$	42	13.5%
	E $> 50\%$	26	8.4%

The accuracy of most spectral levels lies in category B, which within less than 10% of its true value. Assume that there are two different spectral levels with the same accuracy, one contains a low energy level such as a ground level, while the other one is a high energy level. From Eq.(3.9), it can be found that the higher the energy level, the less the influence on partition function due to the uncertainty.

Thus, both high and low spectral energy levels of atomic nitrogen are chosen, the energies are manually increased by 10%, and then substituted into the NEC

calculation. Table 3-6 and Table 3-7 list the original NEC results and the calculated NEC results, taking into account the shifting of the energy of both low and high levels. The composition and NEC calculation are based on initial molar proportions of 50% N_2 -50% PTFE.

3-6: Influence of nitrogen atomic data with low energy level band to NEC

Energy of band (cm^{-1})			Energy of band with 10% increased (cm^{-1})			
19224			21146			
Temperature	5 000K	10 000K	12 000K	14 000K	16 000K	20 000K
Original NEC	1.72E7	1.32E9	7.55E9	2.45E10	3.88E10	8.03E10
Influenced NEC	1.93E7	1.42E9	8.11E9	2.58E10	4.02E10	8.04E10
Influence Rate	12.4%	7.92%	7.41%	5.12%	3.50%	0.20%

Table 3-7: Influence of nitrogen atomic data with high energy levels band to NEC

Energy of band (cm^{-1})			Energy of band with 10% increased (cm^{-1})			
116367			128003.7			
Temperature	5 000K	10 000K	12 000K	14 000K	16 000K	20 000K
Original NEC	1.72E7	1.32E9	7.55E9	2.45E10	3.88E10	8.03E10
Influenced NEC	1.72E7	1.32E9	7.55E9	2.45E10	3.88E10	8.03E10
Influence Rate	< 0.001%	< 0.001%	< 0.001%	< 0.001%	< 0.001%	< 0.001%

From the Table 3-6 and Table 3-7, it can be seen that the influence of uncertainty on the NEC at the high energy level is negligible, but the influence of the low energy level cannot be neglected. However, thanks to the stable low energy level, the results observed from the experiment are usually accurate[34].

3.3.6 Comparison with existing data and verification of methodology

Fig. 3-14 shows the available experimental and theoretical results for NEC with a zero plasma radius at a pressure of 1 bar[35,36,37,38]. For a zero radius plasma (R = 0), by definition self-absorption is not accounted for in the calculation. The results from the present work are close to those of Gleizes[35] for T > 13,000 K with a maximum percentage difference of 13.1%. The discrepancy of up to 29.5% below 13,000 K could be due to the difference between the atomic data used in[35] and in the present work where the most up to date data are used. Fair agreement with the results of Allen[36] and Hermann[37] is achieved. The results of Ernst et al.[38] were obtained experimentally. An increasing discrepancy is observed starting at 17,000 K and it is supposed that there was experimental error arising from the equipment.

Fig. 3-15 shows the available NEC result for pure PTFE calculated by Jan[30] at a pressure of 100 bar. For the NEC lower than 14,000 K, Jan's results have been 5% higher than the calculated results. This is caused by fundamental energy level data accuracy due to the influence of uncertainty on NEC being attenuated when the temperature is higher than 20,000 K. With an uncertainty level, it can be estimated that the number density of species exists in the plasma at temperatures from 10,000 K to 20,000 K.

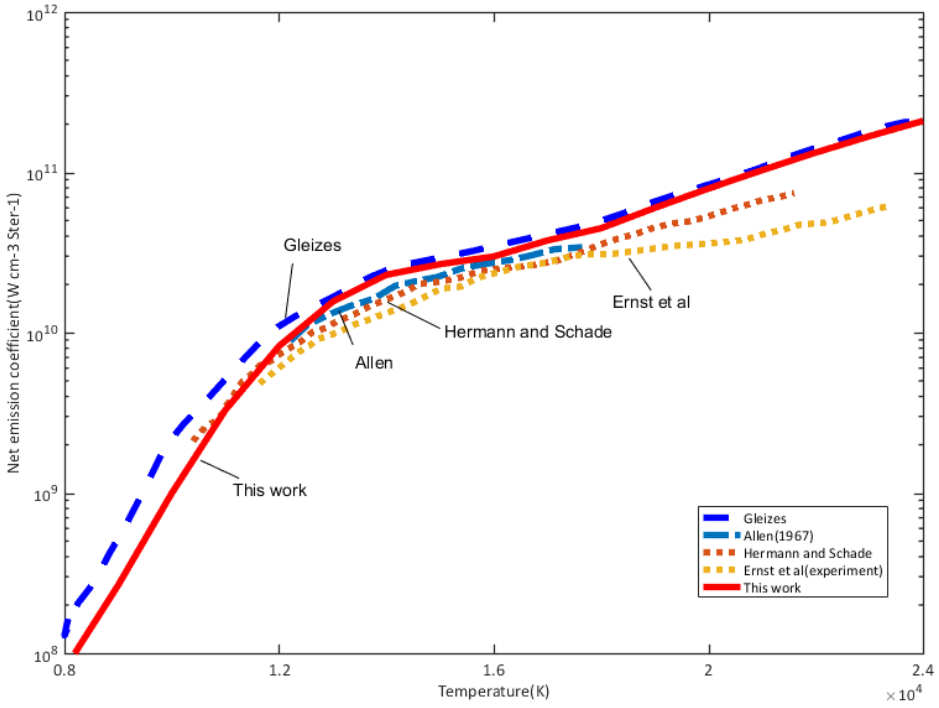

Fig. 3-14: Comparison of calculated NEC results of pure nitrogen gas plasma

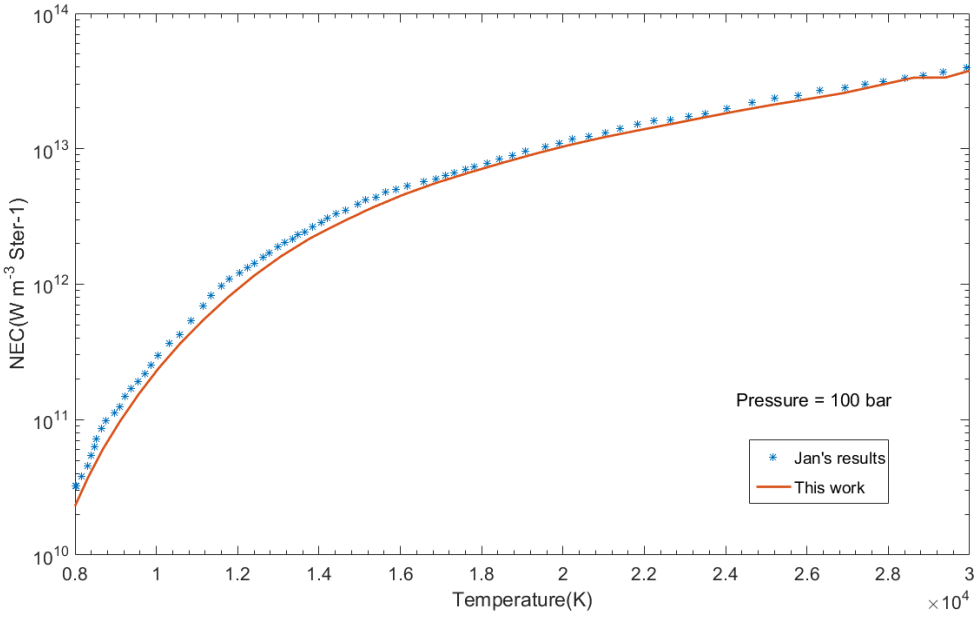

Fig. 3-15: Comparison of calculated NEC results of pure PTFE gas plasma

3.3.7 Line overlapping

In some absorption coefficient calculation case, the overlapping influence is neglected[39], so each line can be treated by means of an escape factor. The escape factor is defined as the ratio of the radiation escaping the plasma to the radiation of an optically thin plasma [40]. In Gleizes[35] calculation, the line overlapping influence is neglected in order to minimise computation costs. To be able to determine the influence of overlapping, a table is introduced below to compare the NEC of a 40%N_2 - 60%PTFE gas mixture both when considering and ignoring the overlapping.

From Table 3-8, it follows that ignoring line overlapping leads to a higher NEC by 21.4% at 8,000 K and 99.1% at 20,000 K. Considering that the influence is not negligible, the NEC results shown in the last section take into account the influence of line overlapping.

Table 3-8: Influence of line overlapping on the NEC of 40% N_2-60% PTFE at different temperature with R = 0 at pressure of 1 bar.

	Temperature					
	8000 K	15 000K	20 000K	25 000K	30 000K	35 000K
NEC with overlapping	8.77E7	9.96E9	2.14E10	6.08E10	1.13E11	2.12E11
NEC without overlapping	1.06E8	1.77E10	4.27E10	1.3E11	2.87E11	6.13E11
Increasing ratio	21.4%	77.5%	99.1%	121.3%	155.2%	189.7%

3.4 Summary

In this chapter, considerable effort is devoted to the calculation of the composition, absorption coefficient and NEC of nitrogen and PTFE gas mixtures

with different initial molar proportions under local thermal equilibrium. The temperature ranges from 300 to 30,000 K and pressure ranges from 1 bar to 100 bar. The calculation model has been checked against the existing results for pure nitrogen gas.

The results of the molar fraction of nitrogen atoms in the 90% N_2 – 10% PTFE gas mixture show that the pressure increase suppresses the dissociation and ionization reactions. It is reasonable as it follows the principle of Le Chatelier's pressure. Due to ionization, the molar fraction of free electrons increases rapidly. Therefore, this increase is suppressed as the pressure increases.

The spectral absorption coefficient was first obtained. At a temperature of 5,000 K, the absorption coefficient is contributed by molecular species, while when the temperature is higher than 15,000 K, atoms and ions dominate the plasma radiation. The spectral line radiation becomes more violent as the temperature increases. Both line and continuum radiation are affected by the pressure; however, at higher temperature the influence of pressure becomes less significant.

The base energy level data of species will affect the NEC results as well. However, by manually changing the data, it shows that a notable influence on NEC is only caused by the low energy level data. The influence of the high energy level to NEC is negligible.

In some cases, in order to reduce the computation cost, the line overlapping influence is not taken into account. Results considering and not considering the overlapping influence are listed.

3.5 References

[1]. W. Hermann, E. Schade, *Transportfunktionen von sticksoff bis 26000 K,* Zeitschrift für Physik A Hadrons and nuclei, 233, 333, (1970).

[2]. A. B. Murphy, *The effects of metal vapour in arc welding*, J. Phys. D: Appl. Phys., 434001, (2010).

[3]. A. Gleizes, J. J. Gonzalez, and P. Freton, *Topical review: thermal plasma modelling*, J. Phys. D: Appl. Phys. 38, 153, (2005).

[4]. A. B. Murphy, *Thermal plasmas in gas mixtures*, J. Phys. D: Appl. Phys. 34, 151, (2001).

[5]. R. Bini, M. Monno, and M. I. Boulos, *Numerical and experimental study of transferred arcs in argon*, J. Phys. D: Appl. Phys. 39, 3253, (2006).

[6]. A. B. Murphy, *Metal vapour causes a central minimum in arc temperature in gas–metal arc welding through increased radiative emission*, J. Phys. D: Appl. Phys. 43, 1, (2010).

[7]. M. Z. Rong, Q. Ma, Y. Wu, T. Xu, and A. B. Murphy, *The influence of electrode erosion on the air arc in a low-voltage circuit breaker*, J. Appl. Phys. 106 ,023308, (2009).

[8]. K. M. Tang, J. D. Yan, C. Chapman, and M. T. C. Fang, *Three-dimensional modelling of a dc arc plasma in a twin-torch system*, J. Phys. D: Appl. Phys. 43, 345201, (2010).

[9]. H. Nordborg and A. A. Iordanidis, *Self-consistent radiation based modelling of electric arcs: I. efficient radiation approximations*, J. Phys. D: Appl. Phys. 41, 135205, (2008).

[10]. R. W. Liebermann and J. J. Lowke, *Radiation emission coefficients for sulfur hexafluoride arc plasmas*, J. Quant. Spec. Radiat. Trans. 16, 253, (1976).

[11]. J. J. Lowke and R. W. Liebermann, *Predicted arc properties in sulfur hexafluoride,* J. Appl. Phys. 42, 3532, (1971).

[12] P. Kloc, V. Aubrecht, M. Bartlova and O. Coufal, *Radiation transfer in air and air-Cu plasmas for two temperature profiles*, J. Phys. D: Appl. Phys. 48, 055208, (2015).

[13]. D. Godin and J. Y. Trepanier, *A robust and efficient method for the computation of equilibrium composition in gaseous mixtures*, Plas. Chem. Plas. Proc. 24, 3, (2004).

[14]. W. P. White, S. M. Johnson, and G. B. Dantzig, *Chemical equilibrium in complex mixtures*, J. Chem. Phys., 28, 751, (1958).

[15]. V. Aubrecht and E. T. Protasevich, *Radiative transport of energy in SF6 arc plasma*, Izdatělstvo Tomskogo polytechničeskogo universitěta, 2000.

[16]. W. L. Wiese, M. W. Smith, and B. M. Glennon, *Atomic transition probabilities*, NSRDS-NBS 4, Vol. 1, (1966).

[17]. H. R. Griem, *Plasma spectroscopy*. McGraw-Hill, (1967)

[18]. H. R. Griem, *Semiempirical formulas for the electron-impact widths and shifts of isolated ion lines in plasmas*, Phys. Rev., 165, 258, (1968).

[19]. A. P. Hitchcock, M. J. Van der Wiel, *Absolute oscillator strengths (5-63 eV) for photoabsorption and ionic fragmentation of SF_6*, J. Phys. B: Atom. Molec. Phys. 12, 2153, (1979).

[20]. A. Gleizes, M. Gongassian and B. Rahmani, *Continuum absorption coefficient in SF_6 and SF_6-N_2 mixture plasmas*, J. Phys. D: Appl. Phys. 22, 83, (1989).

[21]. A. Burgess and M. J. Seaton, *Radiative recombination of He*, Monthly Notices of the Royal Astronomical Society, 120, 121, (1960).

[22]. V. Kokoouline and O. Dulieu, *Radiative electron attachment of molecules of astrophysical interest*, Harvard, (2012).

[23]. S. Eden, P. Limao-Vieira, P. A. Kendall, N. J. Mason, J. Delwiche, M. J. Hubin-Franskin, T. Tanaka, M. Kitajima, H. Tanaka and H. Cho, *Electronic excitation of tetrafluoroethylene, C_2F_4*, Phys. Chem., 297, 257, (2004).

[24]. L. G. Christophorou, J. K. Olthoff and M. V. V. S. Rao, *Electron interactions with CF_4*, J. Phys. Chem. 25, 1341, (1996).

[25]. L. C. Lee, E. Phillips and D. L. Judge, *Photoabsorption cross sections of CH_4, CF_4, CF_3Cl, SF_6, and C_2F_6 from 175 to 770 Å*, J. Chem. Phys. 67, 1237, (1977).

[26]. W. A. Jennifer, G. R. Burton and C. E. Brion, *Quantitative spectroscopic studies of the valence-shell electronic excitation of freons ($CFCl_3$, CF_2Cl_2, CF_3Cl, and CF_4) in the VUV and soft X-ray regions*, Chem. Phys. 221, 151, (1997).

[27]. N. T. Padial, L. A. Collins and B. I. Schneider, *Photoionization of ground-state molecular carbon C2*, Astrophys. J. 298, 36974, (1985).

[28]. A. E. Orel, T. N. Rescign, B. V. McKoy and P. W. Langhoff, *Photoexcitation and ionization in molecular fluorine: Stieltjes-Tchebycheff calculations in the static-exchange approximation*, J. Chem. Phys. 72, 1265, (1980).

[29]. Y. Itikawa, *Cross sections for electron collisions with nitrogen molecules*, J. Phys. Chem. Ref. Data 35, 31, (2006).

[30]. C. Jan, Y. Cressault, A. Gleizes, K. Bousoltane, *Calculation of radiative properties of SF_6-C_2F_4 thermal plasmas—application to radiative transfer in high-voltage circuit breakers modelling*, J. Phys. D: Appl. Phys. 47, 015204, (2014).

[31]. NIST Atomic Spectra Database Levels Form: http://physics.nist.gov/PhysRefData/ASD/levels_form.html

[32]. Atomic Spectral Line Database from CD-ROM 23 of R. L. Kurucz: http://www.pmp.uni-hannover.de/cgi-bin/ssi/test/kurucz/sekur.html

[33]. A. Gleizes, J. J. Gonzalez, B. Liani and G. Raynal, *Calculation of net emission coefficient of thermal plasmas in mixtures of gas with metallic vapour*, J. Phys. D: Appl. Phys. 26, 1921, (1993).

[34]. J. Gallagher and C. E. Moore, *Tables of spectra of hydrogen, carbon, nitrogen, and oxygen atoms and ions*, CRC Press, (1993).

[35]. A. Gleizes, B. Rahmani, J. J. Gonzalez and B. Linai, *Calculation of net emission coefficient in N_2, SF_6 and SF_6-N_2 arc plasmas*, J. Phys. D: Appl. Phys. 24, 1300, (1991).

[36]. R. A. Allen, *Air radiation tables*, NASA Contractor Report, CR-557, (1967).

[37]. W. Hermann and E. Schade, *Radiative energy balance in cylindrical nitrogen arcs*, J. Quant. Spec. Radiat. Trans. 12, 1257, (1972).

[38]. K. A. Ernst, J. G. Kopainsky and H. H. Maecker, *The energy transport, including emission and absorption, in N_2-Arcs of different radii*, IEEE Trans. Plas. Sci. 1, 3, (1973).

[39]. J. A. Fennelly and D. G. Torr, *Atomic data and nuclear data tables*, 23, 63, (1979).

[40]. N. E. Nicolet, C. E. Shepard, K. J. Clark, A. Balakushnan, J. P. Kesseling, K. E. Suchsland, and J.J. Reese Jr., *Analysis and design study for a high pressure, high enthalpy constricted arc heater,* Defense Technical Information Center report, ADA012551, (1975).

Chapter 4 Radiation transfer calculation for LTE nitrogen-PTFE mixture gas plasma

4.1 Introduction of radiation transfer in arc plasma

Radiation plays important roles that can affect the behaviour of plasma in an electric arc or a thermal plasma. During arc processing, the total radiation of an arc plasma is its energy loss, which can cause the electric arc to cool. The aim of a circuit breaker is to rapidly extinguish an electric arc through separating electric contacts. The total radiation, therefore, plays a determining role in a circuit breaker's performance. Furthermore, radiation transfer research can be used for applications like particles heating[1] or plasma torches, but those are not the purpose of this research.

Generally, the direction of radiation transfer within an arc plasma starts from the arc core (hot regions). The energy is emitted from the arc core to the cold regions such as the edge of the plasma. Energy can be transferred completely in hot regions. However, it has to be absorbed partially in relatively cool regions. When the radiation reaches the cold region, the remaining energy will be absorbed. The energy transfer will determine the temperature distribution in an arc plasma. In most cases, an electric arc is generated in the throat of the PTFE nozzle. The throat surface is called the wall. If the dimension of the throat is small enough (less than the edge of the cool region), material ablation will occur due to the high temperature. The PTFE ablation will influence the arc behaviour as well, which is why it is necessary to consider radiation transport in arc plasma modelling.

The physical quantity described in radiation transfer is radiation flux. Simulation of arc plasma modelling is based on the energy balance equation[2], in which radiation flux is one of the most important terms. Chapter three introduced the theory of net emission coefficient (NEC). This is the simplest way to replace radiation flux as a term in the energy balance equation. It can be tabulated as a function of temperature. However, it can only be applied in the hot regions in which reabsorption is usually neglected. Fig. 4-1 shows the typical temperature profile of an electric arc. In the cool region, which is region two in Fig. 4-1, the radiation transfer equation (RTE) must be solved to obtain the radiation flux. Radiation transfer is complicated to compute because it is not only a space-dependent variable (related to plasma temperature or its number density), but also a spectral-dependent variable (related to the absorption coefficient of plasma). This results in a prohibitive computation time being needed to solve the RTE. Therefore, a simpler solution is necessary. The number density of plasma can be determined once the temperature is given. If an efficient way of determining the absorption coefficient can be identified, it will save computation time for solving RTE. Some authors came up with the idea of an effective absorption coefficient as a function of a space variable, such as pressure, temperature or plasma composition. However, the accuracy is doubtful[3,4,5,6]. Another suggestion is averaging the absorption coefficient in frequency bands, which is called the mean absorption coefficient (MAC).

Besides solving the RTE directly, many approximate methods have been developed. A partial characteristics method was developed by Sevast' yanenko[7], who identified two parameters, Som and $\Delta \mathrm{Sim}$, which describe the absorption and emission of radiation in a given direction. Those two values can be tabulated for a specific gas before starting the simulation work. It is complex as well, but the simulation is rapid. P1 approximation is another effective method of calculating radiation flux for plasma modelling. P1 approximation was first

developed by Jeans[8] in 1917, but Kourganoff further described this method in 1952[9]. The value of this method is the governing equation, which is a simple partial differential equation (PDE), which means that this approximation can be solved in low order equations. The computation cost is much less than that required for solving the RTE and it has good accuracy for media near-isotropic radiative intensity [10] . Gelbard improved the P1 method to high-order approximation to increase its accuracy; it is known as SP_N. The discrete ordinate method (DOM) is another approximation method used to simplify RTE. Details of DOM have been given by Charest[11].

In this chapter, the radiation transfer flux in an arc plasma will be calculated. Results obtained by P1, DOM and exact solution of the RTE will be compared. In accordance with the aim of this project, a nitrogen-PTFE mixture plasma will be used as the medium. The results will be plotted with different N_2-PTFE molar proportions at different pressures under LTE conditions. To further discuss the application of the calculation results, simulation of arc modelling will be introduced that corresponds to an existing experimental environment. The results of radiation transfer flux will be applied in the simulation work. The arc behaviour of the simulation will be compared with the experimental results from different methods of radiation transfer. Further introduction to the simulation and the experiment will be provided in a later section.

4.2 Methods of radiation transfer calculation

In general, thermal radiative energy consists of electromagnetic waves because the particles absorb energy. Thus, it is easy to predict the radiation of liquids and solids by applying electromagnetic wave theory, while the radiation of gases can be obtained from quantum mechanics.

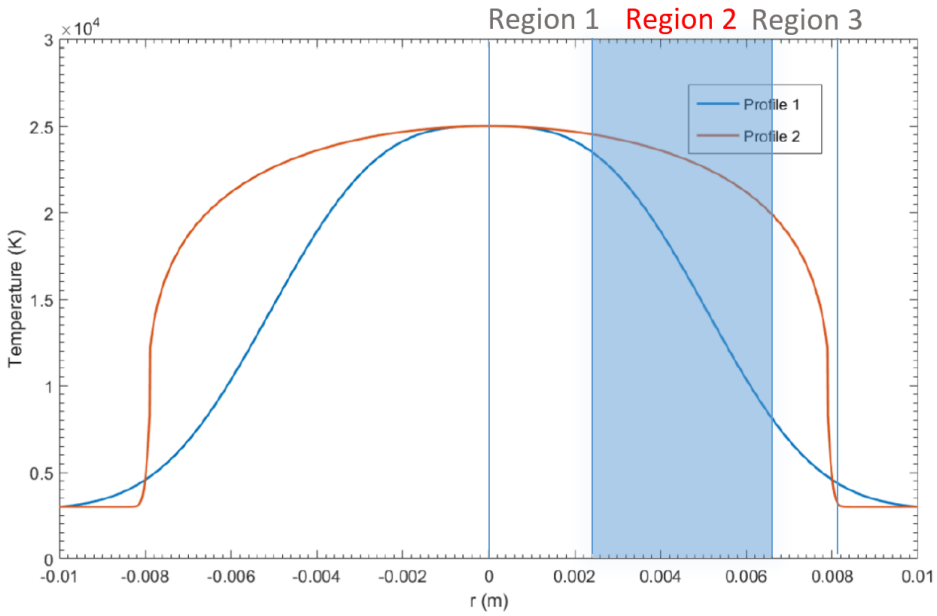

Fig. 4-1: Typical temperature profile of electrical arc: this chapter will focus on the region 2

4.2.1 Radiation intensity

Radiation transfer in plasma can be emitted, absorbed and scattered by the medium. Once radiation is emitted from the source, it is transferred via a path straight to cold regions of plasma. During this process, radiation will be attenuated by absorption and scattering. The amount of radiation absorption is proportional to the magnitude of incident radiation and the distance of radiation has travelled from the source.

$$dI_{v,abs} = -\kappa_v I_v dl \qquad (4.1)$$

where the I_v is the radiation intensity and κ_v is the absorption coefficient at frequency v. The negative sign indicates that the radiation is reduced. Assuming the radiation travelled over path l, the radiation intensity takes into account emitting and absorption only. This can be expressed as Eq.(4.2):

$$\mathrm{I}_v(l) = \mathrm{I}_v(0)\exp(-\int_0^l \kappa_v\, dl) = \mathrm{I}_v(0)\exp(-\tau_v) \qquad (4.2)$$

$$\tau_v = \int_0^l \kappa_v dl \tag{4.3}$$

τ_v is the optical thickness of absorption through the radiation travelling path l.

The $\mathrm{I}_v(0)$ indicates the intensity emitted from the source, which is $l = 0$. With LTE condition, the intensity of the source is equal to the blackbody intensity[42] B_v , which is a function of the magnetic wave frequency:

$$\mathrm{B}_v = \frac{2hv^3}{c^2} \frac{1}{\exp\left(\frac{hv}{kT}\right) - 1} \tag{4.4}$$

where h is the Planck constant, c is the speed of light, and k is the Boltzmann constant.

When the radiation wave meets the particle on its route, it will be partially absorbed by the particle. The radiation intensity is a parameter that describes the radiative flux per unit solid angle. Assume the radiation energy is passing a cross-section, the area of which is dS.

Eq.(4.5) describes the radiation intensity.

$$\frac{dI_v}{dl} = -\kappa_v(B_v - I_v) \tag{4.5}$$

Solution of the radiation transfer equation

The radiation transfer equation (RTE) can be written as Eq. (4.6).

$$\hat{\mathrm{s}} \cdot \nabla I_v(R, \hat{\mathrm{s}}) = \kappa_v(B_v - I_v) \tag{4.6}$$

where I_v is the spectral radiative intensity that was introduced in the last section. $I_v(R, \hat{\mathrm{s}})$ indicates the intensity at point R, and it goes along with direction $\hat{\mathrm{s}}$, while frequency is v.

However, when discussing radiation flux or divergence of radiation flux, it is necessary to describe the quantity of radiation transfer. Radiation flux is also called radiative heat flux, shown below:

$$\mathbf{F}_v(\boldsymbol{r}) = \int_{4\pi} d\hat{\boldsymbol{s}}\hat{\boldsymbol{s}} I_v(\boldsymbol{r}, \hat{\boldsymbol{s}}) \tag{4.7}$$

Furthermore, to diverge the radiative heat flux, it is important to determine the interaction of radiation and the species in plasma:

$$\nabla \cdot \mathrm{F}_v = -\kappa_v \int_{4\pi} d\hat{s} \int_0^{\infty} dl \frac{dB_v}{dl} e^{-\int_0^l dl' \kappa_v(l')} \tag{4.8}$$

4.2.2 Approximate solution of RTE

There is a schematic presentation of the domain cross section in Fig. 4-2. The round shape with the centre at S indicates the cross section of the arc. Along with line SR, point R is where the divergence of radiation flux will be evaluated at. The divergence of radiation flux can be influenced by any point on plane S. Along with the point on line AB, point X is one of the points that contributes radiation on R. Due to difficulty is obtaining the distance between the arc core to X which is r shown in diagram. A reference plane perpendicular to plane S intersects with line AB to explain the calculation of r. The angle φ and ζ, which is the length between X and R along with AB, is known. Assume lines YS and SR are perpendicular to the plane YSR. It is then possible to find the relationship between r and φ, θ, ζ. During the calculation process, the range of θ is from $-\pi$ to π, which can cover all the points on line AB. Once r is obtained, the temperature on point X is obtained according to the temperature profile.

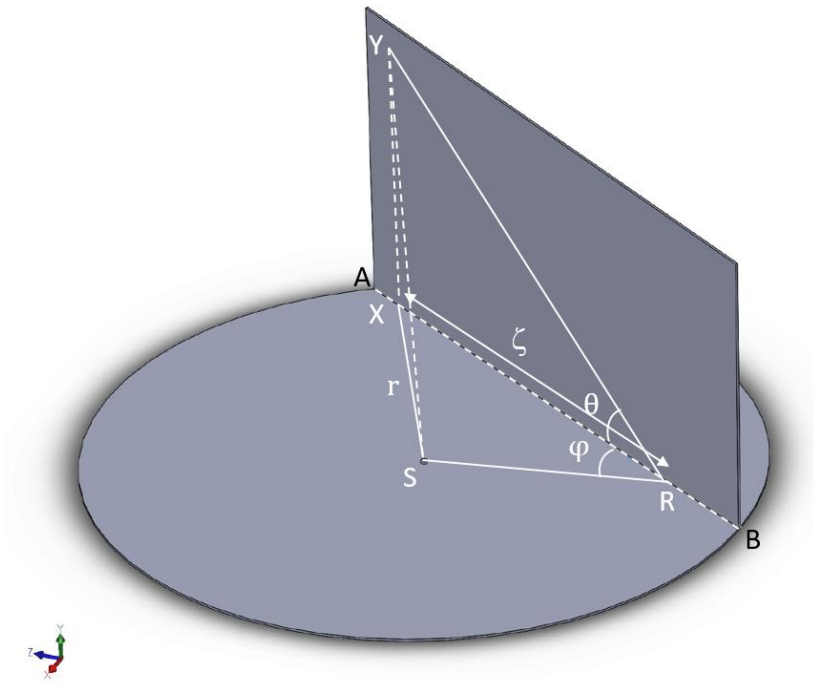

Fig. 4-2: Schematic representation of computational domain cross section.

P1 approximation

P1 approximation actually simplifies the RTE into an elliptic partial differential equation of lower order. The unknown in this PDE is the incident radiation intensity G.

$$\nabla \cdot \left(-\frac{1}{3\kappa_v(T)}\nabla \mathrm{G}_v\right) + \kappa_v(T)G_v = \kappa_v(T)G_v^0(T) \tag{4.9}$$

where $G_v^0(T)$ can be obtained by

$$G_v^0 = 4\pi I_v^0(T) \tag{4.10}$$

Once $G_v^0(T)$ is solved from this equation, G_v can be used to calculate divergence of radiation flux ∇F.

DOM approximation

DOM is the method that replaces integrals over all directions by numerical quadrature. It follows the equation:

$$\nabla \mathrm{F}_{\nu} = \kappa_{\nu} \sum_{j}^{n} \omega_j \left[B_{\nu}(0) e^{-\int_0^{x_{wall,j}} k_{\nu}(x_j) dx_j} - \int_0^{x_{wall,j}} \left(B_{\nu}(x_j) - B_{\nu}(0) \right) \kappa_{\nu}(x_j) e^{-\int_0^{x_j} \kappa_{\nu}(\zeta_j) d\zeta_j} dx_j \right] \tag{4.11}$$

where ω_j is the weight associated with the direction, the number of which is reported in Michael's book[42]. It can be summarized with the equation below:

$$\omega_j = d\varphi * (\sin\left(\theta_j + \frac{1}{2} d\theta\right) - \sin(\theta_j - \frac{1}{2} d\theta)) \tag{4.12}$$

$d\varphi \; and \; d\theta$ are determined by the resolution of DOM bands. As described in the last section, the Discrete Ordinates Method (DOM) chooses several different φ, θ. The choice can, however, influence the accuracy of results. During the calculation of Nordborg[12] and Randrianandraina[13], no more than 40 directions are chosen, but the results retain accuracy well. In this case, eight unique directions of angles of φ from 0 to π and five unique directions of angles of θ from 0 to $\frac{\pi}{2}$ are chosen. Thus, 112 unique directions need to be computed over the whole computational domain. Notably, this is the work for one interesting point, which is R, shown in Fig. 4-2. There are 100 interesting points along the arc core to the edge of plasma.

4.2.3 Mean absorption coefficient (MAC)

The NEC cannot be used to estimate the absorption of radiation in cool and cold regions, leading to huge computation cost if the found spectral absorption coefficient is employed to obtain radiative absorption in the regions in which the temperature is lower than the arc core. It is necessary to find an approximate method to describe absorption coefficient for each temperature. With the MAC method, the integration of absorption coefficient of each frequency can be replaced by integration of the MAC of each band. Calculation of radiation flux requires integration calculation of absorption coefficient with

the same frequency but different temperature, which then integrates results over all frequencies. Without MAC, it costs too much to calculate the absorption coefficient even if it is stored in memory. Thus, the primary step is to split the spectrum into several intervals. Fig. 4-3 shows the absorption coefficient for 90% nitrogen -10% PTFE molar proportion mixture plasma with temperature of 8000K and pressure of 1 bar. The boundary of 9 spectral bands is also plotted. The boundary is given by considering the jumping of the absorption coefficient. The full range of the absorption coefficient is $1X10^{14}$ Hz to $1X10^{16}$ Hz. The frequency of the first band is higher than the second band, and so on. The first band is contributed by most atom ionization such as nitrogen, fluorine and carbon atom. The second band is contributed by dissociation of molecules CF_2 and C_2F_3N. Band six is due to the dissociation of CN. The frequency of the electromagnetic wave because of species dissociation or ionization is the property independent of temperature and pressure. This interval can be applied on a spectrum of different temperatures and pressures.

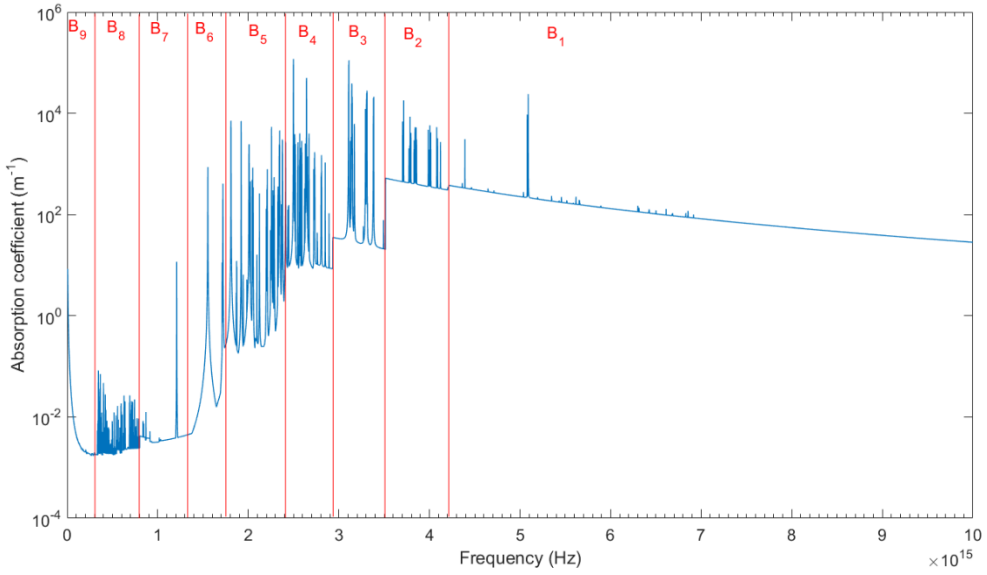

Fig. 4-3: Evolutions of the continuum absorption coefficient for 90% nitrogen -10% PTFE molar proportion at the temperature of 8,000 K and pressure of 1 bar. The 10 intervals are plotted in the vertical full red lines. The numbering of the intervals is indicated in the figure.

Randrianandrain[13] summarized three methods of MAC: normal[14], Roasseland[15], and Planck[16] MAC. Normal MAC is defined by the MAC definition that is expressed in Eq. (4.13). Opaque medium usually causes a high absorption coefficient. Rosseland MAC was derived to resolve this problem. It has better approximation at high pressure. The Planck MAC actually is a 'modified Planck' because an exponential term has been introduced into the original Planck MAC. Randrianandraina reported that the original Planck MAC method yields poor results with high absorption coefficients, making it inappropriate for absorption coefficient due to ionization of most atom species. The exponential term can reduce the atomic lines of the first band. However, calculation of Planck MAC has to be linked to thermal radius R_p in NEC expression.

$$\overline{\kappa_{Nor,Band_i}} = \frac{1}{\Delta v}\int_{v_{down,Band_i}}^{v_{up,Band_i}} \kappa_v dv \tag{4.13}$$

Eq.(4.13) presents the normal MAC expression. $v_{up,Band_i}$ and $v_{down,Band_i}$ indicate the two boundary frequencies for band i. κ_v is the absorption coefficient of fine spectrum at frequency v. dv is the frequency resolution of fine spectrum. Δv is the frequency difference between two boundaries.

$$\overline{\kappa_{Rosseland,Band_i}} = \frac{\int_{v_{down,Band_i}}^{v_{up,Band_i}} \frac{dB_v^0}{dT}\kappa_v dv}{\int_{v_{down,Band_i}}^{v_{up,Band_i}} \frac{dB_v^0}{dT} dv} \tag{4.14}$$

Eq.(4.14) shows the Rosseland MAC method. The only difference from Eq.(4.13) is the term B_v^0, which is the black body radiation intensity that was expressed in Eq.(4.4). In Rosseland MAC, the black body radiation intensity can be obtained according to the frequency v.

$$\overline{\kappa_{Planck,Band_i}} = \frac{\int_{v_{down,Band_i}}^{v_{up,Band_i}} B_v^0 \kappa_v e^{-\kappa_v R_p} dv}{\int_{v_{down,Band_i}}^{v_{up,Band_i}} B_v^0 dv} \quad (4.15)$$

Eq.(4.15) shows the Planck method. As mentioned, an exponential term is multiplied with the original term. R_p is the thermal radius.

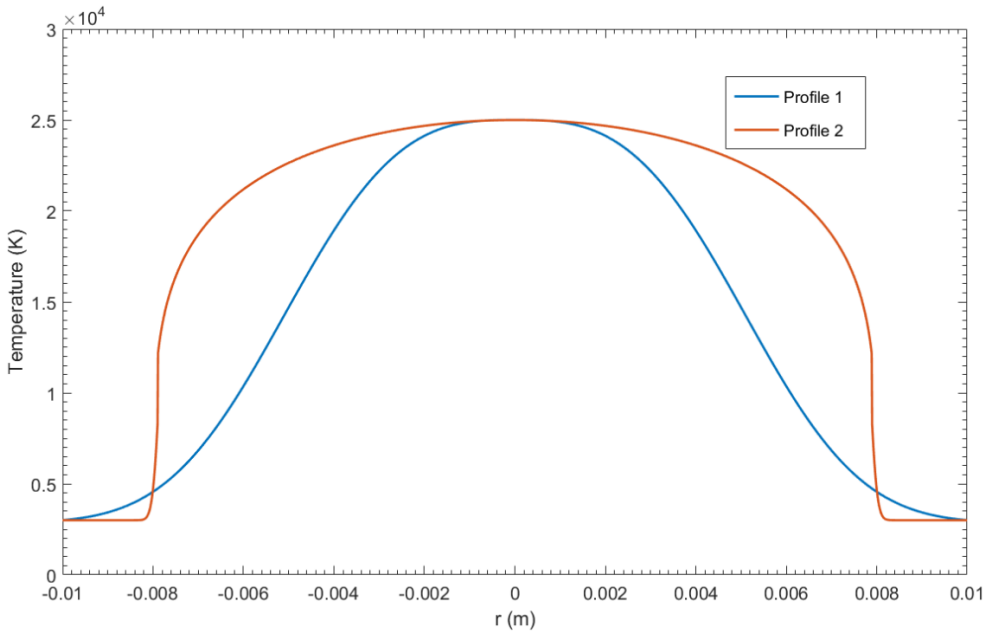

Fig. 4-4: Temperature profiles used in the calculations of the divergence of the radiative flux

4.2.4 Calculation program

The calculation program is developed in C++. Amazon Elastic Compute Cloud (EC2) provides the calculation resources to complete the calculation. It has 36 cores of Intel Xeon E5-2666 v3 processors. The parallel calculation can increase efficiency sufficiently. Each interested point can be calculated individually. The 100 points are separated into 34 files; 3 points are included in 33 files, and one point is in the last file. Thirty-four mirrors of the program were

created, and each of them read one of the files. This produces 34 threads to do calculation in 34 CPU cores with full performance at the same time.

4.3 Results and discussion

4.3.1 Approximation of different MAC

Fig. 4-5 and Fig. 4-6 show the calculated fine spectrum of absorption coefficient for 90% nitrogen and 10% PTFE at 1 bar at 8,000 K and 25,000 K, respectively. The results are compared with normal MAC, Rosseland, Planck and MMP.

Fig. 4-7 shows the NEC results calculated by fine spectra, Normal, Rosseland, Plank, and Mixed Mean Planck method. The results obtained by MAC methods are agree with results by fine spectrum. The Normal MAC leads the radiation taken in account higher than rest of three MAC methods. That results NEC by Normal method slightly higher when temperature is below than 20,000 K. It enlarges the difference when temperature is higher than 20,000 K, due to the Normal MAC is more sensitive at high temperature. The NEC calculated by Rosseland MAC has better agreement when temperature is lower than 25,000 K, while the Mixed Mean Planck MAC has more accurate when temperature higher than that.

4.3.2 Radiation flux by different approximation methods

Different approximations to solve RTE have been discussed. A few selected calculation results for divergence of radiative flux are represented in Fig. 4-8 to Fig. 4-13. Considering that the frequency resolution of the absorption coefficient determines the accuracy of results and calculation time, 10 GHz has been chosen as the frequency step. It has 98% agreement with results obtained by 1 GHz under the same conditions but only costs 8% of calculation time. Corresponding to the temperature profile, the temperature of the arc core is 25,000 K, while the temperature of the wall is 3,000 K. The distance of the arc

core to the wall is 0.01 m. There are 100 interested points distributed over the axis, and the accuracy of points is $1X10^{-4}$ m. The divergence of radiative flux is carried out by DOM 8-5 (8 of φ and 5 of θ), DOM 5-3, P1 approximation, exact angular.

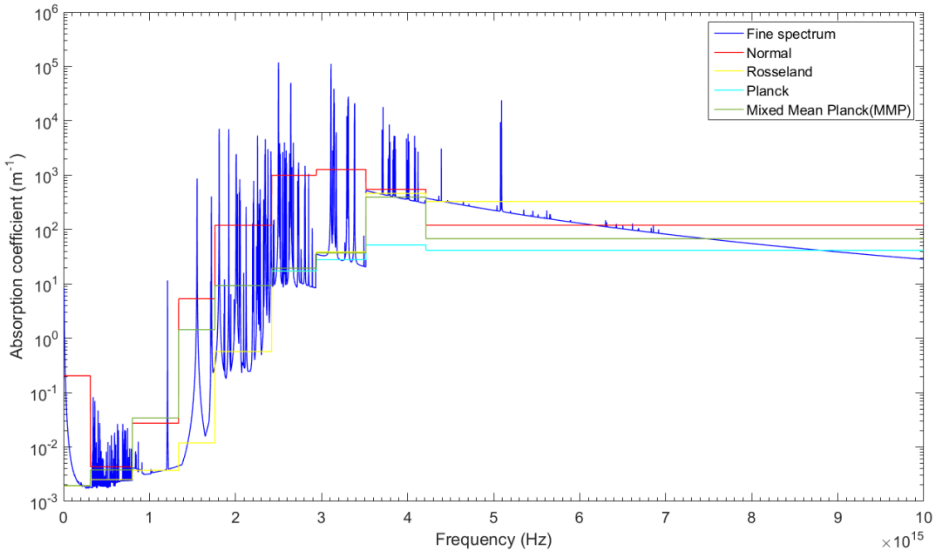

Fig. 4-5: Fine absorption spectrum for 90% nitrogen -10% PTFE molar proportion at temperature of 8000 K and pressure of 1 bar. Normal, Rosseland, Planck and Mixed Mean Planck (MMP) are also presented.

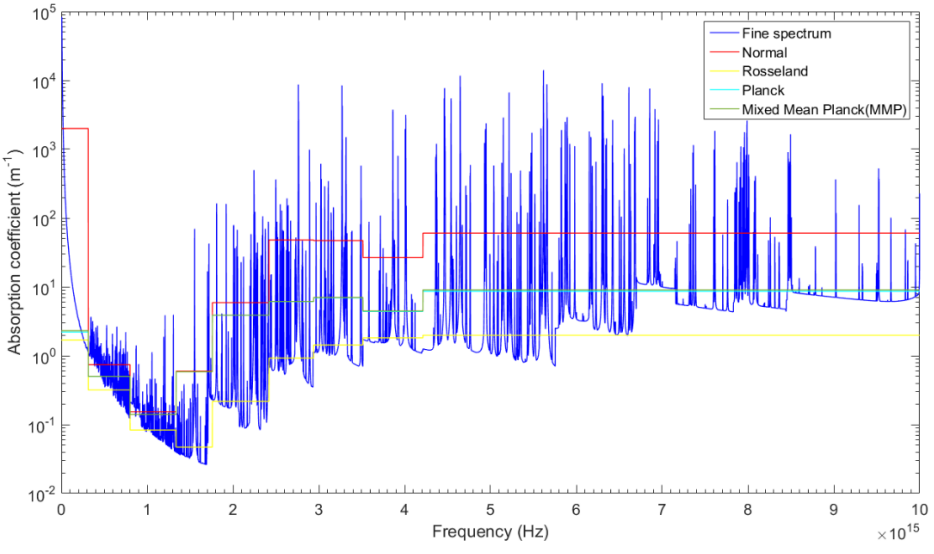

Fig. 4-6: Fine absorption spectrum for 90% nitrogen -10% PTFE molar proportion at temperature of 25000 K and pressure of 1 bar. Normal, Rosseland, Planck and Mixed Mean Planck(MMP) are also presented.

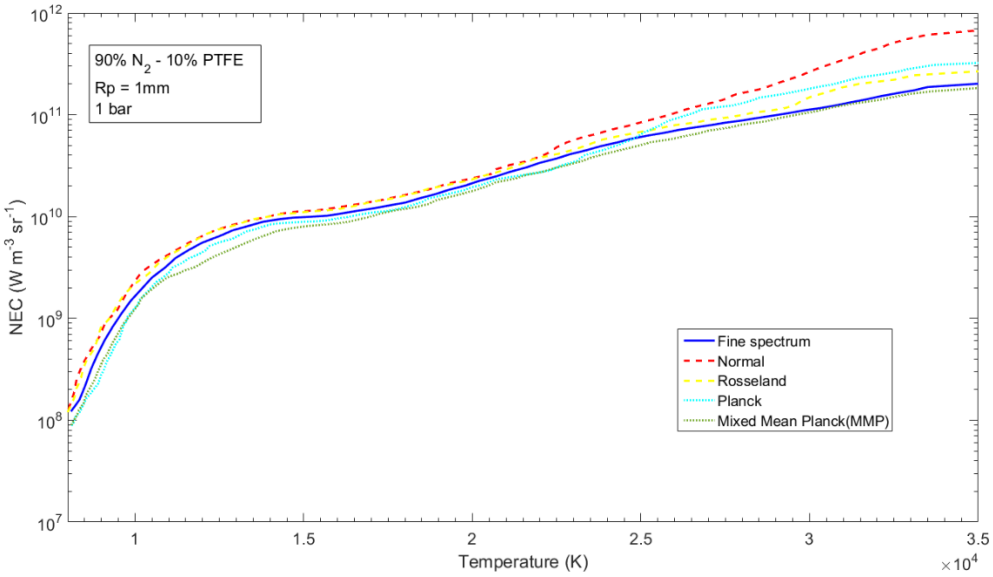

Fig. 4-7: Comparison of NEC calculated by fine spectra and different MAC method from normal, Rosseland, Planck and MMP.

In Fig. 4-8, the influence of different nitrogen and PTFE molar proportions on divergence of radiation flux is represented. The P1 approximation has overestimated the radiation flux on the arc core and wall region. With higher nitrogen molar proportion, P1 results show worse estimation. However, P1 is still the first choice in many arc model simulations because of its much smaller computation cost. The results of radiation flux by DOM with 8-5 bands show better performance than 5-3 DOM on different molar proportions cases. It is reasonable because it considers more directions in 8-5 DOM.

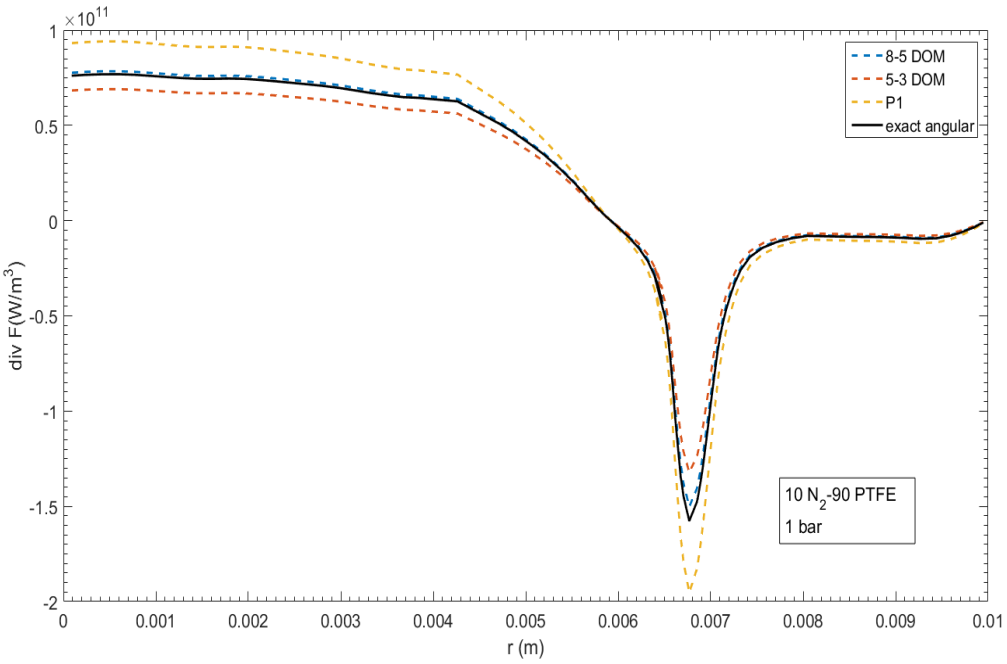

(a)

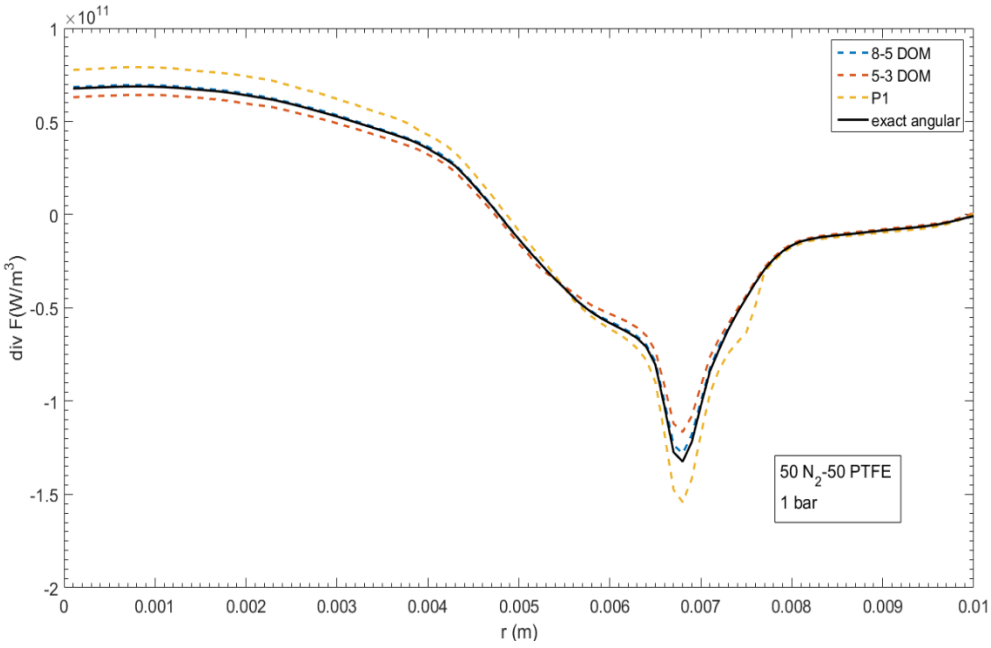

(b)

Fig. 4-8: Calculated divergence of the radiation flux for different molar proportions of nitrogen and PTFE based on temperature profile 1 at 1 bar.

Fig. 4-9 and Fig. 4-10 show different divergences of radiation flux with 8 bar and 32 bar pressures. It results in 402.3% and 2296.7% higher divergence of radiation flux for 10% N_2-90% PTFE at 1 bar. However, the increasing rate drops down to 375% and 2205.3% with 50% nitrogen molar proportion. The overestimation rate of P1 approximation has a tendency to get smaller in higher pressure situations. The computation time for different approximation methods varies. The P1 approximation costs 10 minutes in one interested point. One case of divergence of radiation flux takes 30 minutes (34 threads parallel calculation). Calculation of 5-3 DOM costs about 4 hours total, while 8-5 bands take 7.5 hours for one case. The exact angular yields the most accurate results, but it costs 23 hours to obtain the result for one calculation. This is why P1 approximation is still the most popular method in arc simulation.

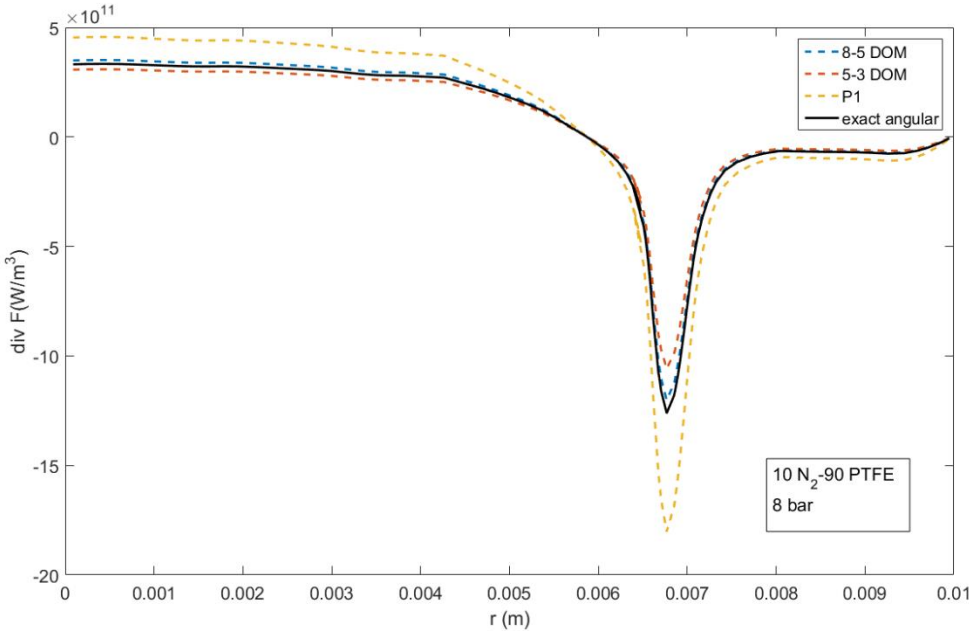

(a)

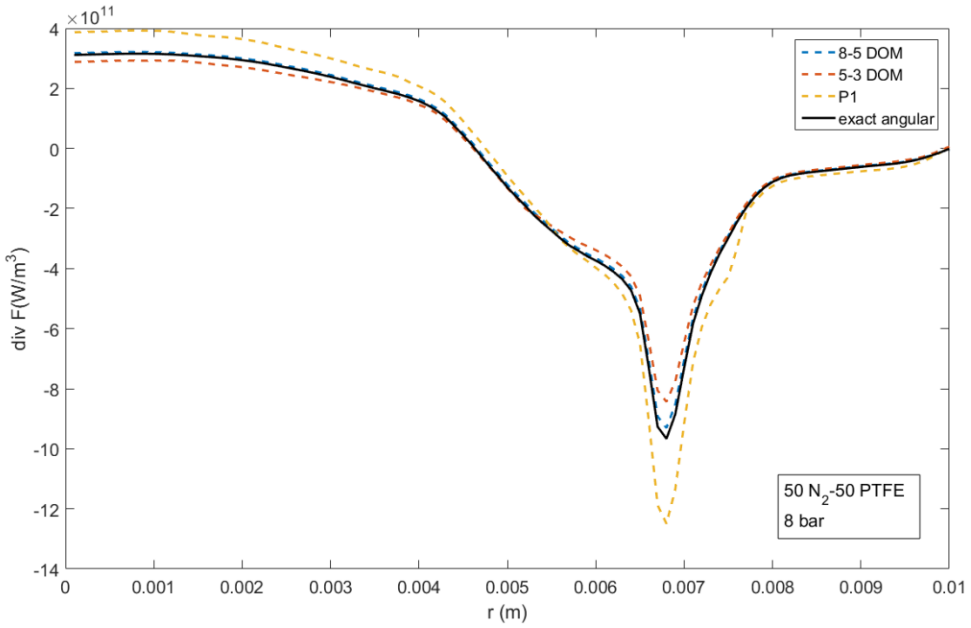

(b)

Fig. 4-9: Calculated divergence of the radiation flux for different molar proportions of nitrogen and PTFE based on temperature profile 1 at 8 bars.

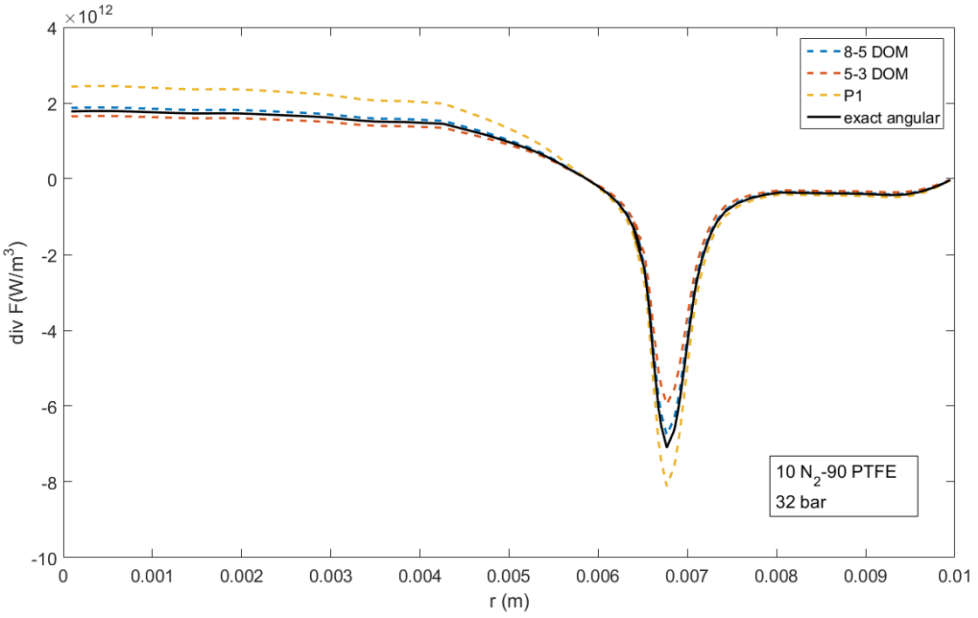

(a)

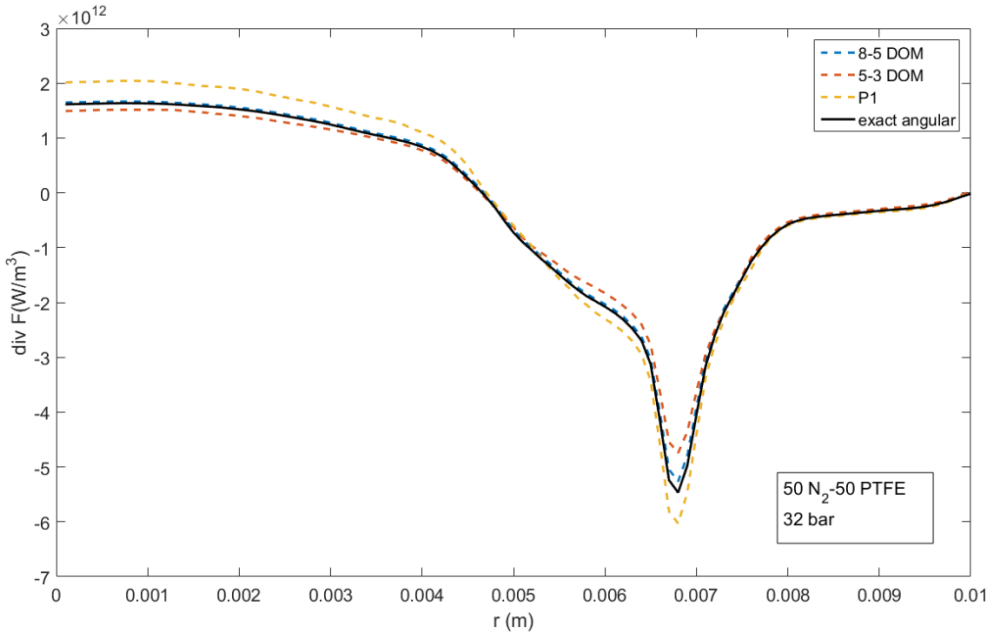

(b)

Fig. 4-10: Calculated divergence of the radiation flux for different molar proportions of nitrogen and PTFE based on temperature profile 1 at 32 bars.

Fig. 4-11 shows that, because the temperature profile has been changed, the divergence of radiation flux remains high until the temperature drops. Like the results for profile 1, P1 approximation overestimated the results, especially in regions close to the arc wall. The best fit approximation method is 8-5 DOM. Fig. 4-12 and Fig. 4-13 represent the divergence of radiation flux in high pressures.

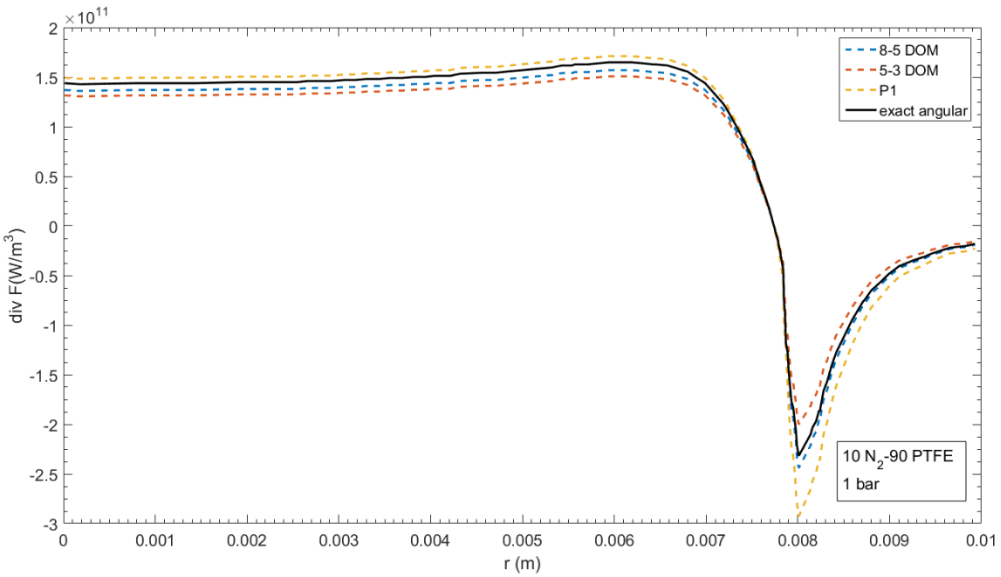
×10^11
2
1.5
1
0.5
0
-0.5
-1
-1.5
-2
-2.5
-3
div F(W/m^3)
0
0.001
0.002
0.003
0.004
0.005
0.006
0.007
0.008
0.009
0.01
r (m)
8-5 DOM
5-3 DOM
P1
exact angular
10 N2-90 PTFE
1 bar

(a)

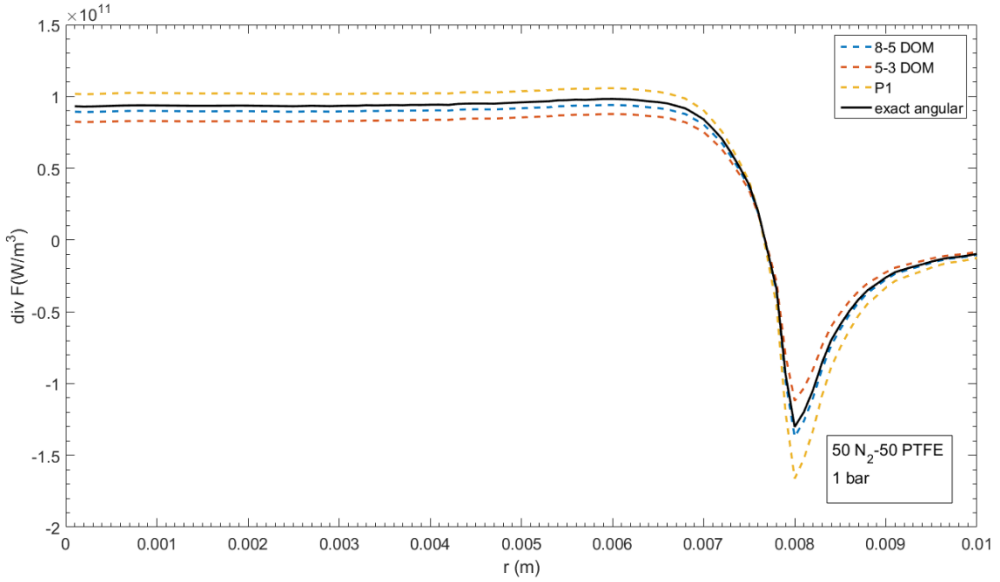
×10^11
1.5
1
0.5
0
-0.5
-1
-1.5
-2
div F(W/m^3)
0
0.001
0.002
0.003
0.004
0.005
0.006
0.007
0.008
0.009
0.01
r (m)
8-5 DOM
5-3 DOM
P1
exact angular
50 N2-50 PTFE
1 bar

(b)

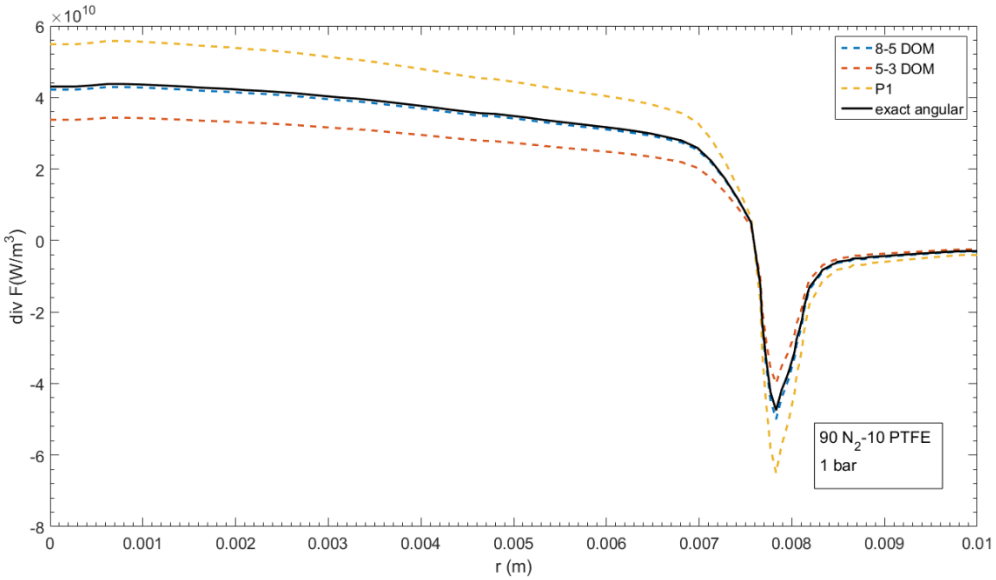

(c)

Fig. 4-11: Calculated divergence of the radiation flux for different molar proportions of nitrogen and PTFE based on temperature profile 2 at 1 bar.

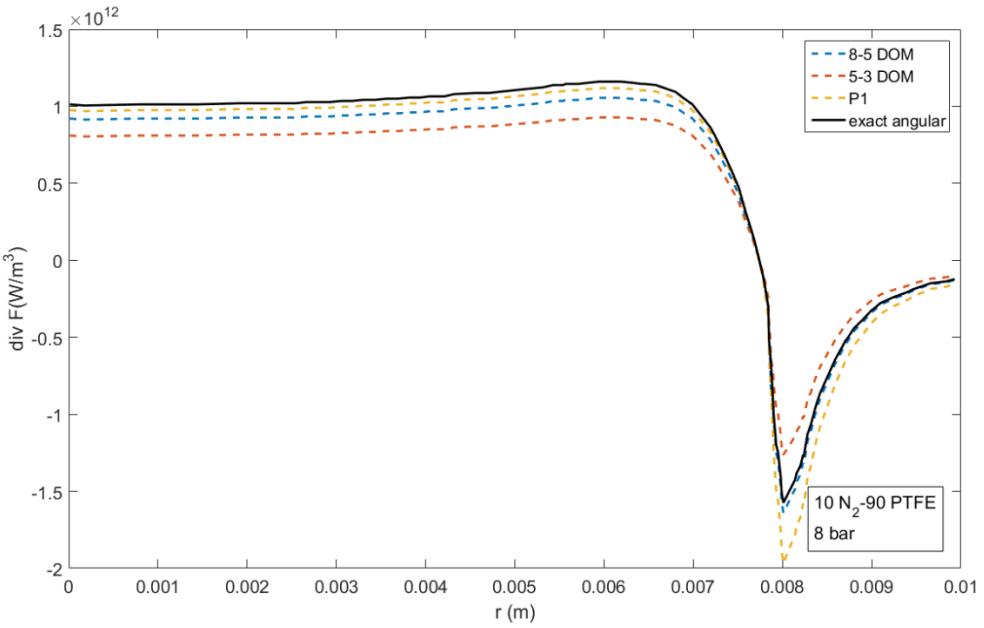

(a)

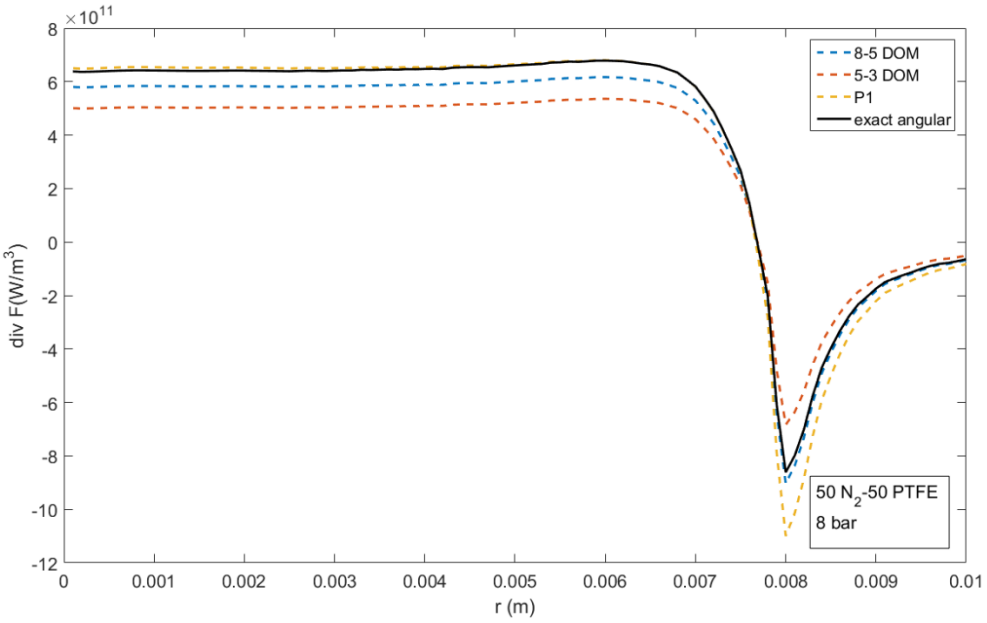

(b)

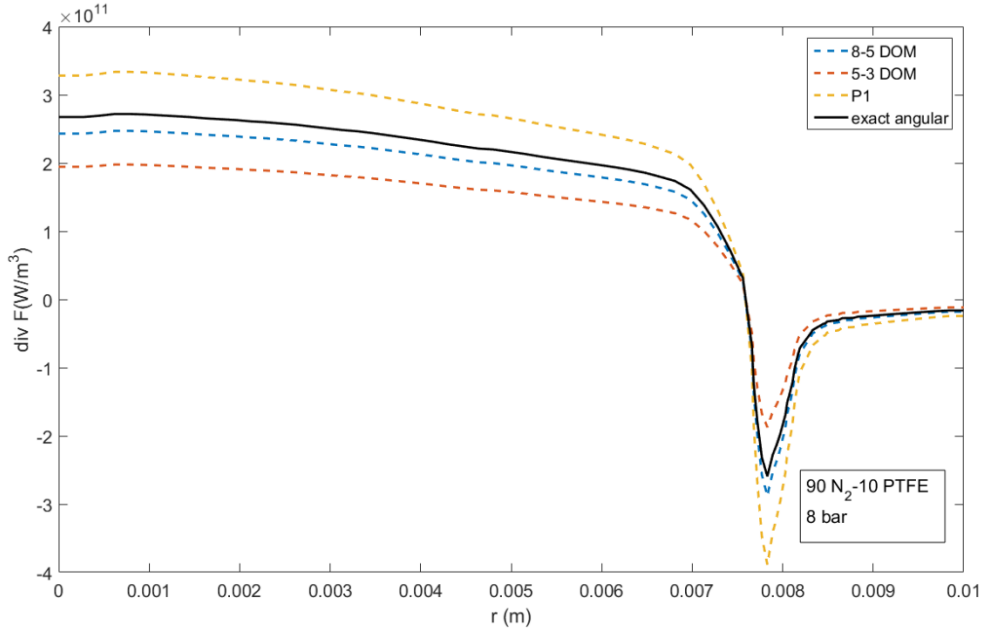

(c)

Fig. 4-12: Calculated divergence of the radiation flux for different molar proportions of nitrogen and PTFE based on temperature profile 2 at 8 bars.

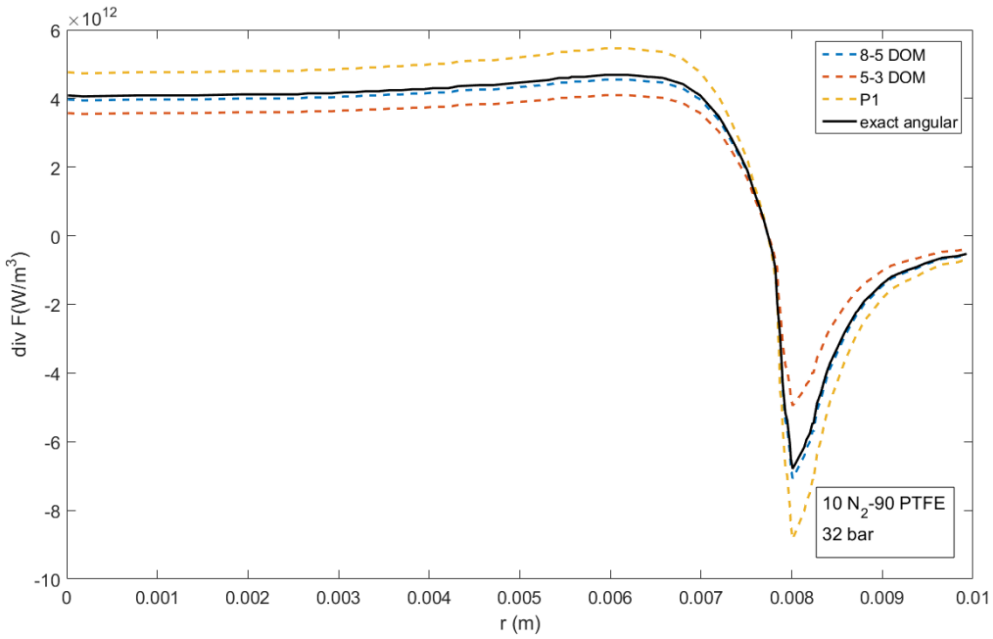
×10^12
6
4
2
0
-2
-4
-6
-8
-10
div F(W/m^3)
0
0.001
0.002
0.003
0.004
0.005
0.006
0.007
0.008
0.009
0.01
r (m)
8-5 DOM
5-3 DOM
P1
exact angular
10 N2-90 PTFE
32 bar

(a)

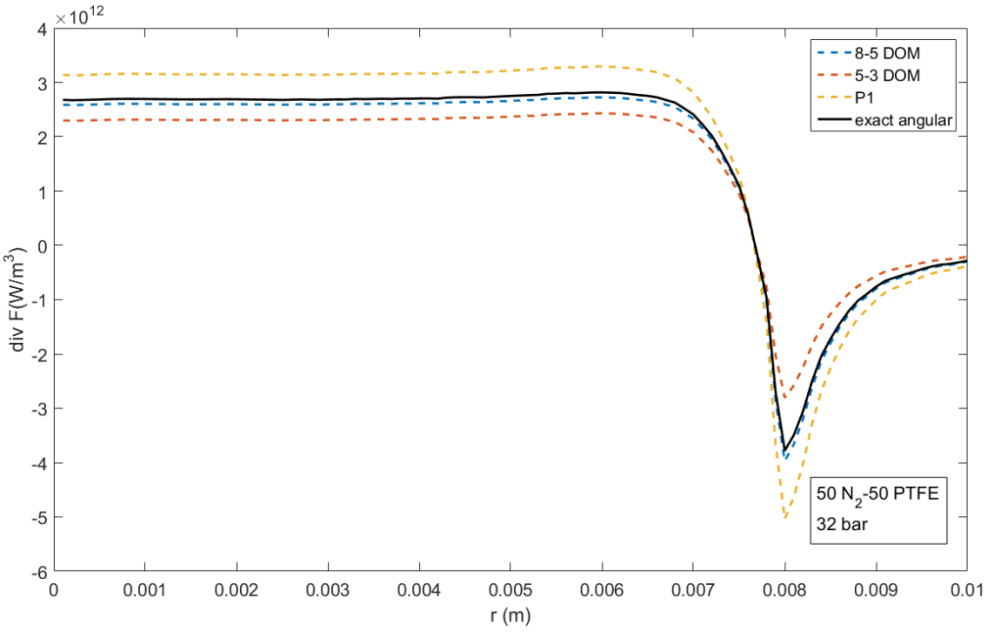
×10^12
4
3
2
1
0
-1
-2
-3
-4
-5
-6
div F(W/m^3)
0
0.001
0.002
0.003
0.004
0.005
0.006
0.007
0.008
0.009
0.01
r (m)
8-5 DOM
5-3 DOM
P1
exact angular
50 N2-50 PTFE
32 bar

(b)

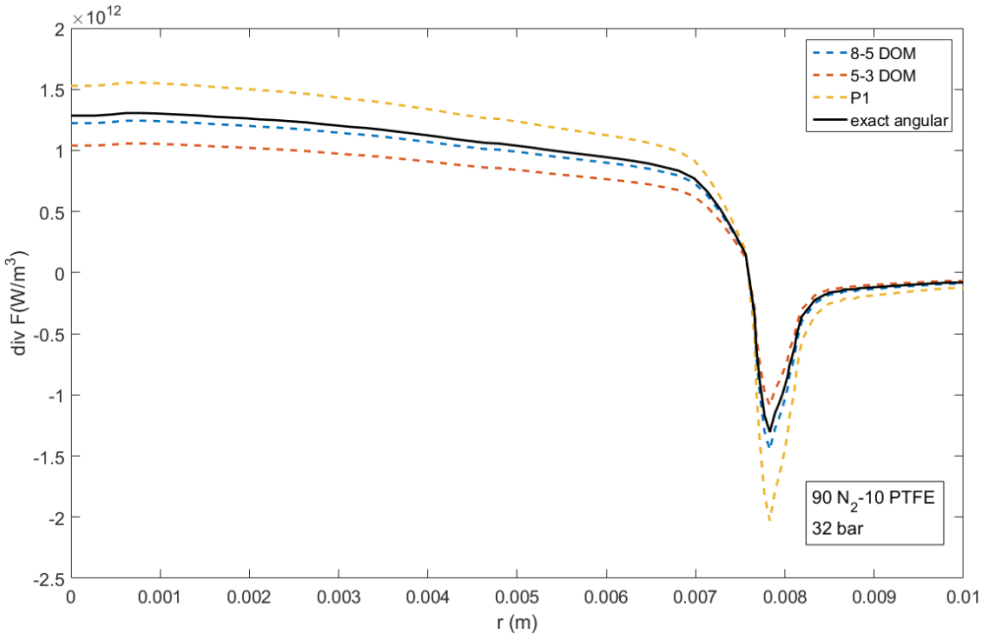

(c)

Fig. 4-13: Calculated divergence of the radiation flux for different molar proportions of nitrogen and PTFE based on temperature profile 2 at 32 bars.

4.3.3 Discussion of NEC and divergence of radiative flux

NEC is an approximation method to describe radiation transfer in an isothermal cylinder. In arc simulation, there is a term related to radiation flux in plasma. Researchers usually replace this term with NEC. It can estimate divergence of radiation to some degree. In the centre of the arc plasma region, the relationship of NEC to divergence of radiation flux can be expressed as:

$$4\pi\varepsilon_N = \nabla F \tag{4.16}$$

Fig. 4-14 shows the results of $4\pi * \mathrm{NEC}$ compared with divergence of radiative flux for two temperature profiles. The red line indicates the temperature profile. In the region of near-constant temperature, the radiation calculated by NEC model has good agreement with the divergence of radiative flux in both

temperature profiles. Once the temperature starts to drop, the NEC model can hardly estimate the real situation of radiation transferring in the arc plasma. This corresponds to the primary assumption of NEC, which describes radiation in an isothermal cylinder.

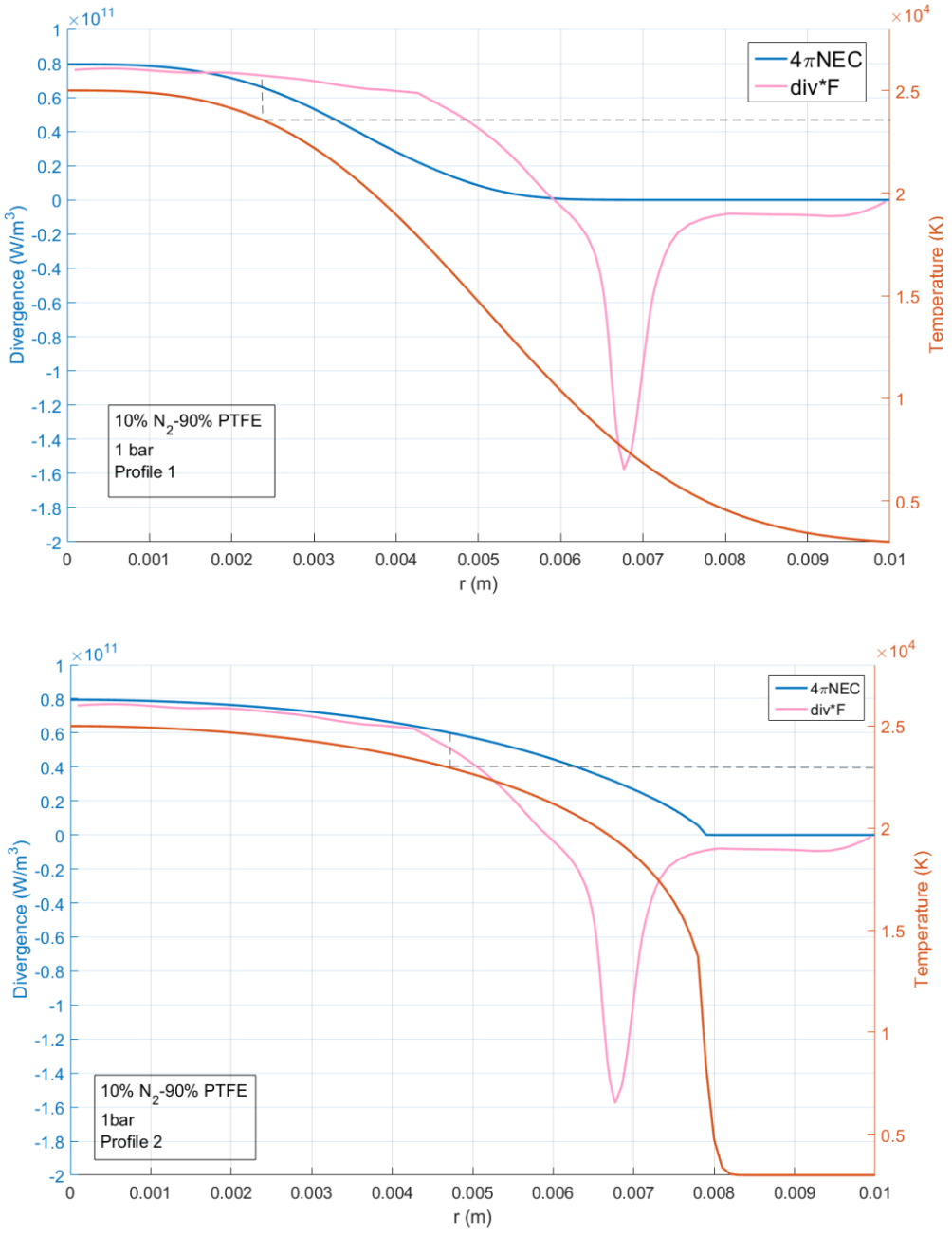

Fig. 4-14: Calculated $4\pi * \mathrm{NEC}$ compared with divergence of radiative flux for two temperature profiles

4.4 Summary

The calculation methods for radiation transfer in nitrogen-PTFE arc plasma have been introduced. The methods include P1 approximation and two DOM approaches. The results yielded by those approximation methods show good performance. P1 approximation requires much less computation resources than the other two methods. However, 8-5 DOM gives the best agreement with the exact value. It is a trade-off between calculation time and accuracy of results.

Comparing these results with the NEC results obtained in the last chapter indicates that $4\pi \cdot$NEC can only be used to replace the divergence of radiative flux in the arc core region. In the cool region and the arc wall, due to the re-absorption of particles, NEC is no long valid.

MAC is another way of saving computation costs for radiation flux calculation. The division of frequency bands and choice of methods determines the accuracy of results. Rosseland MAC has good performance on high pressure.

4.5 References

[1]. A. Gleizes, J. J. Gonzalez and P. Freton, *Thermal plasma modelling*, *J. Phys. D: Appl. Phys.* 38, 153, (2005).

[2]. J. J. Lowke, *Prediction of arc temperature profiles using approximate emission coefficients for radiation losses*, *J. Quant. Spectrosc. Radiat. Transfer,* 14, 111, (1974).

[3]. H. R. Griem, *Principles of plasma spectroscopy,* Cambridge University Press, (1997).

[4]. R. W. Liebermann and J. J. Lowke, *Radiation emission coefficients for sulfur hexafluoride arc plasmas*, J. Quant. Spectrosc. Radiat. Transfer, 16, 253, (1976).

[5]. A. Gleizes, B. Rahmani, J. J. Gonzalez and B. Liani, *Calculation of net emission coefficient in N_2, SF_6 and SF_6-N_2 arc plasmas*, *J. Phys. D: Appl. Phys.* 24, 1300, (1991).

[6]. V. Aubrecht and B. Gross, *Calculations of radiation transfer in SF_6 plasmas using the method of partial characteristics*, *J. Phys. D: Appl. Phys.* 27, 95, (1994).

[7]. V. G. Sevast'yanenko, *Radiant heat transfer in a real spectrum,* Hear Tram. Sov. Res. 9, 36, (1977).

[8]. J. H. Jeans, *The equations of radiative transfer of energy,* Monthly Notices Roy. Astronom. Soc., 78, 28, (1917).

[9]. V. Kourganoff, *Basic methods in transfer problems*, Dover Publications, (1963).

[10]. M. F. Modest, *Radiative heat transfer,* Academic Press, (2013).

[11]. M. R. J. Charest, C. P. T. Groth, and O. L. G¨ ulder, *Solution of the equation of radiative transfer using a Newton–Krylov approach and adaptive mesh refinement*, J. Comp. Phys., 231, 8, 3023, (2012).

[12]. H. Nordborg and A. Iordanidis, *Self-consistent radiation based modelling of electric arcs: I. efficient radiation approximations*, J. Phys. D: Appl. Phys. 41, 135205, (2008).

[13]. H. Z. Randrianandraina, Y. Cressault and A. Gleizes, *Improvements of radiative transfer calculation for SF6 thermal plasmas*, *J. Phys. D: Appl. Phys.* 44, 194012, (2011).

[14]. D. Godin and J. Y. Trepanier, *A robust and efficient method for the computation of equilibrium composition in gaseous mixtures,* Plas. Chem. Plas. Proc. 24, 44773, (2003).

[15]. D. Blechschmidt, R. Haensel, E. E. Koch, U. Nielsen and T. Sagawa, *The optical spectra of gaseous and solid SF_6 in the extreme ultraviolet and soft x-ray region*, *Chem. Phys. Lett.* 14, 336, (1972).

[16]. D. M. P. Holland, D. A. Shaw, A. Hopkirk, MacDonald M A and McSweeney S M., *A study of the absolute photoabsorption cross section and the photoionization quantum efficiency of sulphur hexafluoride from the ionization threshold to 420 A*, *Phys. B: At. Mol. Opt. Phys.* 25, 4823, (1992).

Chapter 5 Calculation of thermodynamic and transport properties of two-temperature model

5.1 Introduction

SF_6 is widely used in high voltage gas-blast circuit breakers because of its excellent dielectric performance and arc quenching ability. It is however a strong greenhouse gas. SF_6 will need to be replaced. There has been research on SF_6 replacement[1]. PTFE, which is used to make the nozzle in high voltage circuit breakers, is an excellent solid insulation material. Ablation of PTFE takes place in the interruption process of a high voltage circuit breaker as a result of strong arc radiation. Both theoretical and experimental investigations[2-3] have been carried out and have shown that ablated PTFE vapour has a significant influence on the performance of circuit breakers. There is better agreement between the predicted and measured values if the influence of PTFE vapour[2] is taken into account. In previous calculations, the main assumption is local thermal equilibrium (LTE). However, LTE is no longer valid when a large temperature gradient exists, such as in the region close to the cold wall or when the number density of electrons is not high enough to allow sufficient transfer of energy between the electrons and heavy-particles. A non-LTE assumption has to be applied to the region with such conditions. Region three in Fig. 5-1 shows such a region in the typical temperature profile of an electric arc.

The purpose of a circuit breaker is to interrupt a high current in a short time (less than 100 ms) when needed. The current-zero period is critical to the interruption performance. During this period convection and turbulent cooling play a dominant role in reducing the arc temperature. As a result of this

phenomenon, the electron number density is not high enough to support the transfer of energy between electrons and heavy particles. In this situation, although the electron energy distribution function still follows Maxwellian, the mean kinetic energies of electrons and heavy-particles are different.

The species in a plasma can be divided into two groups, electrons and heavy particles, because of the large difference in their mass. Depending on the discharge conditions, the plasma could be in local chemical equilibrium (LCE) but the two species have different temperatures. In this case a two-temperature model needs to be used to solve this non-thermal equilibrium problem. There are two temperatures, the electron temperature (T_e) and heavy-particles temperature (T_h). The mass difference between heavy particles is much smaller than that between heavy particles and electrons. Thermal relaxation among heavy particles is thus very efficient and all heavy particles have a common temperature. The composition, thermodynamic properties and transport coefficients of non-thermal equilibrium plasma are therefore needed to model and optimize a two-temperature plasma system.

Work related to two-temperature plasma has been reported on pure SF_6[4,5,6,7], its mixtures, such as SF_6-copper[8] and SF_6-nitrogen[9] and other gas mixtures Ar-O_2 [10] and Ar-H_2 [11]. Two-temperature modelling of pure nitrogen has been reported as well[12],[13]. However, there are no existing publications on nitrogen-PTFE mixture under non-thermal equilibrium conditions.

The determination of plasma composition based on a two-temperature model usually requires the use of Saha and Guldberg-Waage Laws, Dalton's Law and the Species Conservation Law. The methods were derived by Van de Sanden[14], Potapov et al. [15] and Godin's method [16], as mentioned in Chapter three. However, in Godin's work, LTE was assumed. In this chapter, how to apply Godin's method to a non-LTE plasma is explained with two-temperatures. The

results obtained using Godin's method will be compared with those from Van de Sanden's method and Potapov's method.

In this chapter, the plasma composition, thermodynamic properties and transport coefficient of a non-equilibrium N_2-PTFE gas mixture are calculated. Boltzmann distribution can still be used to describe the population density distribution as a function of energy, including discrete energy levels; however, the temperature as a parameter has to be chosen carefully. The plasma pressure ranges from 1 bar to 100 bar and the electron temperature ranges from 300 K to 40,000 K. The composition is calculated using Godin's method. The thermodynamic properties and transport coefficients are then obtained based on the composition of the species. There will be a discussion on the results from different methods to help understand the underlying physical mechanisms responsible for the difference.

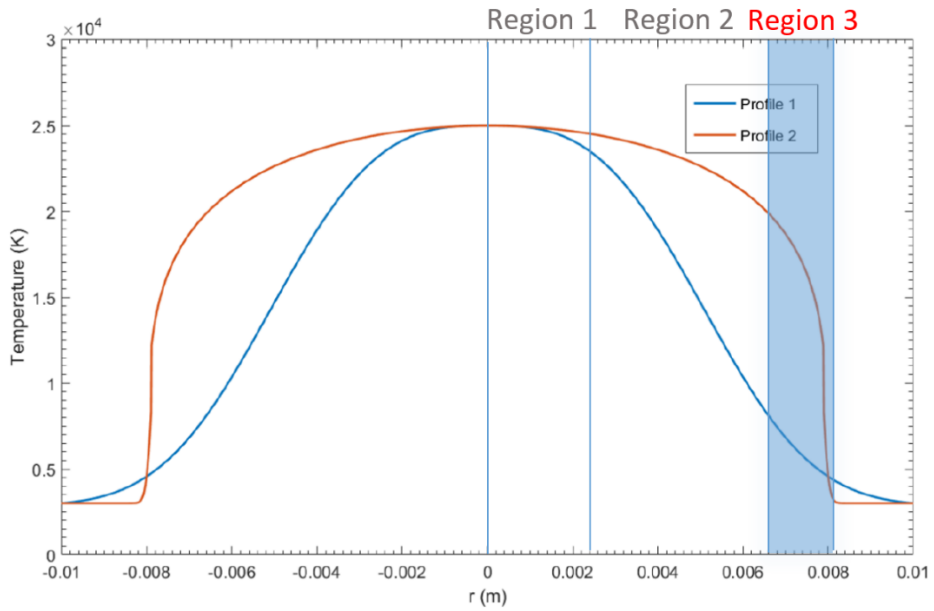

Fig. 5-1:Typical temperature profile of electric arc

5.2 Fundamental principles

5.2.1 Plasma composition

There are mainly four models for computing plasma composition have been derived in literatures by researchers: Potapov[15], Van de Sanden[14], minimization of Gibbs free energy method[17],[18] and Godin[16] method. The basic principle of Gibbs free energy minimization method is the same as Godin's method that was employed to calculate the plasma composition under LTE conditions in Chapter three. Chen and Han argued that Gibbs or Godin's method cannot be used to calculate the composition under non-LTE condition[19]. However, Andre agreed that the method based on minimization of Gibbs free energy can be employed for two-temperature or multi-temperature models for non-LTE plasma[20,21]. Andre further pointed out that Chen and Han's point from statistical mechanics[22].

Conservation of Stoichiometric equilibrium

$$\sum_{i}^{w} c_{s,i} n_{s,i} = C \tag{5.1}$$

Eq. (5.1) represents the conservation of element mass where $n_{s,i}$ is the number density of element s in species i, $c_{s,i}$ the stoichiometric coefficient of element s, C a constant and w the number of species in a plasma.

Dalton's law

$$\mathrm{P} + \Delta\mathrm{P} = \sum_{i \neq e}^{w} n_i k T_h + n_e k T_e$$
$$\Delta\mathrm{P} = \frac{1}{24\varepsilon_0 \pi \lambda_d^3} \sum_{i=1}^{w} Z_i^2 n_i \tag{5.2}$$

$$\lambda_e^{-2} = \frac{e^2}{\varepsilon_0 k}\left[\frac{n_e}{T_e} + \sum_{t=1,t\neq e}^{w} \frac{z_t^2 n_t}{T_h}\right]$$

Eq.(5.2) expresses Dalton' Law with Coulomb field modification[23], where T_h and T_e are the heavy particle and electron temperatures, respectively. P and ΔP are the gas pressure and pressure correction due to interactions among charged particles. λ_d is the Debye length with ion shielding. In the present calculation, a comparison of Debye length due to ion and electron shielding and only due to electrons will be presented. w is the number of species in the plasma, k the Boltzmann's constant, ε_0 the vacuum permittivity, Z_i and n_i are the charge number and number density of species i and n_e is the number density of electron.

Electrically quasi-neutrality

$$\sum_t Z_t n_t - n_e = 0 \qquad (5.3)$$

Eq.(5.3) presents electrical quasi-neutrality in the plasma and Z_t and n_t are the charge number and number density of the charged species t, respectively.

Law of mass action

$$\prod_i^w n_i^{c_i} = \prod_i^w Q_i^{c_i} \qquad (5.4)$$

In Eq.(5.4), c_i presents the coefficient related to the chemical basis in Eq.(3.5). These equations are used in different method of calculation. The difference lies with the equations of describing dissociation and ionization reactions. The advantages of Godin's method are uniting form for both reactions, it allows a

reaction's equations be re-generated dynamically during the calculation process.

Potapov's method and Van de Sanden's method will be first introduced below, a comparison of results between different methods will be discussed later as well.

Potapov's method

The dissociation reaction $\mathrm{ab} \leftrightarrow \mathrm{a} + \mathrm{b}$ describes a chemical reaction in equilibrium under the control of the heavy species temperature T_h. The ionization $\mathrm{a}^{r+} \leftrightarrow \mathrm{a}^{(r+1)+} + \mathrm{e}^-$ reaches equilibrium with T_{ex} is the excitation temperature.

$$\frac{n_a n_b}{n_{ab}} = \frac{Q_a Q_b}{Q_{ab}} \left[\frac{2\pi k T_h}{h^2}\right]^{3/2} \left[\frac{m_a m_b}{m_{ab}}\right]^{3/2} \exp\left[-\frac{E_d}{kT_h}\right] \tag{5.5}$$

$$n_e \left[\frac{n_{r+1}}{n_r}\right]^{1/\theta} = 2\left[\frac{Q_{r+1}}{Q_r}\right]^{1/\theta} \left[\frac{2m_e \pi k T_e}{h^2}\right]^{3/2} \exp\left[-\frac{E_{I,r+1} - \Delta E_{I,r+1}}{kT_{ex}}\right] \tag{5.6}$$

where θ is the non-LTE degree which is given by $\theta = \frac{T_e}{T_h}$, Q is the internal partition function, $E_{I,r+1}$ the ionization energy while subscript *r* indicates *r*-times ionized species and E_d the dissociation energy. $\Delta E_{I,r+1}$ is the lowering of the ionization energy due to the interactions between plasma particles. ab, a and b denote the reactant and the products of the dissociation reactions. T_{ex} is the excitation temperature of the species a^{r+}. The lowering of the ionization energy can be expressed as:

$$\Delta \mathrm{E}_{I,r+1} = (r+1)\frac{e^2}{4\pi\varepsilon_0}\frac{1}{\lambda_d} \tag{5.7}$$

where λ_d is the Debye length due to the shielding effect of charged particles. It is known that the ionization potential lowering is inversely proportional to the Debye length. A comparison[24] of the Debye length with and without considering the contribution of heavy species is made. It can be shown that ions play an equally or more important role in the lowering of the ionization potential in a two-temperature plasma.

Van de Sande et al.'s method

Guldberg-Waage's equation is based on Saha's law, it can be written as below:

$$\frac{n_a n_b}{n_{ab}} = \frac{Q_a Q_b}{Q_{ab}}\left[\frac{2\pi k T_h}{h^2}\right]^{3/2}\left[\frac{m_a m_b}{m_{ab}}\right]^{3/2}\exp\left[-\frac{E_d}{kT_{ex}}\right] \tag{5.8}$$

$$n_e\left[\frac{n_{r+1}}{n_r}\right] = 2\left[\frac{Q_{r+1}}{Q_r}\right]\left[\frac{2m_e\pi k T_e}{h^2}\right]^{3/2}\exp\left[-\frac{E_{I,r+1}-\Delta E_{I,r+1}}{kT_{ex}}\right] \tag{5.9}$$

The kinetic temperature of heavy species T_h in the exponential term of Potapov's method Eq. (5.5) is replaced by an effective excitation temperature T_{ex} as shown in Eq. (5.8) and Eq.(5.9). T_{ex} can be either T_h or T_e, the choice of reaction excitation temperature follows the rule in Table 5-1.

Table 5-1

Reaction		
Dissociation reaction	Molecular ionization reaction	Atomic ionization reaction

$\boldsymbol{T_{ex}}$	T_h	T_h	T_e

Minimization Gibbs free energy

In Chapter three, Godin's method has been shown to be valid for the calculation of the composition of thermal equilibrium plasma. It can also be employed under non-thermal equilibrium conditions as well.

In this chapter, the composition of a total of 34 species contained in nitrogen and PTFE gas mixture is to be calculated. Actually, both methods can be derived from the other and give exactly the same results. It just needs to solve 4 equations based on Godin's method but requires to solve 34 equations with Van de Sande's method. Thus, Godin's method will be used to calculate the composition of nitrogen and PTFE gas mixture plasma.

According to Godin's method, a concept of chemical basis has to be defined. It is denoted by z for the M species of the chemical basis and by *z** for the subset of the other N-M species not belonging to it. In this calculation, there are 4 chemical bases and the remaining 30 bases are listed below:

z = $\{e^-, N^+, CN, C_2F_2\}$

z*=$\{N_2, C_2, F_2, N, N^{2+}, N^{3+}, F, F^+, F^{2+}, F^{3+}, F^{4+}, C, C^+, C^{2+}, C^{3+}, C_2F_4, C_2F_6, CF_2, CF_3, C_2F_3N, CF_4, CN^-, CN_2(CNN), CN_2(NCN), CF, C_3\ C_2N_2, FN, C_2N, C_4N_2\}$

$$\left\{ n_{z_j^*} = Q_{z_j^*} \prod_{i=1}^{M} \left(\frac{n_{z_i}}{Q_{z_i}}\right)^{c_{j,i}} \right\}_{j=1}^{N-M} \tag{5.10}$$

Where Q is the partition function of species z or z^*, c is the coefficient related to the chemical basis.

For species are set as the chemical bases in consideration of the number of chemical elements present in the plasma and the charge (N, C, F, and charge). Therefore, the remaining 30 species are set as chemical species and mass action law is applied. The principles of conservation of atomic nucleus, electrical neutrality and ideal gas law are used to obtain a system of plasma. A total of 34 equations are obtained, which include two equations for conservation of nuclei (ratio of C:F in PTFE + N:F between PTFE and N_2), one equation for charge neutrality, one from the ideal gas law and another 30 equations describing the mass action law for the 30 chemical species. These equations are solved using the Newton-Raphson method to obtain the number density of all 34 species. Logarithm was taken on both sides of the chemical species equations, which results in 30 linear equations and thus greatly simplifies the calculation. The linear equations are then substituted in the base equations to reduce the number of unknowns to only 4. This gives a smaller size of the Jacob matrix in the solution procedure using the Newton-Raphson method, and significantly promotes the convergence of the calculation.

5.2.2 Partition function

The total partition function of a species i is written as

$$\mathrm{Q}_i^{total} = Q_i^{trans} \times Q_i^{int} \times Q_i^{reac} \tag{5.11}$$

According to Gleize's[23] work, T_h dominates the translational, rotational and vibrational activities of heavy species and electronic excitation and translational motion of electrons are governed by T_e.

The translational partition function of species i can be expressed as:

$$\mathrm{Q}_i^{trans} = \left(\frac{2\pi m_i k T_i}{h^2}\right)^{3/2} V \tag{5.12}$$

where V is the volume and T_i the temperature of species i. In this case, only when i is an electron, $T_i = T_e$, otherwise $T_i = T_h$.

Monatomic species

Monatomic species usually dominate the plasma composition when the temperature is higher than 10,000 K. The internal partition function of monatomic species consisting of electronic energy can be expressed as:

$$Q_{int} = Q_{el} = \sum_{j}^{\varepsilon_I} g_{e,j} \exp(-\frac{\varepsilon_j}{kT_e}) \quad (5.13)$$

where ε_I is the ionization energy and $g_{e,j}$ the statistical weight.

$$Q_{reac} = \exp\left[-\left(\frac{E_{reac,1}}{kT_h} + \frac{E_{reac,2}}{kT_e}\right)\right] \quad (5.14)$$

Q_{reac} represents a reaction energy for the formation of the specie. Reaction energy 1 $E_{reac,1}$ is due to molecular dissociation reaction, reaction energy 2 $E_{reac,2}$ is a result of atom ionisation. For example, the reaction energy of N^{2+} is formed by the following process:

$$\mathrm{N_2} \leftrightarrow 2N + \mathrm{E}_{reac,1}$$

$$N \leftrightarrow \mathrm{N^+} + e^- + \mathrm{E}_{reac,2a}$$

$$\mathrm{N^+} \leftrightarrow N^{2+} + e^- + \mathrm{E}_{reac,2b}$$

$$E_{reac,2} = \mathrm{E}_{reac,2a} + \mathrm{E}_{reac,2b}$$

Diatomic and polyatomic species

Eq.(5.15) expresses the internal partition function for diatomic species.

$$\mathrm{Q}_{int} = Q_{ele} \cdot Q_{vib} \cdot Q_{rot} \tag{5.15}$$

where Q_{ele}, Q_{vib} and Q_{rot} are electrical, vibrational and rotational partition functions respectively. The expressions for those partition functions are shown below:

$$\begin{aligned} Q_{ele} &= \frac{1}{\sigma}\sum_{T_e} g_e \exp\left(-\frac{S_e}{k\,T_e}\right) \\ Q_{vib} &= \sum_{v=0} g_v \exp\left(-\frac{G_v(S_e)}{k\,T_h}\right) \\ Q_{rot} &= \sum_{J=0} g_J \exp\left(-\frac{F_v(J)}{k\,T_h}\right) \end{aligned} \tag{5.16}$$

where σ is a constant, it is equal to 2 for homonuclear molecules and 1 for heteronuclear molecules. The electronic levels S_e are limited to the number of states. G_v corresponds to the vibrational energies and depend on the spectroscopic constants expressed in Eq.(5.17)

$$G_v = \left(v+\frac{1}{2}\right)\omega_e - \left(v+\frac{1}{2}\right)^2 \omega_e x_e + \left(v+\frac{1}{2}\right)^3 \omega_e y_e \tag{5.17}$$

$F_v(J)$ corresponds to the rotational energies which is:

$$\begin{aligned} F_v(J) &= B_v J(J+1) - D_v J^2 (J+1)^2 \\ B_v &= B_e - \alpha_e\left(v+\frac{1}{2}\right) \\ D_v &= D_e - \beta_e\left(v+\frac{1}{2}\right) \end{aligned} \tag{5.18}$$

Parameters ω_e,$\omega_e x_e$, $\omega_e y_e$, α_e, β_e, B_e, D_e are spectroscopic constants which are available from the Janaf table[25].

When the vibration-rotation interactions is weak, the internal partition function for polyatomic species is the same as diatomic species given in Eq.(5.15). Polyatomic species exist at low temperatures. The population of the fundamental level is important. The contribution of Q_{ele} to the total internal partition function can be treated as the ground state quantum weight P_s which can be obtained from the Janaf table.

The vibrational partition function can be expressed as:

$$Q_{vib} = \prod_{i=1}^{N} \left[1 - \exp(\frac{-v_i hc}{k\,T})\right]^{-d_i} \qquad (5.19)$$

Where d_i is the degeneracy of the vibrational frequency v_i of species 'i'. It can be obtained from the Janaf table. The contribution of the rotation part to the total partition function, is shown below:

For linear molecules:

$$Q_{rot} = \frac{1}{\sigma}\frac{k\,T}{hcB_0} \qquad (5.20)$$

For non-linear molecules such as C_2F_3N, C_2F_4, F_2F_6:

$$Q_{rot} = \frac{1}{\sigma}\sqrt{\frac{\pi}{ABC}(\frac{k\,T}{hc})^3} = \frac{1}{\sigma}6.93510^{57}\sqrt{T^3 I_A I_B I_C} \qquad (5.21)$$

where the constant of rotation A, B, C or the momenta of inertia I_A, I_B, I_C can be found from the Janaf Table. All the levels need to be considered for each species can be obtained from the Janaf Table as well.

5.2.3 Calculation of thermodynamic properties

Following the calculation of each species' partition function, the thermodynamic properties can then be obtained. The expression for standard thermodynamic properties is reported by Weizong[12]. Moverover, a species' macroscopic temperature was applied in the work of Colombo[13] in the derivation of the internal partition function. It has been accepted that the electronic excitation of a species is governed by the electron temperature while molecular vibration and rotation is governed by the heavy-particles temperature. These mechanisms have to be reflected correctly by following the most appropriate temperature in Eq.(5.5)-(5.9).

Mass density

$$\rho = \sum_{i=1}^{w} m_i n_i \tag{5.22}$$

where m_i is the mass of species i.

Molar weight

$$\mathrm{M} = \sum_{i=1}^{w} x_i n_i \tag{5.23}$$

where x_i is the molar fraction expressed in Eq.(3.13).

Specific enthalpy

For electrons, specific enthalpy is only determined by the electron temperature and the mass density:

$$\mathrm{H}_e = \frac{5}{2}\frac{k}{\rho} n_e T_e \tag{5.24}$$

For monatomic species i, the specific enthalpy can be carried out by the equation below:

$$\mathrm{h}_i = \frac{5}{2}\frac{k}{\rho} n_i T_h + \frac{1}{\rho} n_i E_i + \frac{k}{\rho} n_i \left({T_e}^2 \frac{\partial ln Q_i^{ele}}{\partial T_e} \right) \tag{5.25}$$

For molecular species, the specific enthalpy is more complicated than monatomic species.

$$\mathrm{h}_i = \frac{5}{2}\frac{k}{\rho} n_i T_h + \frac{1}{\rho} n_i E_i + \frac{k}{\rho} n_i \left[{T_e}^2 \frac{\partial ln Q_i^{ele}}{\partial T_e} + {T_h}^2 \frac{\partial \ln(Q_i^{rot} Q_i^{vib})}{\partial T_h} \right] \tag{5.26}$$

Colombo[13] has proposed the definition that with constant pressure p and constant non-thermal equilibrium degree θ, the specific heat can be determined by the differentiation of the specific enthalpy with respect to electron temperature T_e which is expressed below:

$$\mathrm{C}_{p,\theta} = \left. \frac{\partial h}{\partial T_e} \right|_{p,\theta} \tag{5.27}$$

For a strong 2-T plasma, the specific heat of electrons and heavy particles must be treated separately in purposed calculation model of plasma flow. Thus, two specific heat capacities at certain pressure, one for electrons and another one for heavy particles are needed. For each of them, it can be obtained by differentiation of the specific enthalpy with respect to the corresponding temperature.[26].

5.2.4 Determination of transport coefficients

The classical Chapman-Enskog method is used to calculate the transport coefficients of the plasma in a two-temperature state [27]. Devoto [28] and GBonnefoi[29] further simplified the method by neglecting the coupling between the electrons and heavy-particles. Rat[11] has developed a method which considers the coupling between electrons and heavy-particles. Compared with Devoto and Gbonnefoi's methods, this method produces coupling terms in the calculation. However, in a recent study of transport coefficients, Colombo has shown that the influence of the coupling between electrons and heavy-particles on the transport coefficients of non-LTE plasma in two-temperature state is limited. There is no significant difference in the viscosity, total thermal conductivity and the electrical conductivity but the method considering coupling is computationally much more expensive. Thus, Devoto's method is used in the present work to obtain the transport coefficients for N_2-PTFE plasma in two-temperature state.

Diffusion coefficients

To obtain the binary diffusion coefficient is the initial step to determine the thermal conductivity. Based on Ramshaw's reports[30,31], it can be evaluated as

$$\mathrm{D}_{ij}^{b} = \frac{3k^2 T_i T_j}{16 P \mu_{ij} T_{ij}^{*} q_{ij}^{(1,1)}} \tag{5.28}$$

where D_{ij}^{b} is the binary diffusion coefficient of specie i and j. μ_{ij} and T_{ij}^{*} are the reduced mass Eq.(5.29) and temperature Eq.(5.30) of species i and j, respectively. $q_{ij}^{(1,1)}$ is a collision integral, the superscript will be explained.

$$\frac{1}{\mu_{ij}} = \frac{1}{m_i} + \frac{1}{m_j} \tag{5.29}$$

$$T_{ij}^{*} = \frac{\left(m_i T_j + m_j T_i\right)}{m_i + m_j} \tag{5.30}$$

The ordinary diffusion coefficient can be obtained by Eq.(5.31), following Hirschfelder's work[32]

$$\mathrm{D}_{ij}^{m} = \frac{F^{ji} - F^{ii}}{m_j |F|} \tag{5.31}$$

where F^{ji} is the cofactors of F_{ji}, which can be expressed in terms of the binary diffusion coefficient:

$$\mathrm{F}_{ij} = \frac{1}{\rho}\left[\frac{n_i}{D_{ij}^{b}} + \sum_{l \neq i} \frac{n_l m_j}{m_i D_{il}^{b}}\right]\left(1 - \delta_{ij}\right) \tag{5.32}$$

Ambipolar diffusion coefficients are present below by Eq.(5.33)

$$D_{ij}^{a} = D_{ij}^{m} + \frac{\alpha_i}{\beta}\sum_{s} Z_s D_{sj}^{m} \tag{5.33}$$

where coefficient α_i and β are given in Eq.(5.34) where Z_s is the charges' number for specie s.

$$\begin{aligned} \alpha_i &= \sum_{j} \frac{m_j n_j Z_j D_{ij}^{m}}{T_j} \\ \beta &= \sum_{i} Z_i \sum_{j} \frac{m_j n_j Z_j D_{ij}^{m}}{T_j} \end{aligned} \tag{5.34}$$

Eq.(5.35) and (5.36) express the thermal diffusion coefficients for electrons and heavy-particles:

$$\mathrm{D}_e^T = \frac{15n_e^2\sqrt{2\pi kT_e}}{4}\begin{vmatrix} q^{01} & q^{02} \\ q^{21} & q^{22} \end{vmatrix}\left(\begin{vmatrix} q^{00} & q^{01} & q^{02} \\ q^{10} & q^{11} & q^{12} \\ q^{20} & q^{21} & q^{22} \end{vmatrix}\right)^{-1} \tag{5.35}$$

$$\mathrm{D}_i^T = \frac{15n_i^2\sqrt{2\pi m_i kT_h}}{4}\left(\begin{vmatrix} q_{ij}^{00} & q_{ij}^{01} \\ q_{ij}^{10} & q_{ij}^{11} \end{vmatrix}\right)^{-1}\begin{vmatrix} q_{ij}^{00} & q_{ij}^{01} & q_{ij}^{02} \\ q_{ij}^{10} & q_{ij}^{11} & q_{ij}^{12} \\ q_{ij}^{20} & q_{ij}^{21} & q_{ij}^{22} \end{vmatrix} \tag{5.36}$$

where the q terms are collision integrals.

Viscosity

Due to the fact that heavy-particles are much heavier than electrons, thus, the viscosity of a plasma can be treated as the viscosity of heavy-particles. If an electron temperature is given, the heavy-particle temperature will become lower when the non-LTE degree increases. This results in a drop in the momentum transport and viscosity as well.

$$\eta(\xi) = \eta_h + \eta_e \cong \eta_h \tag{5.37}$$

$$\eta_h(\xi) = \frac{kT_h}{2}\sum_{j,j\neq e} b'_{j0}(\xi) \tag{5.38}$$

where $b'_{j0}(\xi)$ is a coefficient which can be obtained by solution of the following equation:

$$\sum_{j,j\neq e}\sum_{m'=0}^{\zeta-1} \tilde{Q}_{ij}^{mm'} b'_{jm'}(\zeta) = -5n_i\delta_{m0} \tag{5.39}$$

Thermal conductivity

The contribution to the thermal conductivity can be divided into two parts: electron's and heavy-particle's. Following by Ghorui the definition can be expressed as

$$\begin{aligned} \lambda_e &= \lambda_{tre} + \lambda_{re} \\ \lambda_h &= \lambda_{trh} + \lambda_{rh} + \lambda_{int} \end{aligned} \tag{5.40}$$

λ_{tre} and λ_{trh} in Eq.(5.40) are the translational thermal conductivity for electrons and heavy-particles, respectively. λ_{re} and λ_{rh} are the reactive thermal conductivity. λ_{int} is the internal thermal conductivity of the heavy-particles.

The electron translational thermal conductivity can be expressed as:

$$\lambda_{tre} = \frac{75 n_e^2 k}{8} \sqrt{\frac{2\pi k T_e}{m_e}} \left(q^{11} - \frac{(q^{12})^2}{q^{22}} \right)^{-1} \tag{5.41}$$

The translational thermal conductivity contributed of heavy-particles can be obtained by Eq.(5.42):

$$\lambda_{trh} = -\frac{75k}{8} \frac{\sqrt{2\pi k T_h}}{|q|} \begin{vmatrix} q_{ij}^{00} & q_{ij}^{01} & 0 \\ q_{ij}^{10} & q_{ij}^{11} & n_i \\ 0 & n_j/\sqrt{m_j} & 0 \end{vmatrix} \tag{5.42}$$

$$\lambda_{int} = \sum_{i \neq e}^{w} x_i D_{ii}^b k \left(\frac{C_{pi}}{R} - 2.5 \right) \left(\sum_{j \neq e}^{w} \frac{x_j}{x_i} \frac{D_{ii}^b}{D_{ij}^b} \right)^{-1} \tag{5.43}$$

$$\lambda_{re} = \left[\sum_{r=1}^{v} \Delta h_r \frac{n}{pkT_h} \sum_{j=1}^{w} \frac{T_h}{T_j} m_j D_{rj}^a \frac{\partial p_j}{\partial T_e}\right] \tag{5.44}$$

$$\lambda_{rh} = \left[\sum_{r=1}^{v} \Delta h_r \frac{n}{pkT_h} \sum_{j=1}^{w} \frac{T_h}{T_j} m_j D_{rj}^a \frac{\partial p_j}{\partial T_h}\right] \tag{5.45}$$

where, v and w are total number of species and chemical reactions, respectively. Eq.(5.43) describes the internal thermal conductivity of the heavy particles. Eq.(5.44) and Eq.(5.45) describe the reactive thermal conductivity contributed by electrons and heavy-particles. Δh_r is the reaction enthalpy due to the reactive r. D_{rj}^a is the ambipolar diffusion coefficient which can be obtained from Eq.(5.33).

Electrical conductivity

The electrical conductivity of a two temperature plasma is determined by the electrons. The following equation relates the electrical conductivity of the gas mixture in a two temperature state to the electron number density and temperature and also the relevant collision integrals.

Eq.(5.46) shows the way to compute the electrical conductivity:

$$\sigma = \frac{3e^2 n_e^2}{2kT_e} \sqrt{\frac{2\pi kT_e}{m_e}} \begin{vmatrix} q^{11} & q^{12} \\ q^{21} & q^{22} \end{vmatrix} \left(\begin{vmatrix} q^{00} & q^{01} & q^{02} \\ q^{10} & q^{11} & q^{12} \\ q^{20} & q^{21} & q^{22} \end{vmatrix} \right)^{-1} \tag{5.46}$$

5.2.5 Calculation program

The calculation program is developed by C++. There are two parts in calculation program: composition calculation and properties calculation. In the first part, program employs armadillo library to carry out the matrix inverse in Newton-

Raphson method. The program runs on a personal computer of windows 10 operation system with Intel i5-2320 and 8G RAM.

5.3 Results

5.3.1 Species composition

The chemical equilibrium composition of pure nitrogen, PTFE vapour and their mixture were calculated. In a thermal equilibrium plasma, species composition is a function of temperature and pressure only. However, in a non-thermal equilibrium plasma in two-temperature state, the species composition is determined by two independent temperatures, the heavy-particle temperature and electron temperature at a given pressure. Since the system of equations required the Newton-Raphson algorithm to solve, solution of equations system lies on convergence of equations system. It is necessary to change the form of equations in different temperatures or pressures in order to achieve convergence. Another reason of using Godin's method is that it is possible to reduce order of equations system so that it will save the calculation cost which has been explained in chapter three. In this chapter, the default temperature axis in all diagrams is the electron temperature.

Fig. 5-2 shows the composition of pure PTFE vapour in the electron temperature range of 300 K to 40 000 K with the non-equilibrium degree $\theta = \mathrm{T}_e/T_h$ being 1 and 5 and the pressure being at 1 atmosphere. When $\theta = 1$, it is a thermal equilibrium case. It is shown that the number density of C_2F_4 is quite low at room temperature. Its number density starts to increase rapidly over the temperature in the range of 330 K to 850 K, then it is reduced when C_2F_4 starts to decompose.

With a non-thermal equilibrium degree of 5, the composition of heavy particles such as C_2, C_3 molecules and F atoms are quite different from the case of thermal equilibrium. Since the electron temperature is much higher than that of the heavy particles, the number density of free electron is much higher than that in the equilibrium. For example, ionization of atoms starts at an electron temperature of 16 000 K while the heavy particle temperature is only 3,200 K.

Fig. 5-3 shows the composition of pure nitrogen plasma under thermal and non-thermal equilibrium conditions. There are several features coming out from the comparison. Firstly, the peak number density of nitrogen atom in the non-thermal equilibrium case is two orders of magnitude lower. The maximum number density of N is reached in the LTE case ($\theta = 1$) at $\mathrm{T}_e = T_h = 8{,}000\ K$ while in the non-LTE case at $\mathrm{T}_e = 20{,}000\ K$ and $\mathrm{T}_h = 4{,}000\ K$. The reason is that in the latter case when N_2 starts to dissociate, energetic electrons are already able to ionise the N atoms. As a result, the majority of the N atoms resulting from dissociation are quickly ionised, leading to a situation where N+ density is substantially higher than the N atoms in the non-LTE case. Secondly, the composition of pure nitrogen at $\mathrm{T}_e \geq 30{,}000\ \mathrm{K}$ is controlled by the electron activities, not sensitive to the heavy particle temperature. The gas is already fully ionised with an ionisation degree of $\geq 10^4$.

The composition of nitrogen and PTFE mixture under thermal and non-thermal equilibrium conditions are given Fig. 5-4. The temperature ranges of Fig. 5-4(a)(b)(c) are from 300 K to 5,000 K, 5,000 K to 15,000 K and 15,000 K to 40,000 K at $\theta = 1$, Fig. 5-4(d)(e) present the plasma composition at $\theta = 5$, the temperature ranges are from 300 K to 25,000 K and 300 K to 40,000 K, separately. Fig. 5-4(a) and (d) are plotted for comparison because they have the same heavy-particles temperature range. The composition for $\theta = 1$ is presented in three diagrams. The molar fraction ratio of nitrogen and PTFE is 1:1. It can be observed that when $\theta = 1$ large number density of C_3 are present

in pure PTFE as shown in Fig. 5-2, it attains a much lower number density in the mixture at the temperature below 2,000 K. This molecule is replaced by C_4N_2 in the mixture. FCN is generated rapidly above 1,000 K due to the existence of free atoms of these three elements but it is not a steady species. It starts to dissociate at temperatures higher than 2,200 K. Free carbon and fluorine atoms are combined to form CF_2. It is dissociated when the temperature is higher than 3,000 K. The number density of molecules can be neglected when the temperature is higher than 10,000 K.

When $\theta = 5$, due to the electron temperature is different from heavy-particles, there are more electrons at the same heavy-particles temperature, thus speeds up the dissociation of molecules at lower heavy-particle temperature. It can be found out that, in this non-LTE case, the number density of molecular species can be neglected when heavy-particles temperature is 4,200 K in Fig. 5-4(d).

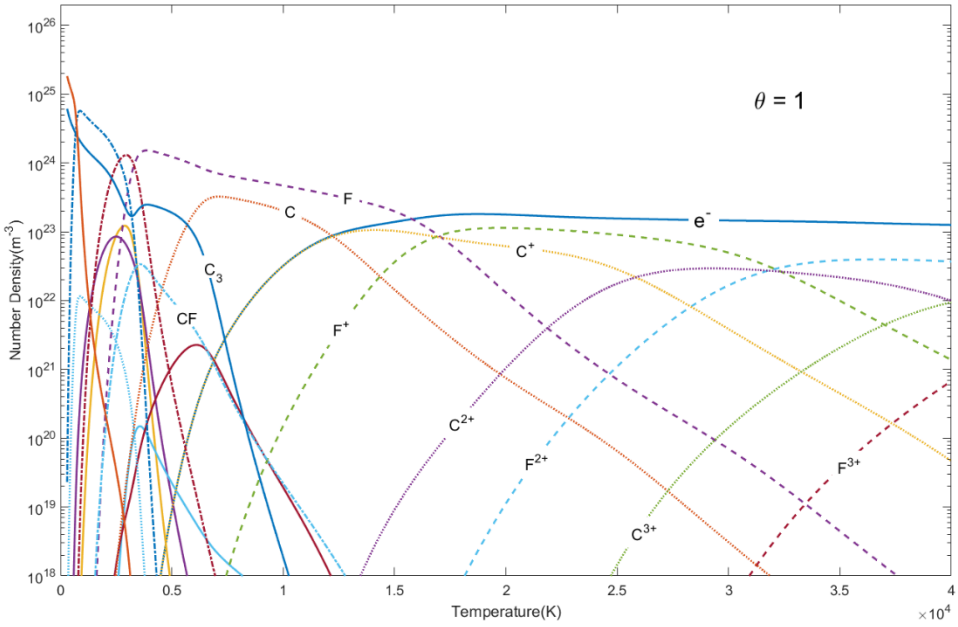

Fig. 5-2 (a)

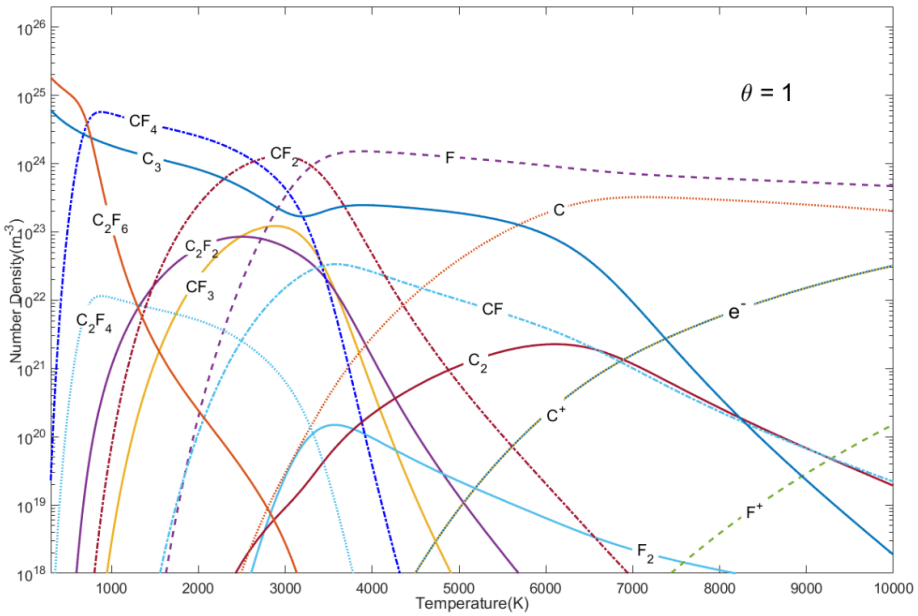

Fig. 5-2 (b)

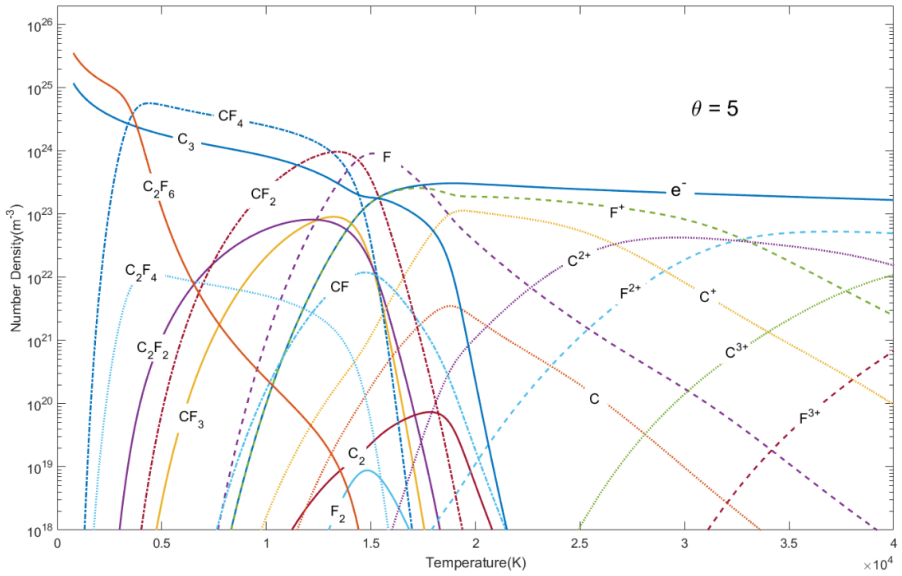

Fig. 5-2 (c)

Fig. 5-2: Temperature dependence of the number density of PTFE vapor under non-equilibrium degree of 1 (a), (b) and 5 (c) at atmospheric pressure.

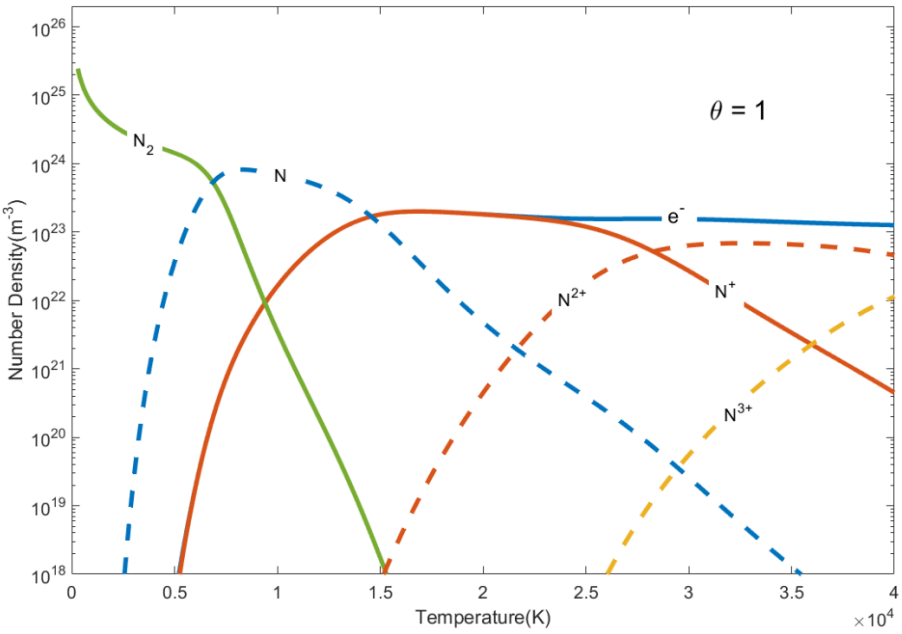

Fig. 5-3 (a)

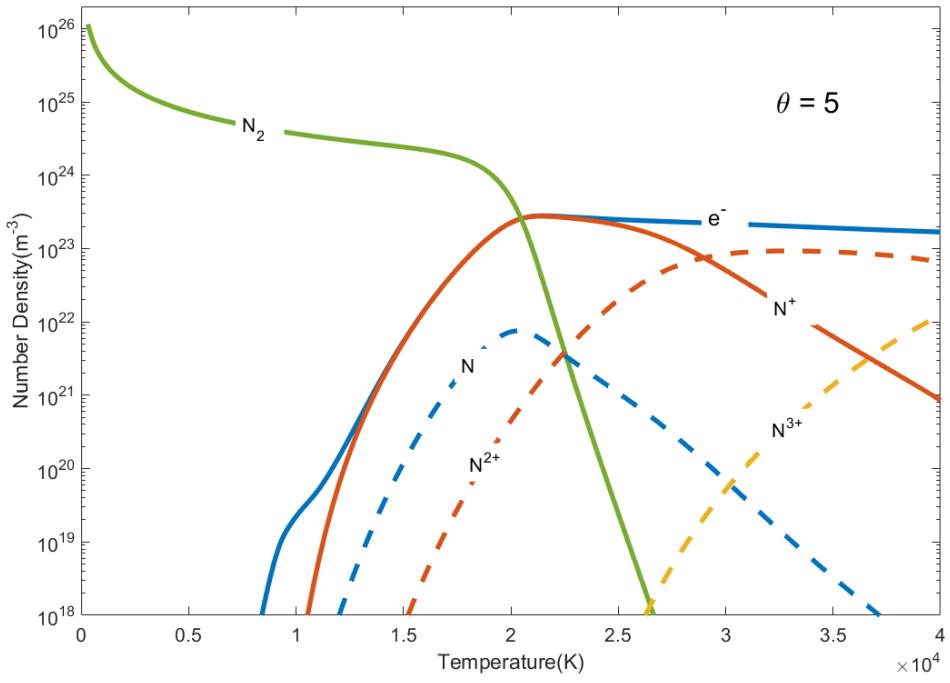

Fig. 5-3 (b)

Fig. 5-3: Temperature dependence of the number density of pure nitrogen gas plasma under non-equilibrium degree of 1 (a) and 5 (b) at atmospheric pressure

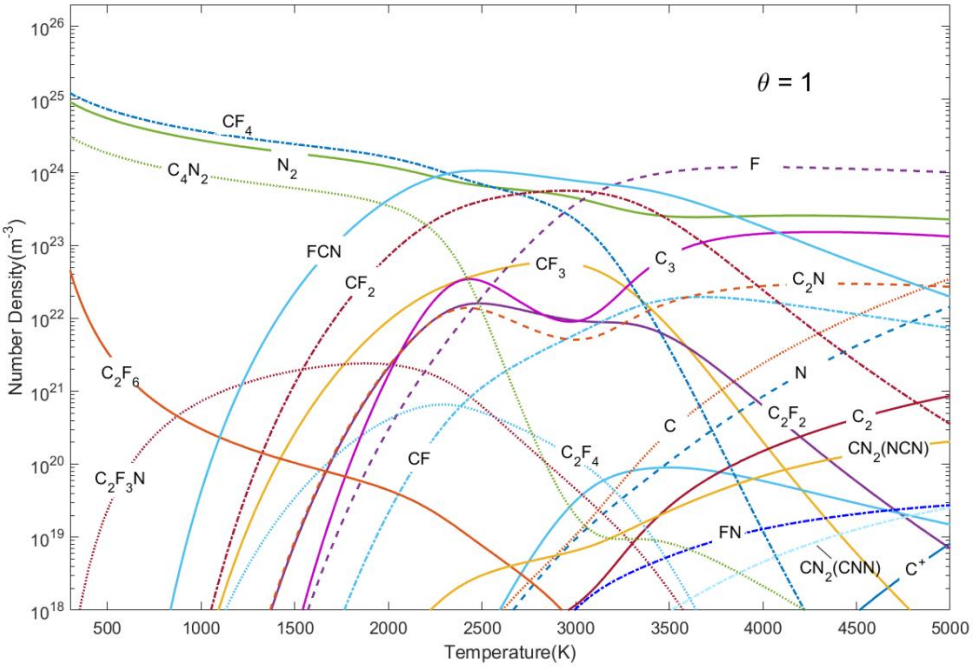

Fig. 5-4 (a)

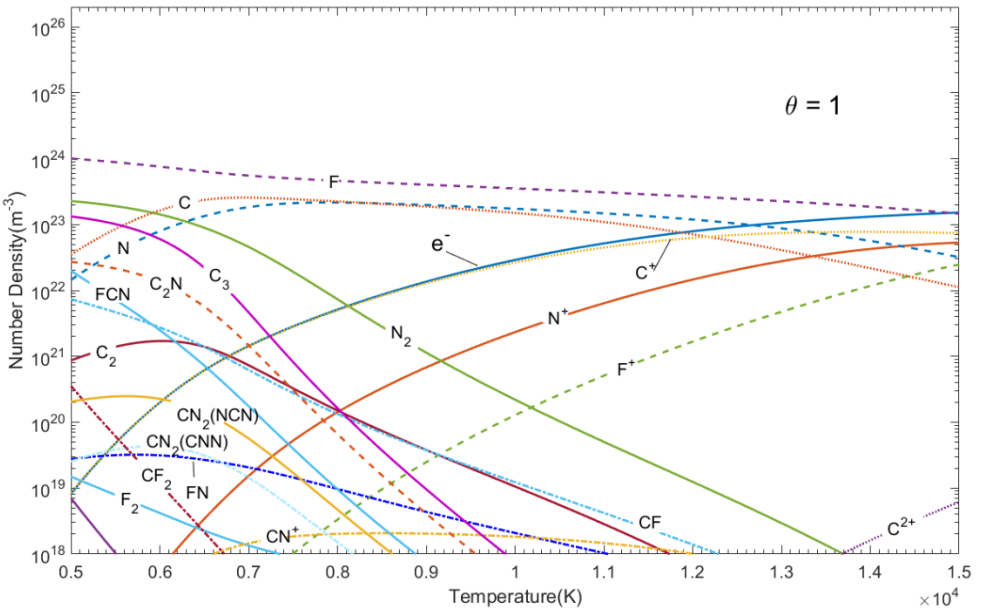

Fig. 5-4 (b)

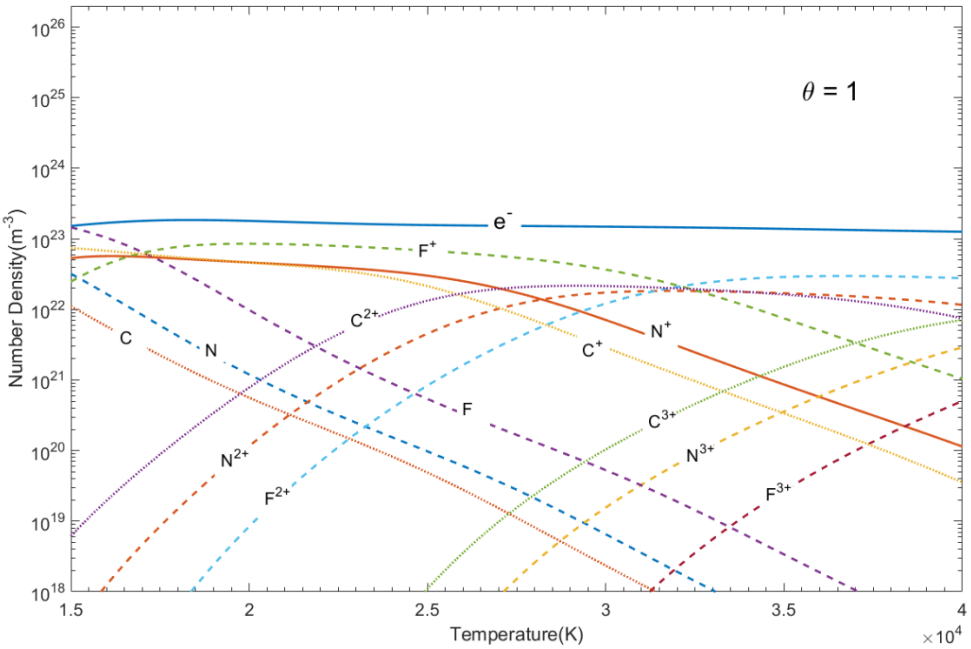

Fig. 5-4 (c)

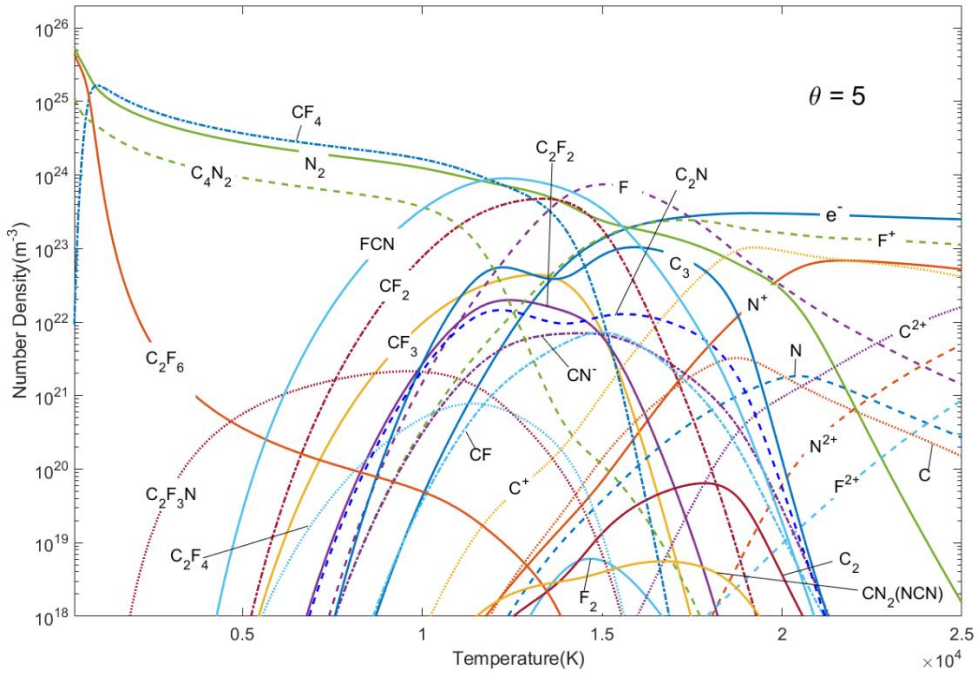

Fig. 5-4 (d)

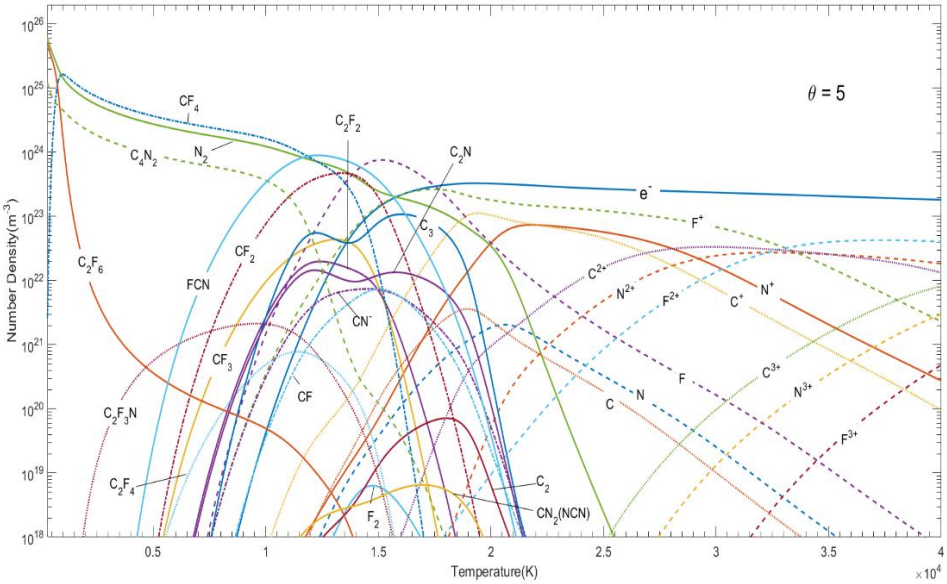

Fig. 5-4 (e)

Fig. 5-4: Temperature dependence of the number density of 50% nitrogen - 50% PTFE initial volume ratio gas plasma under non-equilibrium degree of 1 (a)(b)(c) and 5 (d)(e) at atmospheric pressure

A numbers of diagrams are shown in Fig. 5-5 comparing the number density of different species under different non-thermal equilibrium degree. Some important features can be described.

The number density of electrons indicates the severity of the ionization processing. It can found that the ionization process is governed by both electron and heavy-particle temperatures. It is noticed that for $\theta = 1, 2 \text{ and } 3$, ionization starts from 7,500 K, 8,500 K and 10,000 K respectively. The higher degree shifts the ionization of heavy particles towards higher electron temperature. This phenomenon is manifested clearly when θ is larger than 5(Fig. 5-5(d)).

The main species of PTFE vapour are C_2F_6 and CF_2, their dissociation is only governed by heavy-particles temperature. However, C_2F_6 is dissociated rapidly once the heavy-particles temperature rises above room temperature. CF_2 is

much more stable than C_2F_6. It is clear that CF_2 remains at high density at high electron temperatures with a high θ. It is due to the low dissociation excitation temperature. The number density of ions is higher than their atoms at large θ . The reason is that the ionization of atoms takes place immediately when electrons contain high energy and dissociation reactions occur, at high θ.

The influence of Debye length cannot be neglected. The influence of the Debye length due to all charged species and that due to electrons only are both given in Fig. 5-5. For heavy-particles, the influence of Debye length considering all charged species and considering electrons only is small when θ is lower than 10. It is evident that, when θ is 20, there is significant difference in the heavy-particles number density with the Debye length calculated based on electrons and ions increased rapidly at high temperate. It drops eventually at about temperature of 50,000-60,000 K that will not be present.

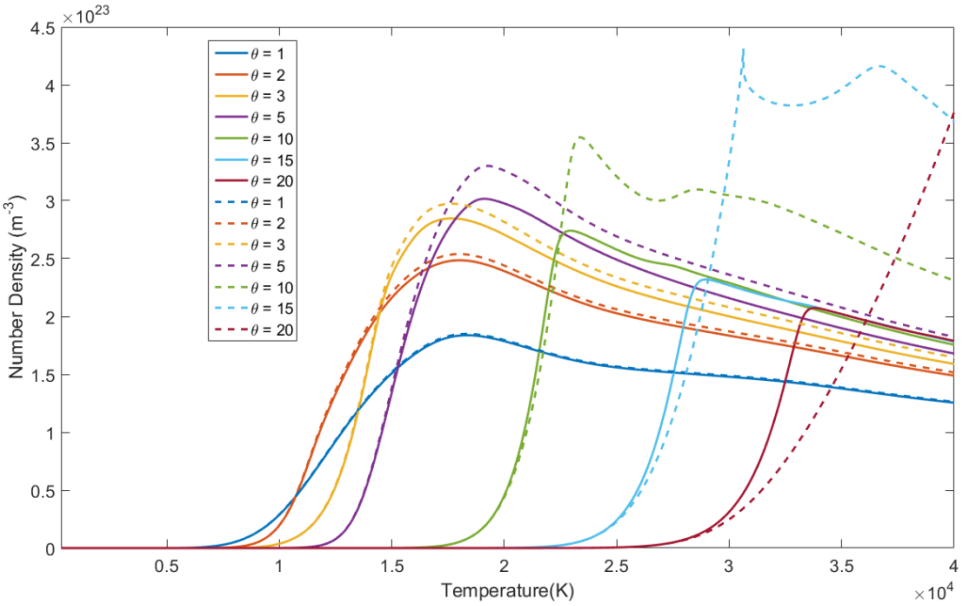

Fig. 5-5(a): electrons

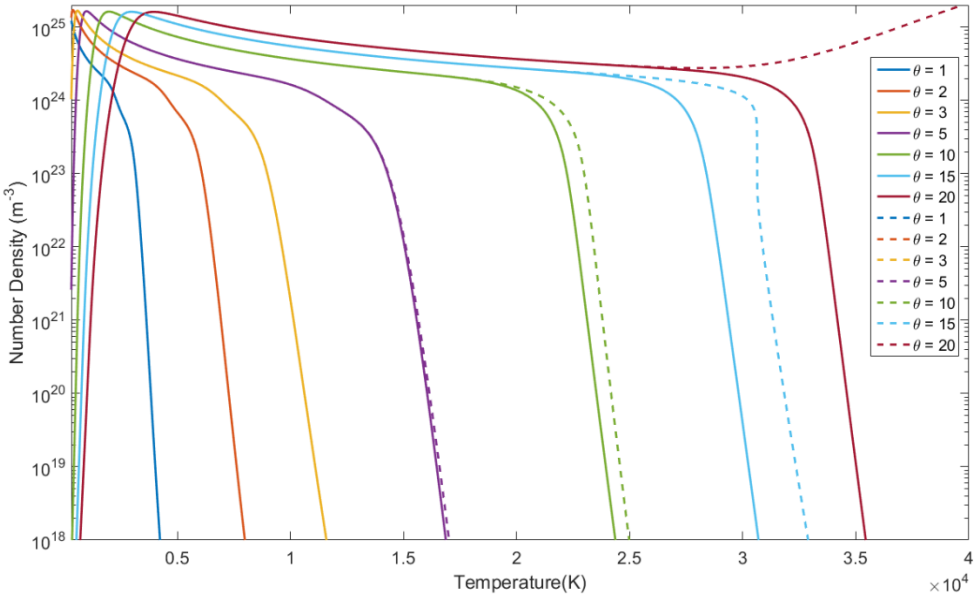

Fig. 5-5(b): CF_2

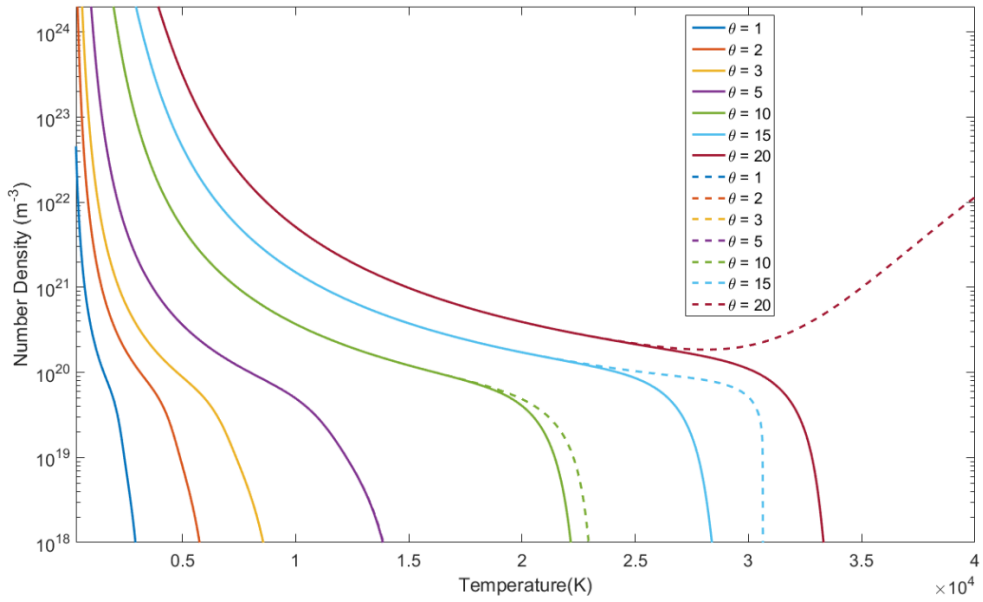

Fig. 5-5(c): C_2F_6

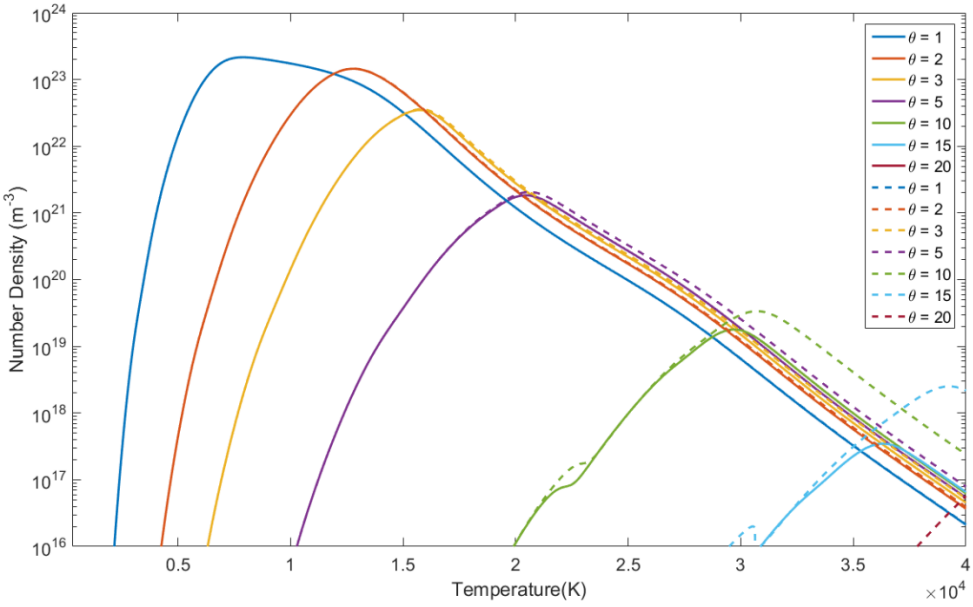

Fig. 5-5(d): N

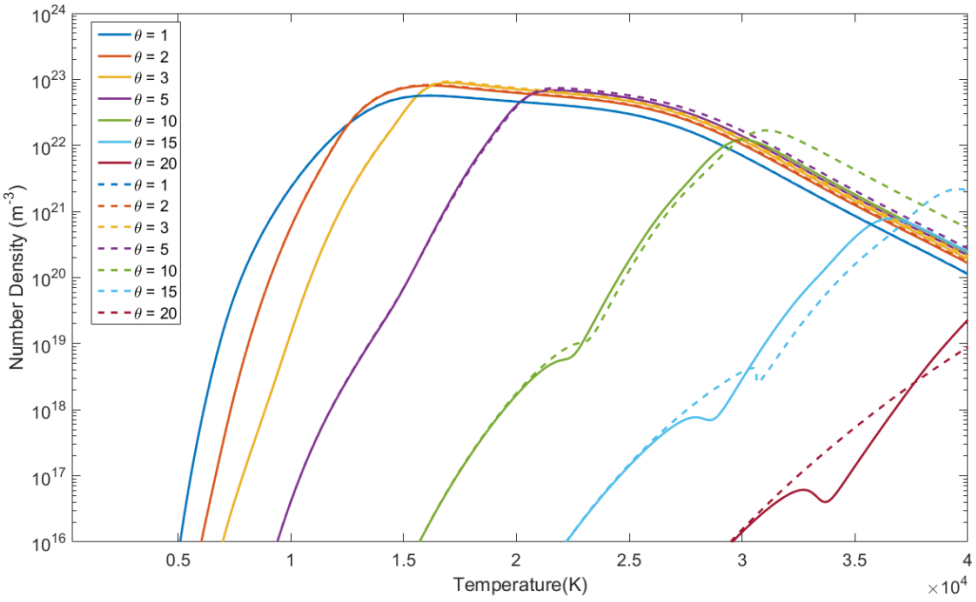

Fig. 5-5(e): N^+

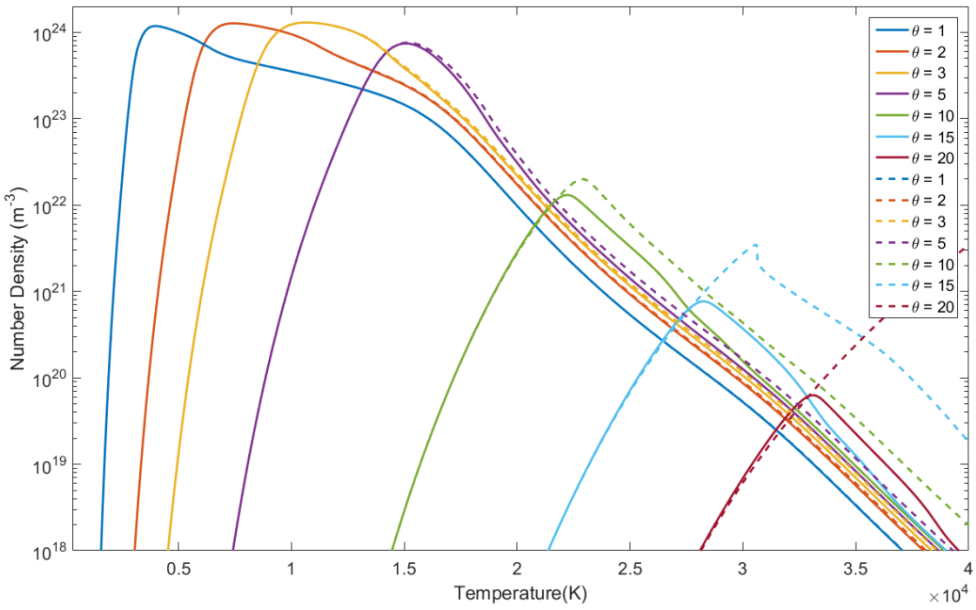

Fig. 5-5(f): F

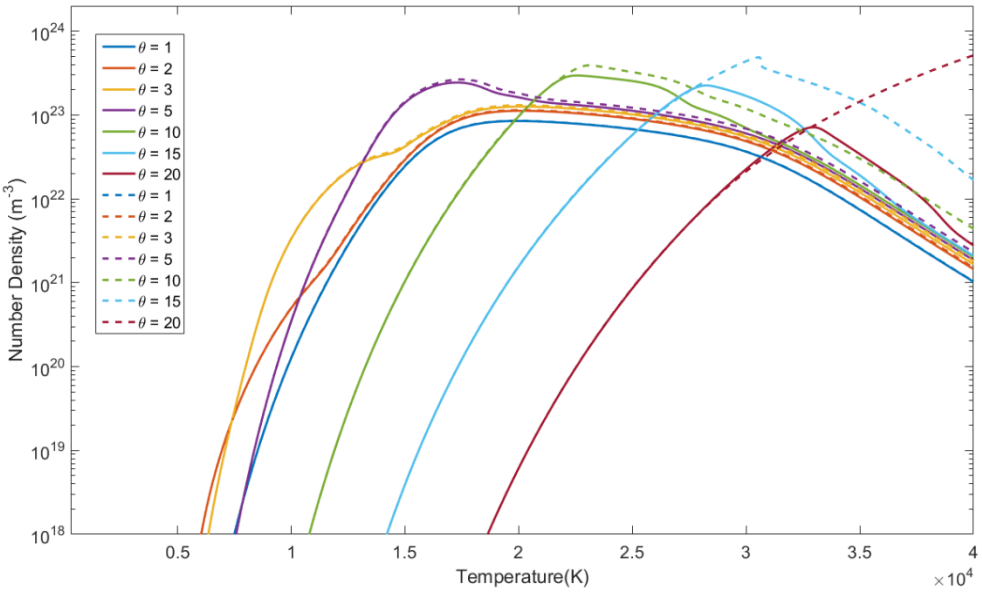

Fig. 5-5(g): F^+

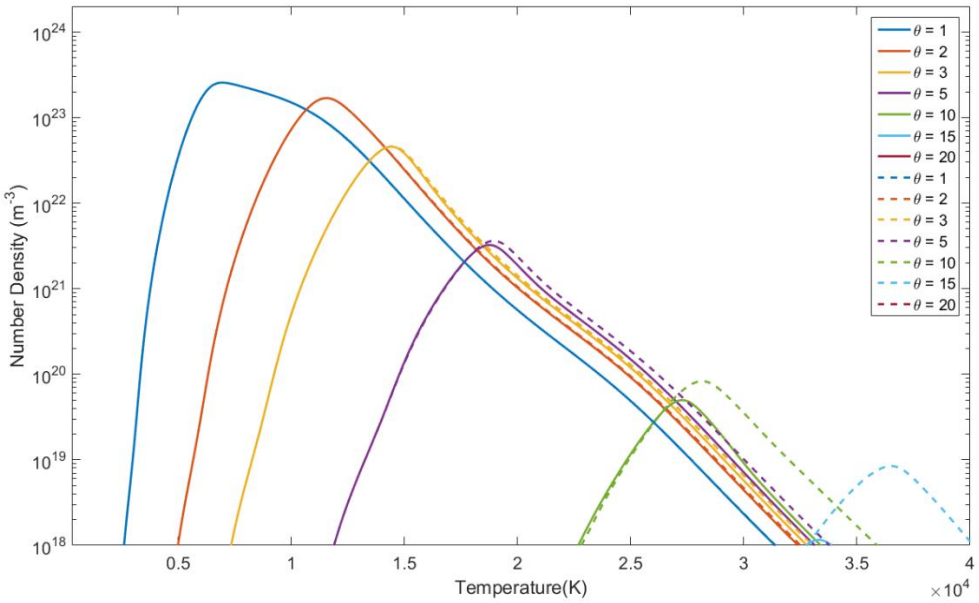

Fig. 5-5(h): C

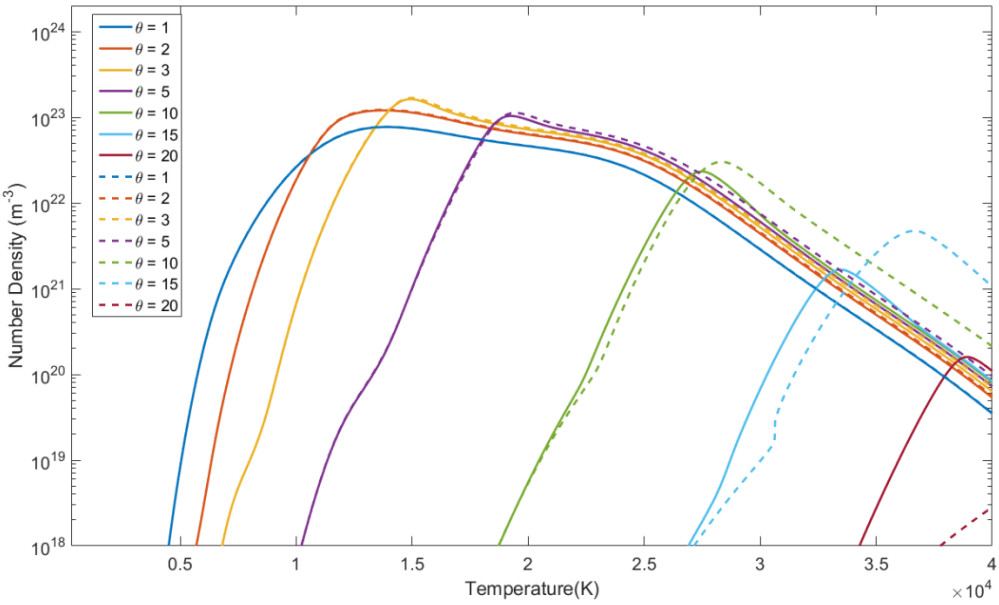

Fig. 5-5(i): C^+

Fig. 5-5: Temperature dependence of the number density of different species (a) free electron (b)CF2 (c) C2F6 (d)nitrogen atom (e) N+ (f) F atom (g) F+ (h) C atom (i) C+ of 50% nitrogen - 50% PTFE initial volume ratio gas plasma with different non-equilibrium degree at atmospheric pressure: The solid line indicates the Debye length including only electrons while dashed line indicates the Debye length including electrons and ions.

The molecule dissociation temperature is shifted higher when non-LTE degree is getting higher. It results in larger mass density in higher θ. Due to the shielding effect, the number density of some species increased rapidly at $\theta = 20$, it leads to the increase in mass density increased at high temperature with $\theta = 20$.

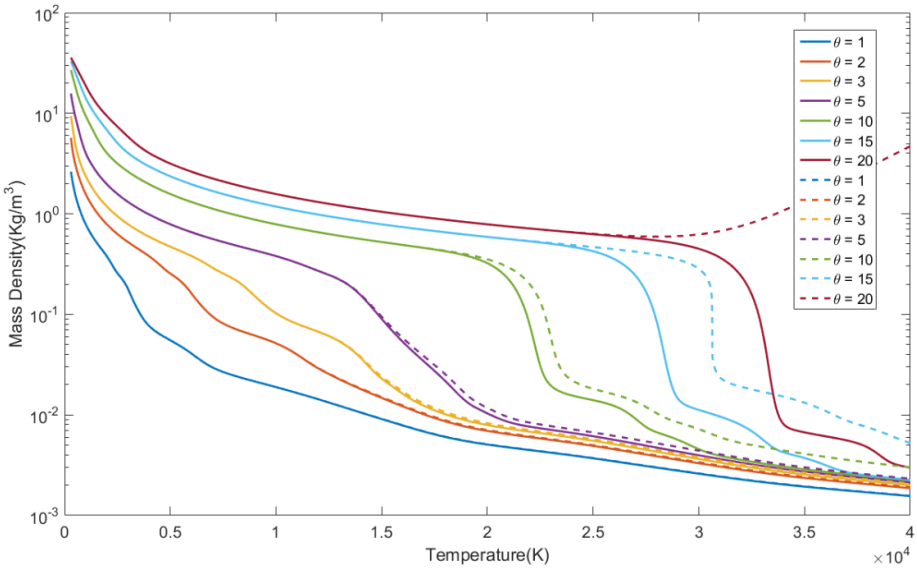

Fig. 5-6: Temperature dependence of mass density of nitrogen plasmas under different degrees of 50% nitrogen - 50% PTFE initial volume ratio gas plasma with different non-equilibrium degree at atmospheric pressure

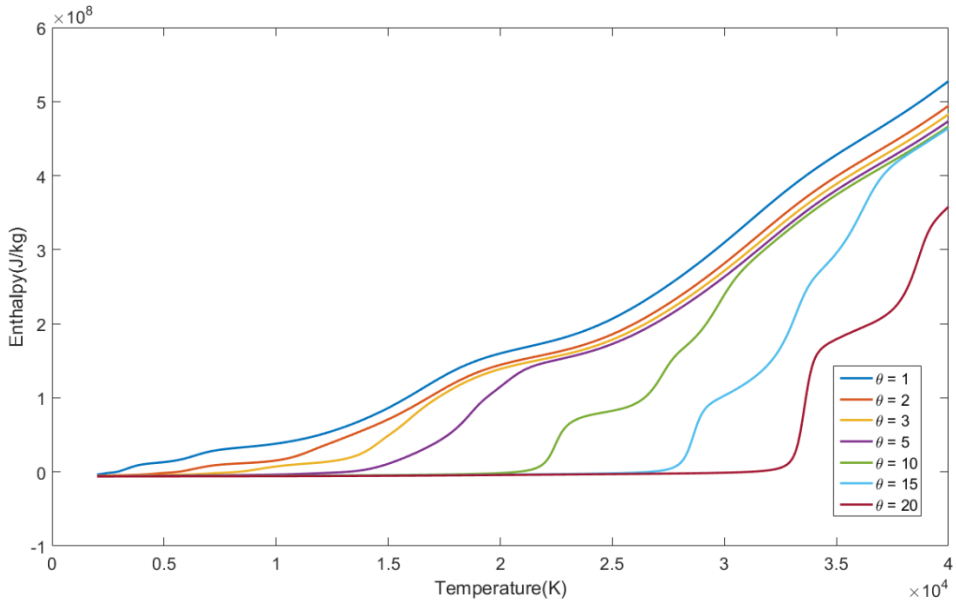

Fig. 5-7: Temperature dependence of enthalpy of 50% nitrogen - 50% PTFE initial volume ratio gas plasma with different non-equilibrium degree at atmospheric pressure

The enthalpy and total specific heat are present in Fig. 5-7 and Fig. 5-8 for 50% nitrogen and 50% PTFE molar concentration with different non-LTE degrees. Due to the heavy-particles dissociation is shifted to higher electron temperature by non-LTE degree getting larger, the peak of total specific heat is shifted to higher electron temperature as well.

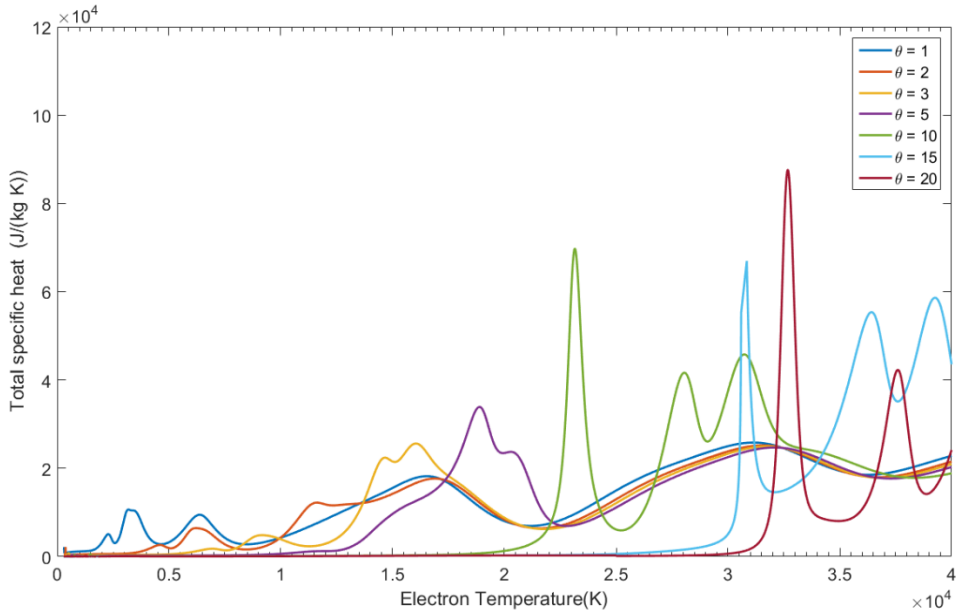

Fig. 5-8: Temperature dependence of total specific heat of 50% nitrogen - 50% PTFE initial volume ratio gas plasma with different non-equilibrium degree at atmospheric pressure

5.3.2 Transport coefficients

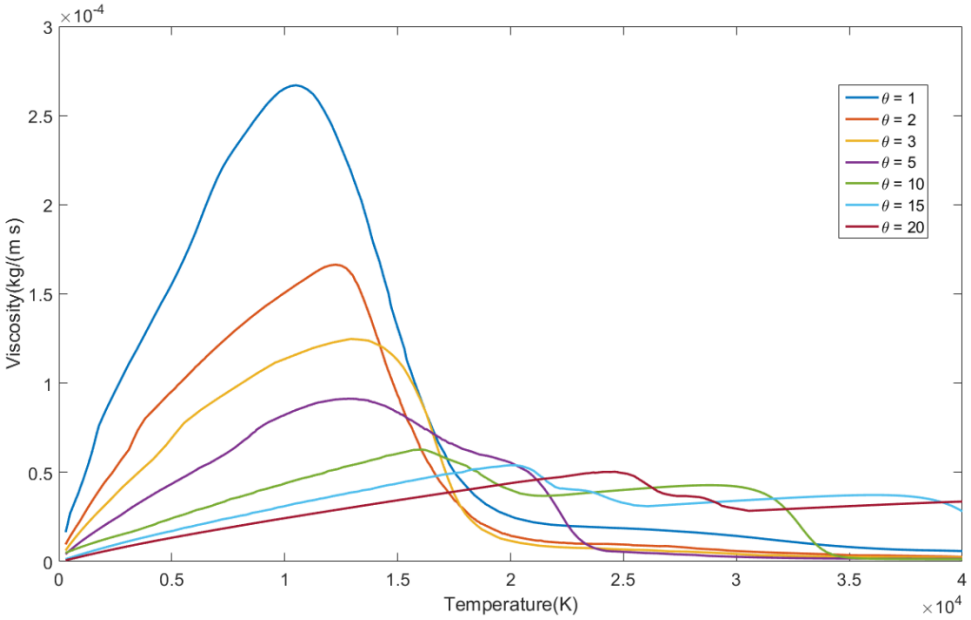

Fig. 5-9: Temperature dependence of viscosity of 50% nitrogen - 50% PTFE initial volume ratio gas plasma with different non-equilibrium degree at atmospheric pressure

Heavy particles are only considered in the calculation of the viscosity. It reaches its first peak around 10,000 K in the LTE case. The electron temperature corresponding to the first peak increases with an increasing non-LTE degree. It has been stated that the viscosity of the mixture is determined by the heavy-particles. Thus, T_e should not affect the viscosity. However, T_h is linked to T_e through $\theta = \frac{\mathrm{T}_e}{T_h}$. Taking $\theta = 10$ as an example. In this case $\mathrm{T}_h = 1{,}600\ K$ at the peak of the viscosity. When $T_e = 16{,}000\ K$, the peak value is equal to the LTE value at $\mathrm{T}_h = 1{,}600\ K$. The other peaks can be explained in a similar way.

Thermal conductivity

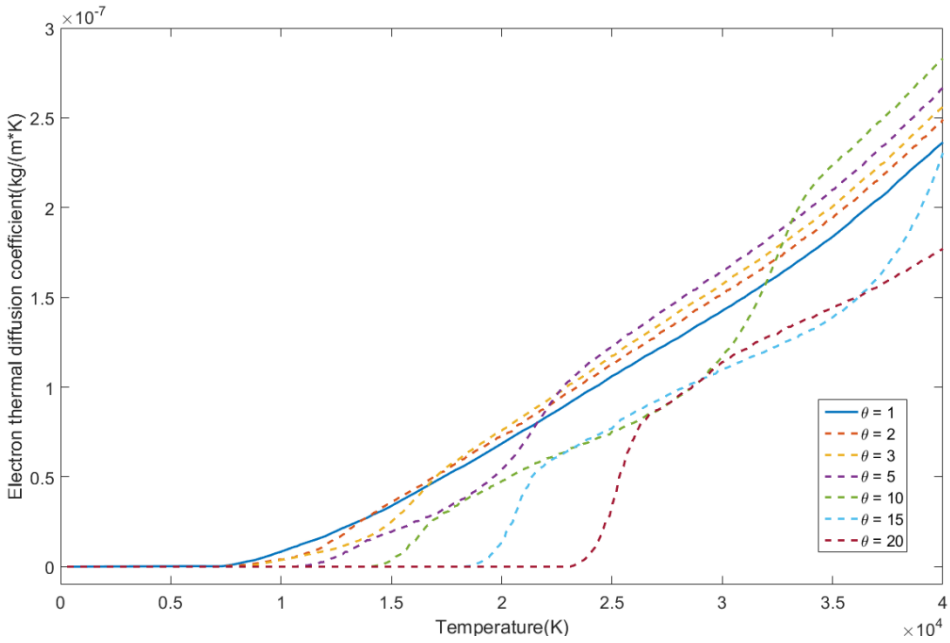

Fig. 5-10: Temperature dependence of diffusion coefficient of 50% nitrogen - 50% PTFE initial volume ratio gas plasma with different non-equilibrium degree at atmospheric pressure

The electron and heavy species translational thermal conductivities of a N_2-PTFE 50%-50% mixture plasma are shown below in Fig. 5-11 and Fig. 5-12. The translational thermal conductivity of the heavy-particles peaks at 11,000 K at $\theta = 1$, very close to the temperature corresponding to the viscosity peak of $\theta = 1$. Deviation from LTE tends to broaden envelop. The peak value drops from 0.5 W(m*K) to 0.06 for a change of θ from 1 to 10. This variation is a reflection

of the change in the gas composition. The pattern of variation is strikingly similar to the change in electron diffusion coefficient (Fig. 5-10). The variation as a function of temperature (T_e) tends to be more nonlinear when $\theta = \frac{T_e}{T_h}$ increases. There is an initial exponential increase which is followed by a slower and smoother increase. Comparing Fig. 5-11 and Fig. 5-12, it is immediately evident that electrons play a much more important role in conducting heat in a plasma when $T_e > 15{,}000\ K$. The electron translational thermal conductivity on the other hands depends on its number density and temperature.

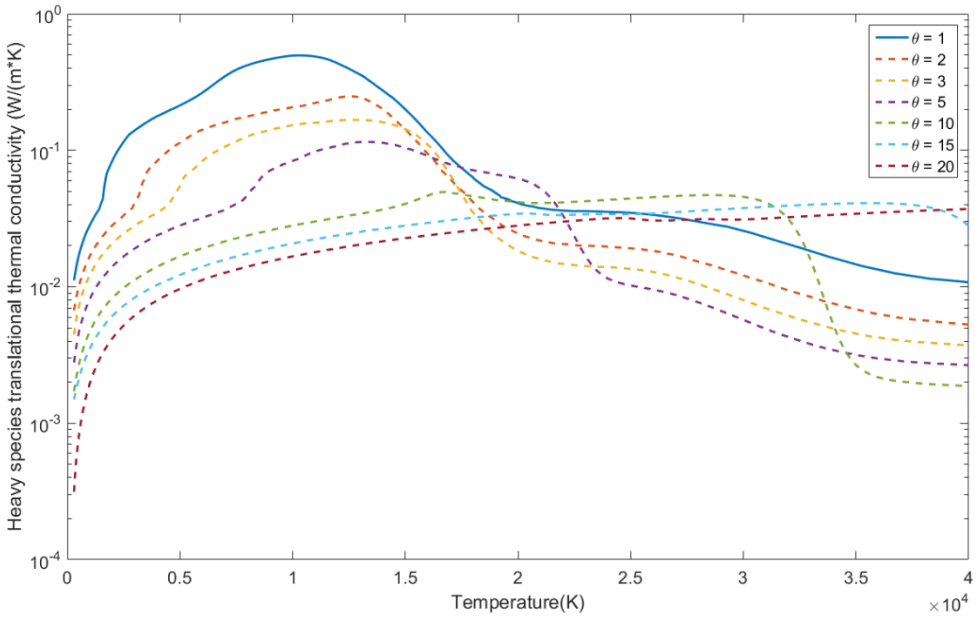

Fig. 5-11: Heavy species translational thermal conductivity for 50%-50% N_2-PTFE mixture plasma with different non-LTE degree at the pressure of 1 bar.

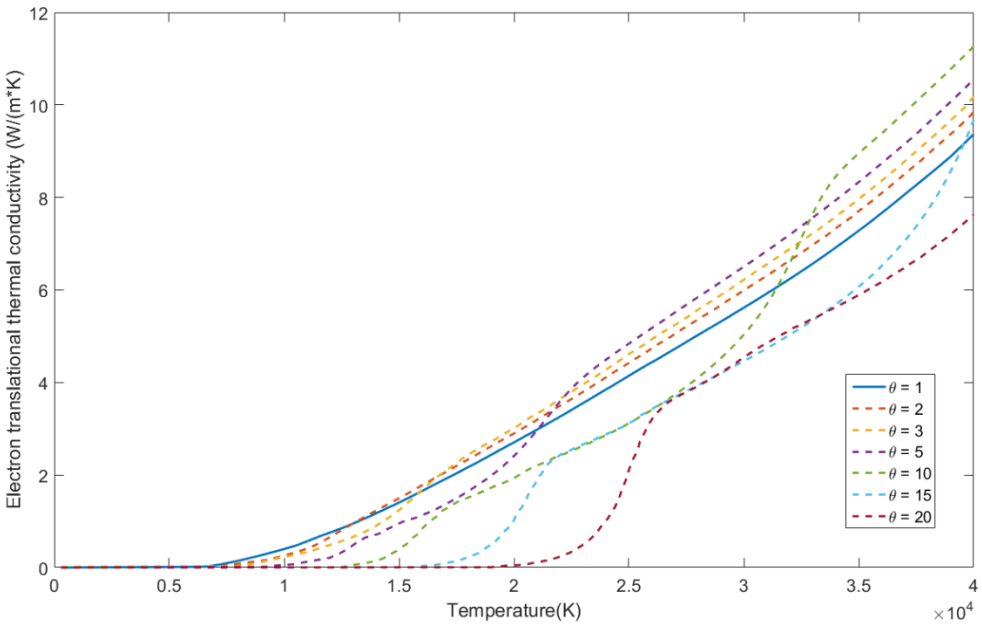

Fig. 5-12: Electron translational thermal conductivity for 50%-50% N_2-PTFE mixture plasma with different non-LTE degree at the pressure of 1 bar.

Electrical conductivity

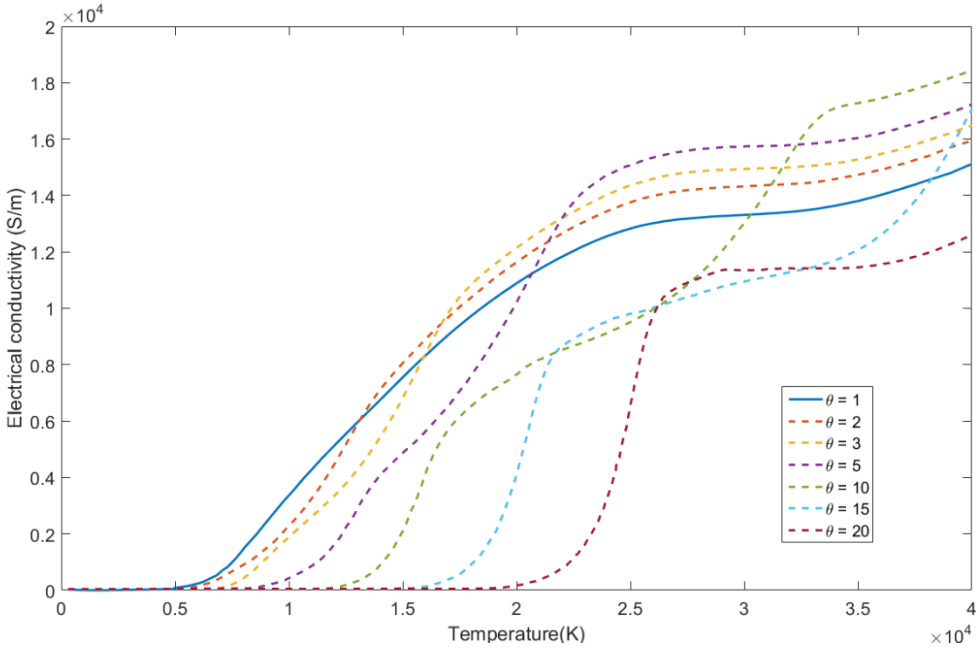

Fig. 5-13: Temperature dependence of electrical conductivity of 50% N_2- 50% PTFE mixture gas plasma with different non-LTE degree at atmospheric pressure (p = 1 bar)

The electrical conductivity is shown in Fig. 5-13 with different non-LTE degrees. To produce free electrons, the molecules have to be first dissociated into atoms. Collisions between heavy-particle are most efficient for dissociation. Therefore, for $\theta = \frac{T_e}{T_h} > 1$, significant dissociation takes place at a higher T_e and this shifts the rapid increase in electrical conductivity to higher T_e. The higher electrical conductivity of the non-LTE plasma when $T_e > 13{,}000\ K$ for $\theta = 2$ is a result of the higher electron number density in comparison with the LTE case, as shown in Fig. 5-5(a). In fact, n_e of $\theta = 2$ is already higher than n_e of $\theta = 1$ at $T_e = 12{,}000\ K$. However, in explaining the electrical conductivity charge, it must take into account the fact that electrical conductivity is not purely determined by the electron number density, the heavy-particle number density will also affect it through the mean free path of the electrons.

5.3.3 Influence of different molar proportions of N_2 and PTFE to transport coefficients

Fig. 5-14 shows the mass density for different molar fraction of Nitrogen and PTFE. It is clear that the total mass density decreases and become lower as higher PTFE molar concentration when $T_e < 15{,}000\ K$. It is interesting to note that the density curves reverse their order over the temperature range of 14,500 K to 21,500 K. At these two temperature all curves overlap.

Fig. 5-15 displays the enthalpy of the two temperature plasma as a function of electron temperature with the PTFE concentration as a parameter. The curves can be divided into three parts, T_e <14,500 K, 14,500 K ~ 21,500 K, >21,500 K. When temperature is at 18,000 K, the total specific heat of pure PTFE gas increases rapidly due to dissociation reaction of CF_4, C_3 and ionization of fluorine. The second peak at 28,500 K is a result of F^+ being ionized to F^{2+} and C^+ ionized to C^{2+}. The total specific heat of pure nitrogen plasma starts to increase rapidly around 15,000 K, this is caused by the dissociation of nitrogen

molecules. When the temperature is higher than 22,000 K, the total specific heat of pure nitrogen plasma increases again smoothly as the nitrogen atoms start to be ionised. Pure PTFE vapour has the highest specific heat. With the presence of 20% N_2, the peak value reduces to half of that of pure PTFE.

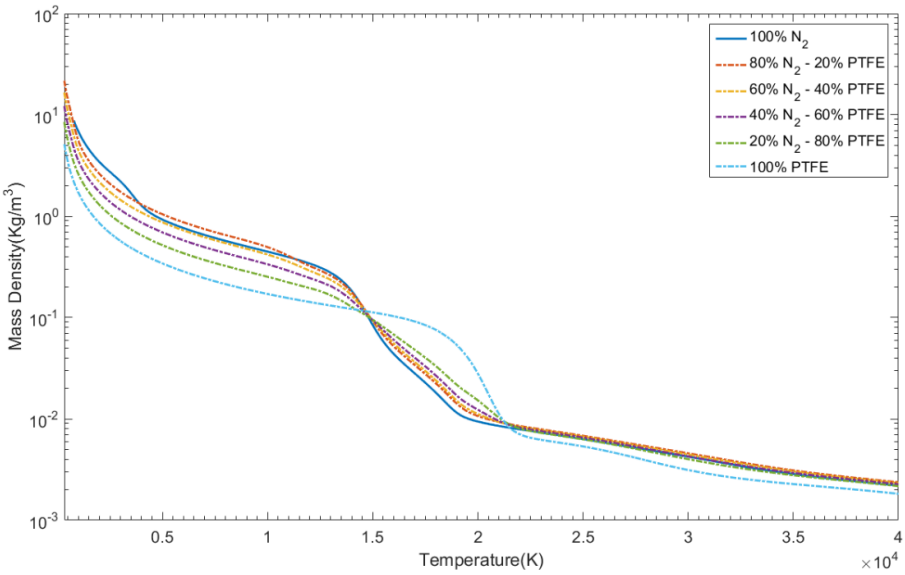

Fig. 5-14: Temperature dependence of mass density of N_2-PTFE mixture gas plasma with different molar proportions at non-LTE degree $\theta = 5$ at atmospheric pressure (p = 1 bar)

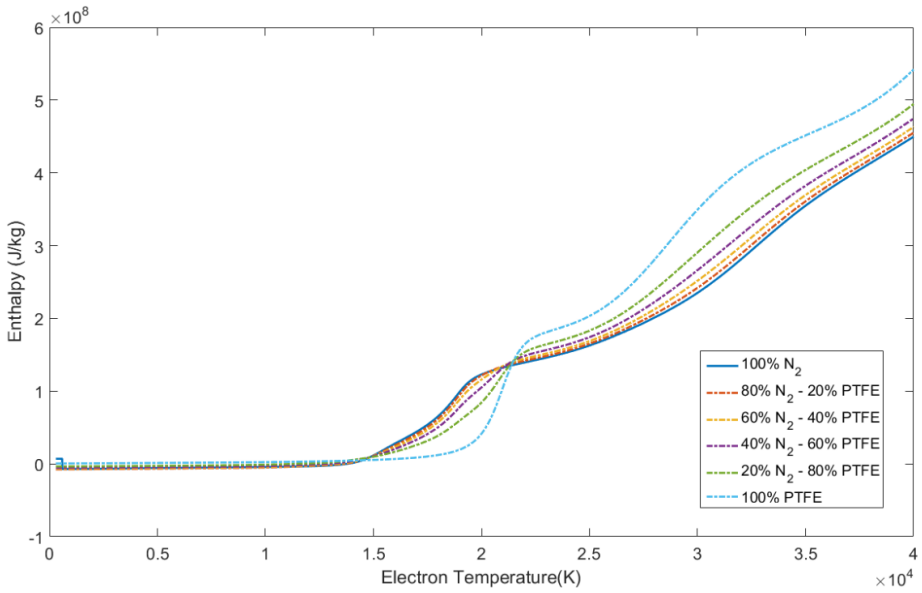

Fig. 5-15: Temperature dependence of enthalpy of N_2-PTFE mixture gas plasma with different molar proportions at non-LTE degree $\theta = 5$ at atmospheric pressure (p = 1 bar)

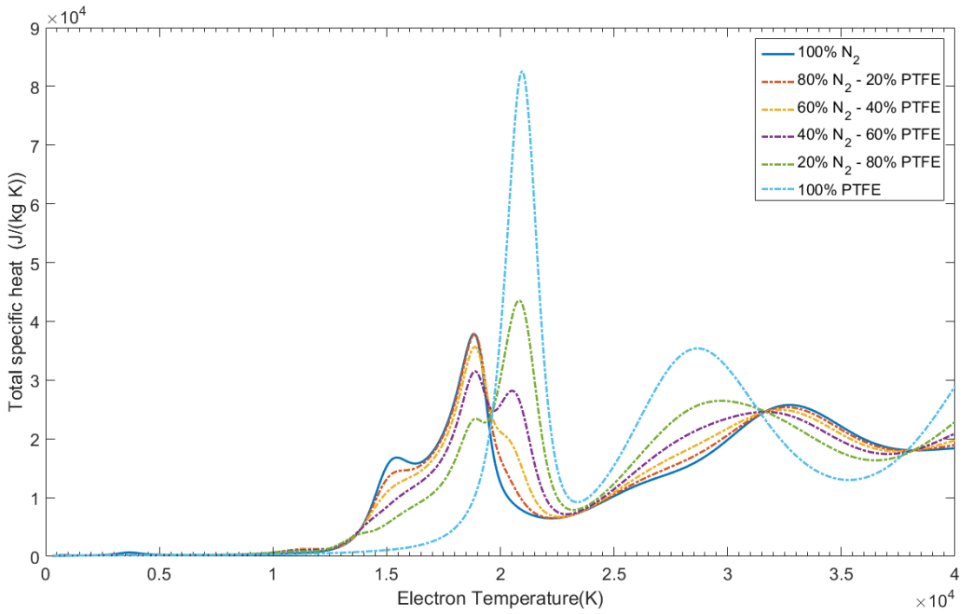

Fig. 5-16: Temperature dependence of total specific heat of N_2-PTFE mixture gas plasma with different molar proportions at non-LTE degree $\theta = 5$ at atmospheric pressure (p = 1 bar)

Fig. 5-17 and Fig. 5-18 show the heavy species and electron translational thermal conductivity with different PTFE concentration for a non-LTE plasma.

The heavy species translational thermal conductivity curves change their order at $T_e = 12{,}500\,K$ and $16{,}500\,K$. The electron translational thermal conductivity depends on the number density of electrons and electron temperature. Its value at higher PTFE molar concentration tends to be higher, which agrees with what is shown in Fig. 5-2 and Fig. 5-3.

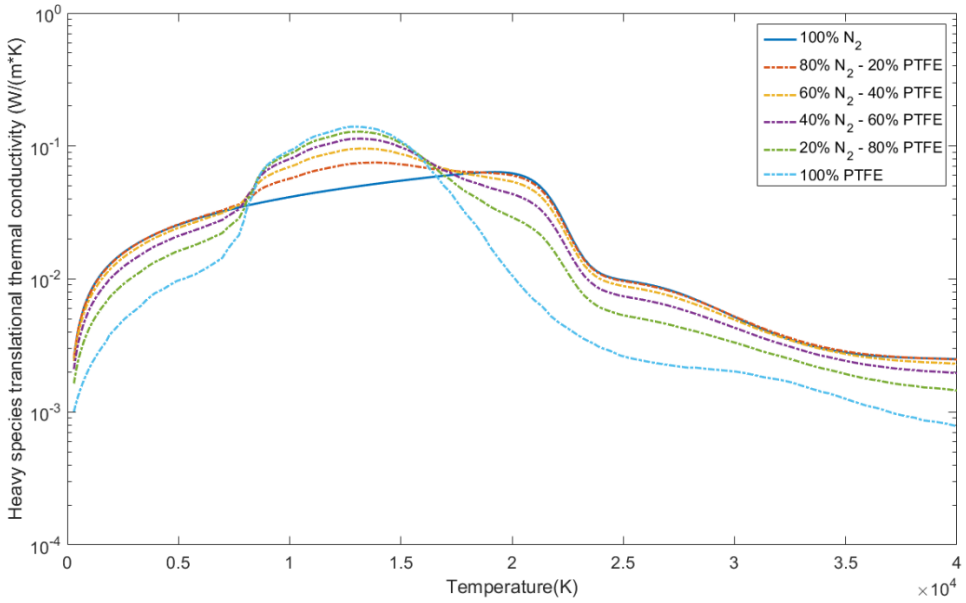

Fig. 5-17: Temperature dependence of Heavy species translational thermal conductivity of N_2-PTFE mixture with different molar concentration at non-LTE degree of $\theta = 5$ at atmospheric pressure (p = 1 bar)

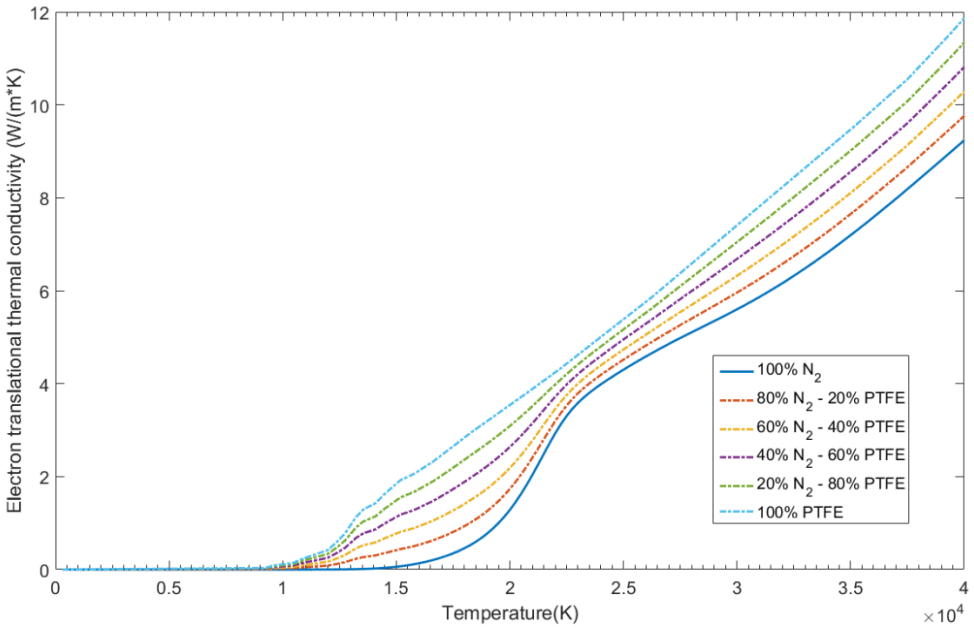

Fig. 5-18: Temperature dependence of electron translational thermal conductivity of N_2-PTFE mixture gas plasma with different molar proportions at non-LTE degree $\theta = 5$ at atmospheric pressure (p = 1 bar)

The viscosity results in Fig. 5-19 show that higher collision integrals of nitrogen molecules and atoms results in lower viscosity when N_2 molar concentration increases. The peak of viscosity also shifts towards higher T_e when the PTFE concentration increases, which is due to the higher ionisation energy of nitrogen atoms.

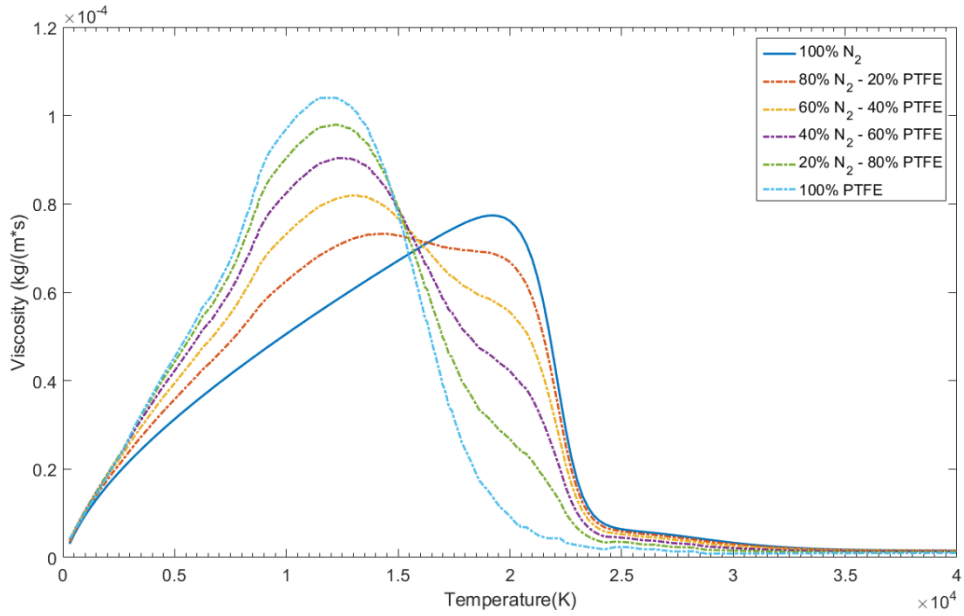

Fig. 5-19: Temperature dependence of viscosity of N_2-PTFE mixture gas plasma with different molar proportions at non-LTE degree $\theta = 5$ at atmospheric pressure (p = 1 bar)

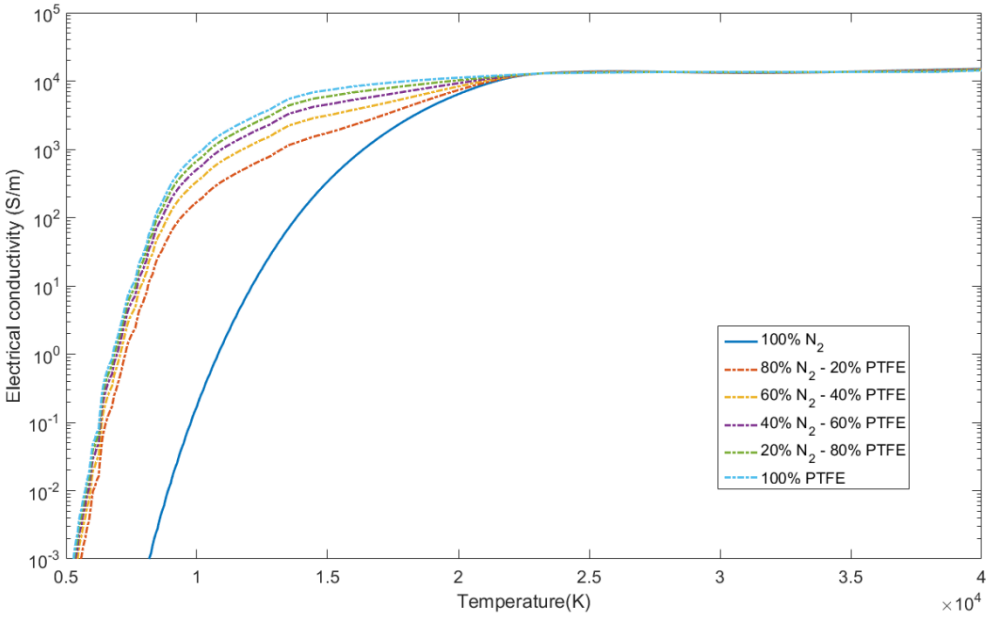

Fig. 5-20: Temperature dependence of electrical conductivity of N_2-PTFE mixture gas plasma with different molar proportions at non-LTE degree $\theta = 5$ at atmospheric pressure (p = 1 bar)

The electrical conductivity of pure PTFE vapour and N_2 gas are very different below 20,000 K due to the different ionisation potentials of their constituting atoms. The presence of PTFE vapour even at a low concentration, significantly affects the electrical conductivity of the mixture. For example, at $T_e = 10{,}000\ K$, the number density of electron in pure N_2 is still low and the electrical conductivity is only 0.1 S/m. With only 20% of PTFE, the electrical conductivity of the mixture increases by three orders of magnitude, reaching 100 S/m. The influence of PTFE on the electrical conductivity of the mixture weakens when the PTFE concentration is about 40%. Above 20,000 K, both gases have nearly the same conductivity and the PTFE concentration has very limited influence on the conductivity.

5.3.4 Discussion on the different methods used to calculate the plasma composition

As mentioned early in this chapter, there are four existing methods to calculate the plasma composition. Godin's method is based on the same principle as that Gibbs's free energy minimisation method, but uses different expressions. These two methods are similar with Van de Sanden's method. The fourth method is Potapov's method. It would be informative to select a case to compare the differences in the results. Fig. 5-21 contains the results of electron number density from three methods with non-LTE degree of 1,2 and 5 and 50% PTFE concentration. With $\theta = 1$, all three methods produce the same composition. However, Potapov's method behaves very differently in the non-LTE cases ($\theta = 2\ and\ 5$). Assume T_p is the electron temperature when the number density reaches highest value, when $T_e < T_p$ the results produced by Godin and Van de Sanden et al. methods are matched each other. Beyond T_p, all three methods produce very similar results.

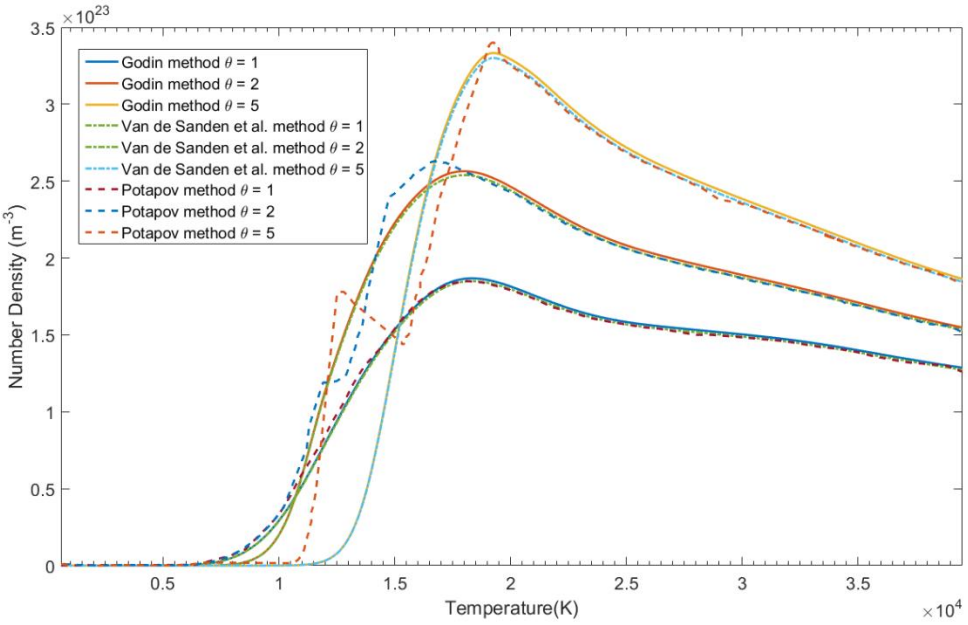

Fig. 5-21: Comparison of equilibrium number density for electrons in 50% N_2- 50% PTFE plasma from Godin's method (our calculation), Van de Sanden et al.'s method and Potapov's method with different non-LTE degree.

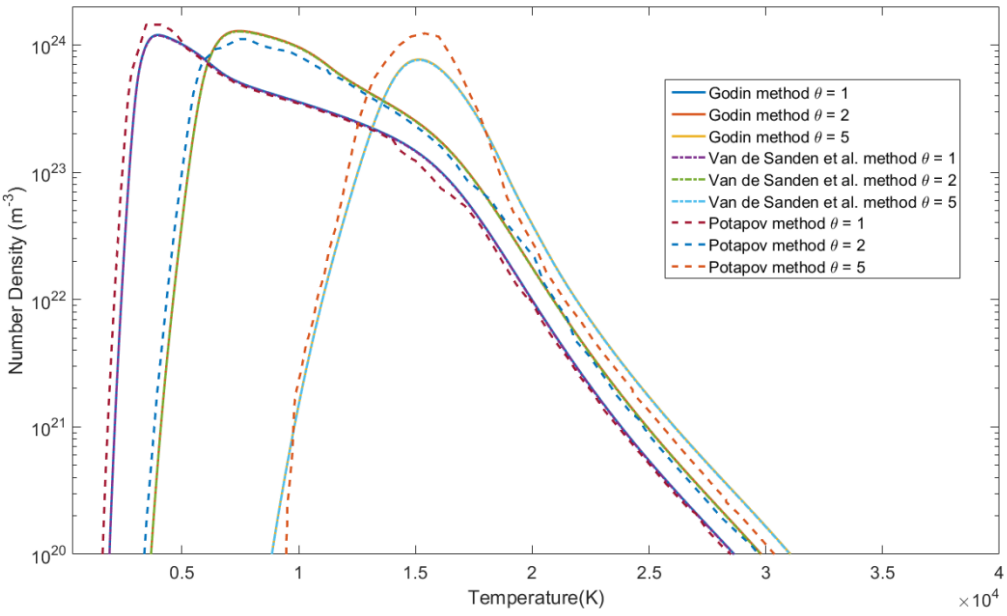

Fig. 5-22: Comparison of equilibrium number density for fluorine in 50% N_2- 50% PTFE plasma from Godin's method (our calculation), Van de Sanden et al.'s method and Potapov's method with different non-LTE degree.

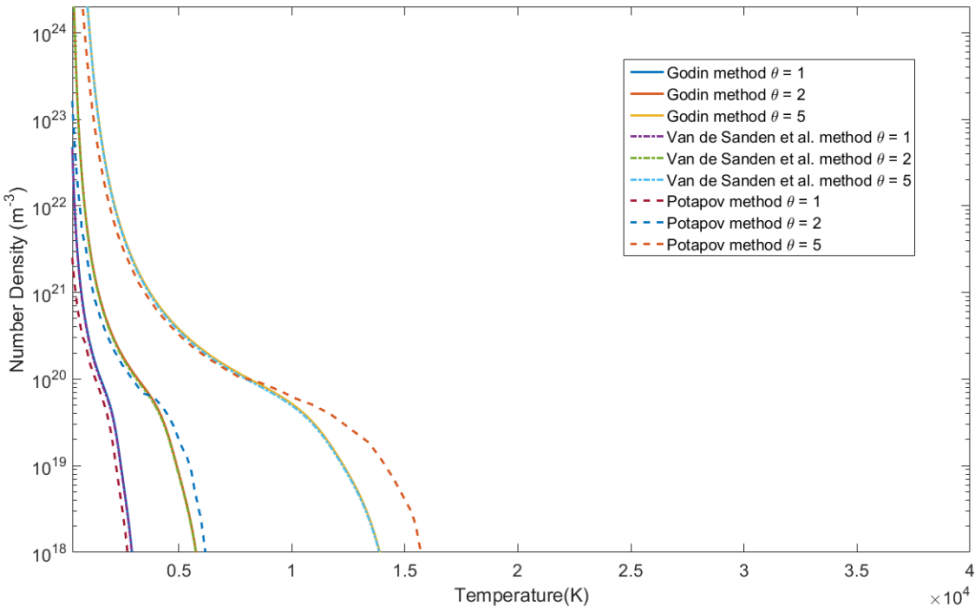

Fig. 5-23: Comparison of equilibrium number density for C_2F_6 in 50% N_2- 50% PTFE plasma from Godin's method (our calculation), Van de Sanden et al.'s method and Potapov's method with different non-LTE degree.

5.4 Comparison with existing data

In order to verify the model, a comparison with existing data has been made and presented in Fig. 5-24 and Fig. 5-25. Since there are no results for nitrogen-PTFE mixture, the results for pure PTFE vapour are compared with those of Wang[33]. The electron number densities in a pure PTFE plasma with different non-LTE degrees are given in Fig. 5-24 and the mass density in Fig. 5-25. There is good agreement between the two sets of data. There is slight difference in electron number density, which might be caused by the difference in fundamental energy data used in the calculation.

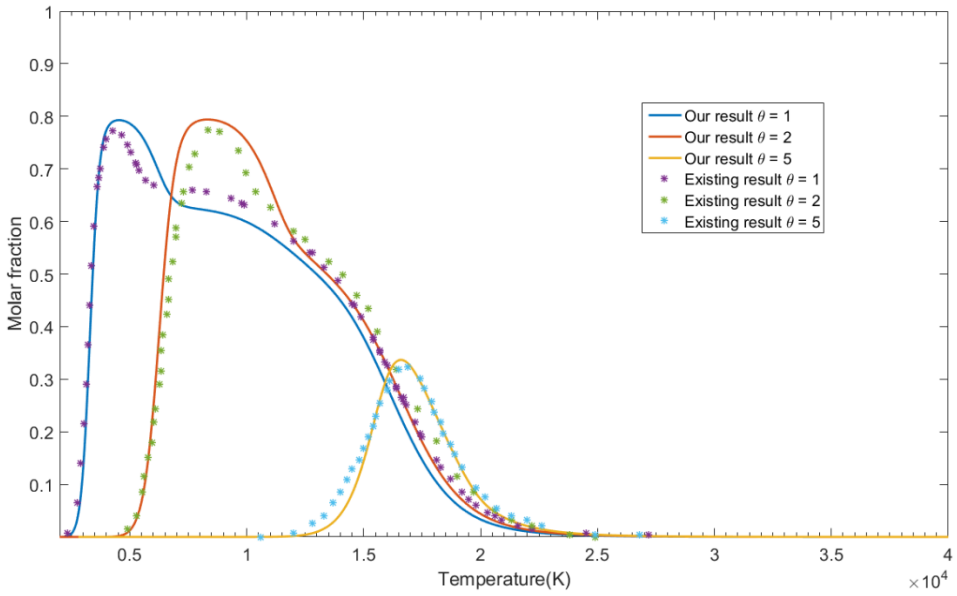

Fig. 5-24: Comparison with existing results of molar fraction for pure PTFE with different non-LTE degree at 1 bar

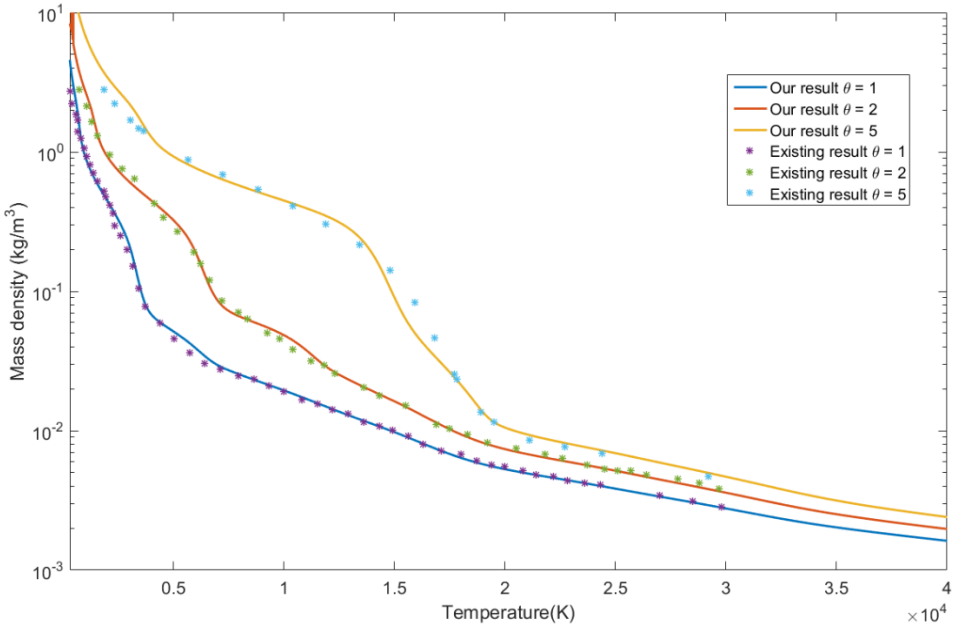

Fig. 5-25: Comparison with existing results of mass density for pure PTFE with different non-LTE degree at 1 bar

5.5 Summary

The composition, thermodynamic properties and transport coefficients of N_2-PTFE mixture with different molar concentration of PTFE have been calculated under LTE and non-LTE conditions assume chemical equilibrium.

The calculation was carried out for electron temperature range from 300 K to 40,000 K with PTFE concentration of 0%, 20%, 40%, 60%, 100%. For the non-LTE plasma cases, the ratio of electron temperature to heavy particle temperature has been set to 1, 2, 5, 10 and 20. The main features present in the results are analysed. A comparison of the results calculated using three methods was made, showing that Godin's method produces results very close to those of Van de Sanden's method. The composition results from the present work were compared with existing results, showing good agreement for pure PTFE vapour. A comparison for N_2-PTFE mixture has not been possible since no existing results are available.

5.6 References

[1]. G. Steward, M. P. Wilson, *The suitability of N_2 to replace SF_6 in a triggered spark-gap switch for pulsed power applications*, Universities Power Engineering Conference (UPEC), 1, (2009).

[2]. J. L. Zhang, J. D. Yan, A. B. Murphy, W. Hall and M. T. C. Fang, *Computational investigation of arc behaviour in an auto-expansion circuit breaker contaminated by ablated nozzle vapor*, IEEE Trans. On Plas. Sci., 30, 706, (2002).

[3]. W. Z. Wang, Y. Wu and M. Z. Rong, *Influence of ablated PTFE vapor entrainment on critical dielectric strength of hot SF6 gas*, IEEE Trans. On Diel. and Elec. Insu., 14, 4, 1478, (2014).

[4]. A. Gleizes, B. Chervy, and J. J. Gonzales, *Calculation of a two-temperature plasma composition: bases and application to SF_6*, J. Phys. D: Appl. Phys. 32, 2060, (1999).

[5]. Y. Tanaka, Y. Yokomizu, M. Ishikawa, and T. Matsumura, *Particle composition of high-pressure SF_6 plasma with electron temperature greater than gas temperature*, IEEE Trans. Plasma Sci. 25, 991 (1997).

[6]. G. J. Cliteur, K. Suzuki, Y. Tanaka, T. Sakuta, T. Matsubara, Y. Yokomizu, and T. Matsumura, *On the determination of the multi-temperature SF_6 plasma composition*, J. Phys. D: Appl. Phys. 32,1851, (1999).

[7]. V. Rat, P. Andre, J .Aubreton, M. F .Elchinger, P. Fauchais, and A. Lefort, *A modified pseudo-equilibrium model competing with kinetic models to determine the composition of a two-temperature SF_6 atmosphere plasma*, J. Phys. D: Appl. Phys. 34, 2191, (2001).

[8]. P. Krenek, *Thermophysical properties of the reacting mixture SF6 and Cu in the range 3000 to 50000 K and 0.1 t 2 MPa*, Acta Tech. CSAV, 37, 399, (1992).

[9]. F. Yang, Z. Chen, Y. Wu, M. Rong, A. Guo, Z. Liu and C. Wang, *Two-temperature transport coefficients of SF6–N2 plasma*, Phys. of Plas. 22, 103508, (2015).

[10]. J. Aubreton, C. Bonnefoi, and J.M. Mexmain, *Calcul de proprietes thermodynamiques et des coefficients de transport dans un plasma Ar-O_2 en non-equilibre thermodynamique et a la pression atmospherique*, Rev. Phys. 21, 365, (1986).

[11]. V. Rat, P. Andre, J. Aubreton, M.F. Elchinger, P. Fauchais, and A. Lefort, *Two-temperature transport coefficients in argon–hydrogen plasmas—I: elastic processes and collision integrals*, Plas. Chem. Plas. Proc. 22, 475, (2002).

[12]. W. Z. Wang, M. Z. Rong, J. D. Yan, A. B. Murphy, and J. W. Spencer, *Thermophysical properties of nitrogen plasmas under thermal equilibrium and non-equilibrium conditions*, Phys. Plas., 18, 113502, (2011).

[13]. V. Colombo, E. Ghedini, and P. Sanibondi, *Thermodynamic and transport properties in non-equilibrium argon, oxygen and nitrogen thermal plasmas*, Prog. Nucl. Ener. 50, 921, (2008).

[14]. M. C. M. van de Sanden, P. P. J. M Schram, A. G. Peeters, J. A. M.van der Mullen, and G. M. W. Kroesen, *Thermodynamic generalization of the Saha equation for a two-temperature plasma*, Phys. Rev. A, 40, 5273, (1989).

[15]. A. V. Potapov, *Chemical equilibrium of multitemperature systems*, High Temp. 4 (1), 48 (1966).

[16]. D. Godin and J. Y. Trepanier, *A robust and efficient method for the computation of equilibrium composition in gaseous mixtures,* Plas. Chem. Plas. Proc., 24, 3, (2004).

[17]. P. Andre, *Partition functions and concentrations in plasmas out of thermal equilibrium*, IEEE Trans. Plasma Sci. 23, 453, (1995).

[18]. P. Andre, M. Abbaoui, A. Lefort, and M. J. Parizet, *Numerical method and composition in multi-temperature plasmas: application to an Ar-H_2 mixture*, Plas. Chem. Plas. Proc. 16, 379, (1996).

[19]. X. Chen and P. Han, *On the thermodynamic derivation of the Saha equation modified to a two-temperature plasma*, J. Phys. D: Appl. Phys, 32, 1711, (1999).

[20]. P. Andre, *Partition functions and concentrations in plasmas out of thermal equilibrium,* IEEE Trans. Plas. Sci., 23, 453, (1995).

[21]. P. Andre, M. Abbaoui, A. Lefort and M. J.M. Parizet, *Numerical method and composition in multi-temperature plasmas: application to an Ar-H_2 mixture*, Plasma Chem. Plasma Process, 16, 379 (1996).

[22]. P. Andre, J. Aubreton, M.F. Elchinger, V. Rat, P. Fauchais, A. Lefort and A. B. Murphy, *A statistical mechanical view of the determination of the composition of multi-temperature plasmas*, Plas. Chem. Plas. Proc., 24, 435, (2004).

[23]. A. Gleizes, B. Chervy, and J. J. Gonzales, *Calculation of a two-temperature plasma composition: bases and application to SF_6*, J. Phys. D: Appl. Phys. 32, 2060, (1999).

[24]. A. B. Murphy, *Transport coefficients of hydrogen and argon–hydrogen plasmas*, Plas. Chem. Plas. Proc. 20, 279, (2000).

[25]. M. W. Chase and Jr. C. A. Davies, NIST-JANAF Thermochemical Tables, 4th edn, American Institute of Physics for the National Institute of Standards and Technology, (1998).

[26]. J. P. Trelles, J. V. R Heberlein, and E. Pfender, *Non-equilibrium modelling of arc plasma torches*, J. Phys. D: Appl. Phys. 40, 5937, (2007).

[27]. J. O. Hirschfelder, C. F. Curtiss, and R. B. Bird, *Molecular theory of gases and liquids,* Wiley, (1964).

[28]. R. S. Devoto, *Simplified expressions for the transport properties of ionized monatomic gases*, Phys. Flui. 10, 2105, (1967).

[29]. C. Bonnefoi, *Contribution to theoretical calculation of transport coefficients of a nitrogen plasma using the Chapman-Enskog method with the fourth approximation of Sonine polynomial expansion*, Ph.D. thesis, Limoges University, France, (1983).

[30]. J. D. Ramshaw, *Hydrodynamic theory of multicomponent diffusion and thermal diffusion in multi-temperature gas mixtures*, J. Non-Equilibrium Thermodyn. 18, 121, (1993).

[31]. J. D. Ramshaw, *Simple approximation for thermal diffusion in ionized gas mixtures*, J. Non-Equilibrium Thermodyn. 21, 233, (1996).

[32]. J. O. Hirschfelder, C. F. Curtiss, and R. B. Bird, *Molecular theory of gases and liquids,* Wiley, (1964).

[33]. W. Z. Wang, M. Li and X. Tu, *Two temperature plasma properties of ablated PTFE vapor used for pulsed plasma thrusters*, 20th International Conference on Gas Discharges and their Applications, (2014).

Chapter 6 Conclusions and future work

6.1 Conclusions

To investigate the full potential of nitrogen for use in high voltage circuit breakers, knowledge of how to calculate the properties and radiation characteristics for nitrogen is necessary. PTFE vapour in high voltage circuit breakers due to nozzle ablation which affects radiation characteristics significantly when mixture with gas such as SF_6. Therefore, the calculation of radiation properties in this thesis considers the plasma of a nitrogen mixture with PTFE.

The species composition of the nitrogen-PTFE gas mixture was computed firstly in chapter three. The chemical equilibrium composition is determined by a modified Gibbs's free energy minimisation method under LTE conditions. The results were presented as a function of temperature and pressure at given molar proportions of nitrogen and PTFE. The net emission coefficient (NEC) for the gas mixture was then computed. The absorption coefficient was obtained by considering both continuum and line radiation contributed by atoms, ions and molecules. The Lorentz profile was employed to describe the sharp of the spectral line. The NEC calculation is followed by Lowke's method. The influence of uncertainty in atomic data on the calculated NEC was discussed. Although the accuracy of the high energy level is poor, the influence of uncertainty in the high energy level to NEC is negligible. Due to finding a significant influence of line overlapping on the NEC, line overlapping influence is considered in the calculation. The validity of the model was confirmed by good agreement between the results calculated in the present work and those obtained by experiment or predicted by other research groups for pure nitrogen gas and

pure PTFE vapour. The results indicate that the influence of PTFE vapour on the radiation is substantial.

In contrast with NEC in isothermal plasma, the real radiation model was introduced in chapter four. Since it is computationally expensive to solve the radiation transfer equation (RTE) to obtain the exact radiation flux, two approximation methods, the discrete ordinate method (DOM) and the P1 approximation method, were used to calculate radiative flux. P1 is computationally cheaper than DOM but it has poor accuracy. The accuracy of DOM is determined by the number of calculation bands. Two DOM bands were calculated and compared with a given temperature profile. The comparison of DOM 8-5 and 5-3 indicates a balanced compromise between accuracy and cost of calculation with DOM 8-5. As an approximation method for spectral radiation, the mean absorption coefficient (MAC) method saves the computation cost when it is calculating radiative flux. The influence of the MAC method on radiative flux was analysed. The comparison of $4\pi * \mathrm{NEC}$ and divergence of radiative flux for both temperature profiles was taken to understand the regions in arc plasma that are suitable to employ NEC for describing radiative transfer.

The calculations in chapter three and four are based on LTE assumption. However, LTE is no longer valid when a large temperature gradient exists such as the region close to the cold wall or when the number density of electrons is not high enough to allow sufficient transfer of energy between the electrons and heavy-particles. Thus, a two-temperature calculation model was introduced in chapter five. Different plasma composition calculation methods were discussed. A modified Godin's method was developed to fulfil the requirement of the two-temperature model. Composition results obtained by different calculation methods were taken to verify the validity of the modified Godin's method. Thermodynamic properties and transport coefficients of N_2

mixtures with different molar concentrations of PTFE were calculated under LTE and non-LTE conditions assuming chemical equilibrium. The calculation was carried out for electron temperatures ranging from 300 K to 40,000 K with PTFE concentrations of 0%, 20%, 40%, 60% and 100%. For the non-LTE plasma cases, the ratio of electron temperature to heavy particle temperature was set to 1, 2, 5, 10 and 20. The main features present in the results are analysed. A comparison of the results calculated using three methods was made, showing that Godin's method produces results very close to those of Van de Sanden's method. The composition results from the present work were compared with existing results, showing good agreement for pure PTFE vapour. A comparison for N_2-PTFE mixtures was not possible since no existing results are available.

Finally, in chapter two, with a nozzle, the nitrogen arc was experimentally investigated using various diagnostic actions, such as voltage and current waveforms, a pressure sensor and a displacement sensor. A detailed introduction to the experimental apparatus and calibration of equipment was provided. The arc is sustained by a slowly decreasing, low magnitude direct current, which is supplied by a capacitor bank. The gas flow is directed to a converging-diverging nozzle from a gas tank of 10 bar upstream stagnation pressure in a two pressure system. Three current levels are used, which are 100 A, 160 A and 333 A. The dynamic behaviour of the arcs was analysed.

6.2 Future work

The research on radiation property calculation of arc plasmas aims to provide accurate theoretical investigation of arc modelling. However, the calculations are based on many approximation methods, which can be improved in the future. Further work needs more effort on improvement of the calculation model to make it approach the real arc plasma. Firstly, the radiative flux calculation in chapter four is based on a given temperature profile. However, depending on the structure of the circuit breaker being used, the temperature

profile of arc plasma is variance. A prediction of the temperature profile from the radiation transport within an arc plasma can be done by equation. Coupling MAC with DOM or P1 can produce a more accurate temperature profile and the radiative flux of such a temperature profile. Secondly, only the two-dimensional radiation model is considered in this thesis. However, the real arc exists in a three-dimensional geometry, so a three-dimensional calculation of radiation flux can better describe the radiation characteristics in a real arc. The radiation flux of non-LTE arc plasma is the third area that requires further investigation in the future. Non-LTE plasma exists in some regions of a high voltage circuit breaker so the radiation contributed by different particles must be considered.